POLYPUBLIE
Polytechnique Montréal

POLYTECHNIQUE MONTRÉAL
UNIVERSITÉ D'INGÉNIERIE

Titre: Title:	Tailoring Absorption in Optical Thin Films Using Atomic Layer Deposition of High Quality Titanium Nitride
Auteur: Author:	Sasha Woodward-Gagné
Date:	2019
Type:	Mémoire ou thèse / Dissertation or Thesis
Référence: Citation:	Woodward-Gagné, S. (2019). Tailoring Absorption in Optical Thin Films Using Atomic Layer Deposition of High Quality Titanium Nitride [Mémoire de maîtrise, Polytechnique Montréal]. PolyPublie. https://publications.polymtl.ca/4121/

Document en libre accès dans PolyPublie
Open Access document in PolyPublie

URL de PolyPublie: PolyPublie URL:	https://publications.polymtl.ca/4121/
Directeurs de recherche: Advisors:	Ludvik Martinu, & Jolanta-Ewa Sapieha
Programme: Program:	Génie physique

Ce fichier a été téléchargé à partir de PolyPublie, le dépôt institutionnel de Polytechnique Montréal
This file has been downloaded from PolyPublie, the institutional repository of Polytechnique Montréal

https://publications.polymtl.ca

POLYTECHNIQUE MONTRÉAL
affiliée à l'Université de Montréal

Tailoring absorption in optical thin films using atomic layer deposition of high quality titanium nitride

SASHA WOODWARD-GAGNÉ
Département de génie physique

Mémoire présenté en vue de l'obtention du diplôme de *Maîtrise ès sciences appliquées*
Génie physique

Décembre 2019

© Sasha Woodward-Gagné, 2019.

POLYTECHNIQUE MONTRÉAL
affiliée à l'Université de Montréal

Ce mémoire intitulé :

Tailoring absorption in optical thin films using atomic layer deposition of high quality titanium nitride

présenté par **Sasha WOODWARD-GAGNÉ**
en vue de l'obtention du diplôme de *Maîtrise ès sciences appliquées*
a été dûment accepté par le jury d'examen constitué de :

Stéphane KÉNA-COHEN, président
Ludvik MARTINU, membre et directeur de recherche
Jolanta-Ewa SAPIEHA, membre et codirectrice de recherche
Clara SANTATO, membre

DEDICATION

To Tuvok, who introduced me to experimental science...
...may he live long and prosper.

ACKNOWLEDGEMENTS

I would first like to thank my director Ludvik Martinu for lending me his great expertise in thin film science and his time as a supervisor. I feel that Ludvik and my co-director Jolanta Sapieha have truly succeeded in creating a welcoming and supportive yet rigorous and challenging work environment in which students like myself can grow both personally and professionally.

To Oleg Zabeida, I thank you for your invaluable support throughout my time in the lab and for being my go-to person for bouncing around ideas, and asking questions. To Bill Baloukas, I am always impressed by the competence and dedication with which you work and by how you notice and remember every little detail. It goes without saying that I thank both of you very much for your mentorship and for the revisions you did on all of my papers, presentations and posters.

I would also like to thank my other collaborators and co-authors Bruce Raynor, Noel O'Toole, Kenneth Scott Alexander Butcher, Nicolas Desjardin-Lecavalier and Julien Gagnon for their tremendous help and for the interesting discussions they all provided. I particularly want to thank Richard Vernhes who introduced me to ALD and thin film science and spiked my interest in these topics.

Many thanks to Thomas Schmitt and Etienne Bousser for training me on equipment, and for being the only two research associates with which I have gone out to drink a beer! I also thank: Jacques Lengaigne and Erika Herrera for being great office partners and interesting conversationalists; Antonin Riera, Louis Dubé Riopelle and Philip Rumsby for providing fun and incredibly effective distractions; Sophie Berthelette by recurrence; Francis Blanchard, Yuxiao Wu, Rodrigue Beaini, Veronika Simova, Amaury Kilicaslan, Michael Laberge, Jincheng Qian, Stephen Brown, Sourouch Hafezian, Erwens Broustet, Josefina Crespo-Villegas, Fabrice Pougoum, Anna Jedrzejczak, Frédérik Poitevin, Julien Schmitt and Simon Loquai for the time we spent together in the labs, meetings and corridors discussing our research and hobbies and drinking too much coffee. I am also grateful to have worked with two talented interns Zachary Allaire and Justin Duby on projects related to this thesis.

For their incredible talent and support with characterization equipment, I also want to thank Josianne Lefebvre, Marie-Helene Bernier, Martin Chicoine, Philippe Plamondon, Jean-Philippe Masse and Patricia Moraille. I would have accomplished a lot less were it not for your help. The same goes for Francis Turcot, Sébastien Chénard, Francis Boutet and Samuel Cardinal for all the technical support they provided throughout my master's and for every-

thing I learned from them regarding deposition system maintenance and construction.

I also thank my family for attempting to understand my field of research and for supporting me in it nonetheless. Among them, Jeanne Clermont for supporting me during this process, correcting my work once in a while and sharing her own scientific culture with me, and for making me forget those odd days where nothing seems to function as it should.

On a final note, I thank the members of my jury Stephane Kéna-Cohen and Clara Santato for taking the time to review this thesis.

RÉSUMÉ

Le dépôt par couche atomique (ALD) est un type de dépôt chimique en phase vapeur (CVD) dans lequel la croissance se produit par monocouches atomiques successives. La méthode présente un grand potentiel pour le traitement de revêtements optique car l'épaisseur précise et la haute conformité des dépôts ALD les rendent très utiles pour adapter les propriétés optiques de matériaux nanostructurés. En effet, de nombreux travaux ont été réalisés sur la modification de structures photoniques utilisant diverses épaisseurs de matériaux diélectriques déposés par ALD. La même technique pourrait être utilisée pour contrôler l'absorption optique dans des matériaux similaires, mais les revêtements métaliques et les nitrure métaliques produit par ALD demeurent d'une qualité inférieure à ceux produit par d'autres méthodes.

Dans cette thèse, nous optimisons le dépôt de TiN par ALD pour des applications optiques et proposons un moyen d'améliorer ses propriétés grâce à l'utilisation du dépôt de couche atomique assisté par plasma à cathode creuse (HC-PEALD). Des couches de TiN sont d'abord déposées par ALD, puis par HC-PEALD, et les paramètres de dépôt sont variés dans les deux cas afin de déterminer leur effet sur les propriétés des revêtements. Comme le second processus est plus complexe et relativement nouveau, une grande attention est accordée à sa caractérisation. Nous constatons que l'utilisation d'un plasma à cathode creuse peut diminuer la contamination au chlore et augmenter le taux de croissance par rapport à d'autres types de source plasma dans le dépôt de couche atomique amélioré par plasma.

Notre TiN optimisé est ensuite utilisé pour ajuster l'absorption de revêtements colonnaires inclinés (SCTF) en SiO_2 en déposant de fines couches conformes de TiN absorbant autour des colonnes diélectriques. Ces colonnes core-shell présentent une séléctivité angulaire similaire à celle observée dans les revêtements colonnaires métalliques. Nous déterminons que l'utilisation du dépôt de couche atomique dans ce contexte permet un réglage précis de l'absorption visible qu'il serait difficile d'obtenir uniquement à l'aide de SCTF métalliques. De plus, le procédé proposé permet l'utilisation de matériaux à partir desquels les SCTF ne pourraient normalement pas être fabriqués.

ABSTRACT

Atomic layer deposition (ALD) is a type of chemical vapour deposition (CVD) in which growth occurs though successive atomic monolayers. The method is of great interest for optical coating processing as the precise thickness and high conformity of ALD films make them very useful for tailoring the optical properties of nanostructured coatings. Indeed much work has been done pertaining to the tuning of photonic structures using varying thicknesses of dielectric materials deposited by ALD. The same technique could be used to tune optical absorption in similar types of nano-structured films however much less research has been done on this topic as the quality of metal and metal nitride films processed by ALD lags behind those processed by other methods.

In this thesis, we optimize TiN ALD for optical applications and propose a way of improving its quality through the use of hollow cathode plasma enhanced atomic layer deposition (HC-PEALD). Films are deposited first by ALD and then by HC-PEALD and process parameters are varied in both cases to determine their effect on film properties. Since the second process is more complex and relatively novel, great attention is given to characterising it. We find that using a hollow cathode plasma source can reduce chlorine content and increase growth rate as compared to competing sources in PEALD.

Our optimized TiN is used to tune absorption in SiO_2 slanted columnar thin films (SCTFs) by depositing thin conformal layers of absorbing material around the dielectric columns. These core-shell columns are found to exhibit angular selective properties similar to what is observed in metallic columnar films. We find the use of ALD in this context enables precise tuning of visible absorption that would be difficult to obtain only using metallic SCTFs. Furthermore, with the proposed method, materials can be used from which SCTFs could not normally be made.

TABLE OF CONTENTS

DEDICATION iii

ACKNOWLEDGEMENTS iv

RÉSUMÉ vi

ABSTRACT vii

TABLE OF CONTENTS viii

LIST OF TABLES xi

LIST OF FIGURES xii

LIST OF SYMBOLS AND ACRONYMS xv

LIST OF APPENDICES xvii

CHAPTER 1 INTRODUCTION 1
- 1.1 Foreword 1
- 1.2 Titanium Nitride: a case for metal nitride ALD in optical thin films 2
- 1.3 Core-shell SCTFs : a case for tuning absorption in metamaterial films 3
- 1.4 Thesis objectives 4
- 1.5 Patent, conferences and publications 5
- 1.6 Thesis outline 6

CHAPTER 2 LITERATURE REVIEW 7
- 2.1 Atomic layer deposition 7
  - 2.1.1 Thermal atomic layer deposition 7
  - 2.1.2 Plasma enhanced atomic layer deposition 11
  - 2.1.3 Atomic layer deposition of titanium nitride 14
  - 2.1.4 Uses of hollow cathode plasma in PEALD 17
- 2.2 Optical properties of TiN 20
- 2.3 Angular selective thin films 22
  - 2.3.1 Glancing angle deposition of SCTFs 23
  - 2.3.2 Angular selectivity of SCTFs 25

2.3.3 Challenges in the fabrication of SCTFs 27
2.4 Core-shell SCTFs 29
2.5 Tuning optical properties with ALD 31

CHAPTER 3 METHODOLOGY 32
3.1 Atomic layer deposition 32
3.1.1 Experimental setup 32
3.1.2 Thermal atomic layer deposition of TiN 34
3.1.3 Plasma enhanced atomic layer deposition of TiN 34
3.2 Glancing angle deposition 35
3.3 Spectroscopic ellipsometry 35
3.3.1 *In situ* SE 38
3.3.2 *Ex situ* SE 39
3.4 Sample characterization 39
3.4.1 Optical properties 39
3.4.2 Thickness and structure 41
3.4.3 Composition 42

CHAPTER 4 ARTICLE 1: PLASMA ENHANCED ATOMIC LAYER DEPOSITION OF HIGH PURITY TITANIUM NITRIDE: COMPARISON OF HOLLOW CATHODE AND INDUCTIVELY COUPLED DISCHARGES 43
4.1 Foreword 43
4.2 Article : Plasma enhanced atomic layer deposition of high purity titanium nitride: comparison of hollow cathode and inductively coupled discharges . . 43
4.2.1 Abstract 43
4.2.2 Introduction 44
4.2.3 Experimental 44
4.2.4 Results and discussion 46
4.2.5 Conclusions 51
4.2.6 Acknowledgements 51
4.3 Further work on atomic layer deposition of TiN 52
4.3.1 Thermal atomic layer deposition of TiN 52
4.3.2 *In situ* and *ex situ* spectroscopic ellipsometry of TiN 52
4.3.3 Plasma exposure time 54
4.4 Concluding remarks 56

CHAPTER 5 ARTICLE 2: TAILORING ANGULAR SELECTIVITY IN SiO_2 SLANTED

COLUMNAR THIN FILMS USING ATOMIC LAYER DEPOSITION OF TITANIUM NITRIDE . . . 57
5.1 Foreword . . . 57
5.2 Article: Tailoring angular selectivity in SiO_2 slanted columnar thin films using atomic layer deposition of titanium nitride . . . 57
5.2.1 Abstract . . . 57
5.2.2 Introduction . . . 57
5.2.3 Experimental methodology . . . 59
5.2.4 Results and discussion . . . 60
5.2.5 Conclusions . . . 65
5.2.6 Acknowledgements . . . 65
5.3 Further work on core-shell SCTFs . . . 65
5.4 Concluding remarks . . . 68

CHAPTER 6 GENERAL DISCUSSION . . . 69

CHAPTER 7 CONCLUSION . . . 72

REFERENCES . . . 73

APPENDICES . . . 86

LIST OF TABLES

Table 2.1 Comparing the quality of published nitride films obtained by HC-PEALD and IC-PEALD. 19
Table 2.2 Resistivity of TiN films found in literature for common types of thin film deposition techniques along with films thickness and resistivity measurement method. 22
Table 4.1 Comparing deposition parameters for films deposited in part 2. 45
Table 4.2 Thickness, growth per cycle, roughness, resistivity and contamination for films deposited using 100 W and 300 W hollow cathode plasmas. . 47
Table 4.3 Material properties of TiN films deposited on native oxide using hollow cathode (HCP) and inductively coupled (ICP) discharges. 50
Table 4.4 Comparing TiN film thickness and resistivity measured by *In situ* spectroscopic ellipsometry, variable angle spectroscopic ellipsometry, x-ray reflectivity, scanning electron microscopy and four point probe. . . . 53
Table 5.1 SiO_2 SCTF characteristics prior to ALD functionalization. Thickness, porosity and refractive index were determined by ellipsometry whereas column angle was measured by SEM imaging. 59
Table 6.1 Comparing the properties of our IC-PEALD and HC-PEALD coatings to selected results from other authors. 69
Table 6.2 Comparing the three deposition methods presented in chapter 4. . . . 70

LIST OF FIGURES

Figure 1.1 All articles indexed in Compendex on the topic of ALD for every year since 1990 as well as those pertaining to microelectronic and energy applications of ALD. 1

Figure 2.1 Schematic representation of a binary ALD process. 7

Figure 2.2 An ALD half-reaction of titanium tetrachloride ($TiCl_4$) with hydroxyl groups on a sample surface. 8

Figure 2.3 Defining the ALD temperature window for self-limiting growth. . . . 8

Figure 2.4 (a) A viscous flow reactor setup for ALD and (b) a typical ALD cycle. 9

Figure 2.5 Optimization uptakes for (a) precursor exposure and (b) purging time. 10

Figure 2.6 Comparing conformity in PVD, CVD and ALD. 11

Figure 2.7 Comparing PEALD to thermal ALD. The second half-cycle is replaced by a plasma exposure. 12

Figure 2.8 Three types of PEALD: (a) Radical enhanced ALD, (b) Direct PEALD and (c) Remote PEALD. 13

Figure 2.9 Key findings from Elers et al. when comparing TiN films obtained from ALD and PEALD. A third process (*in situ*) is also compared where metallic titanium is used as a catalyst for *in situ* reduction of the titanium chloride precursor. (a) Growth rate and (b) chlorine concentration at a given temperature are significantly improved when using PEALD as opposed to ALD. One can also significantly reduce chlorine concentration in PEALD with longer and higher power plasma exposures, as shown in (c). 15

Figure 2.10 Comparing resistivity as a function of temperature for TiN films processed by PEALD and ALD. 16

Figure 2.11 Resistivity (a) as well as electron mean free path and density (b) as a function of thickness for TiN films deposited by PEALD. 16

Figure 2.12 Typical I-V curve of a hollow cathode system exhibiting three regimes. 17

Figure 2.13 Experimentally determined dielectric constants of TiN in literature as compiled by Patsalas et al.. 20

Figure 2.14 (a) E_{ps} and (b) resistivity as a function of N/Ti ratio in TiN. 21

Figure 2.15 Column growth mechanism in GLAD and sample placement respective to the material source. 23

Figure 2.16 Scanning electron micrograph of a SiO_2 SCTFs made by GLAD. . . . 24

Figure 2.17 Understanding the cause of anisotropic absorption in SCTFs and how it relates to the geometry of the columns. 25

Figure 2.18 Angular selective properties of evaporated chromium SCTFs. 26

Figure 2.19 Relative unpolarised luminous AS at 60° as a function of unpolarised luminous transmission at 60° for SCTFs found in literature. 27

Figure 2.20 Relative p-polarized luminous AS at 60° as a function of p-polarized luminous transmission at 60°. Films are simulated from an anisotropic bruggeman effective medium approximation of WO_3 and void. 28

Figure 2.21 Density profiles determined by XRR as a function of (a) glancing angles a: 40, b:6- and c: 70; and (b) thicknesses a: 18. b: 100 and c: 110 nm, α for different materials. 29

Figure 2.22 Density (a) and column angle, β, (b) as a function of glancing angle, α for different materials. 30

Figure 2.23 Tuning (a) transmission and (b) spectral shift in a nanohole-based SPR sensor as a function of the thickness of an ALD alumina overcoat. . . 30

Figure 2.24 Optical reflection of Ag coated Si nanopillar arrays with varying diameter and interparticle gap. 31

Figure 3.1 Making core-shell SCTFs through successive GLAD and ALD. 32

Figure 3.2 (a) The *Kurt J. Lesker Co. ALD-150LX* used in the current thesis, with the control unit (back) and depositions chamber (front). (b) Inside view of the system and its constituent parts. 33

Figure 3.3 Schematic representation of the ALD system. 33

Figure 3.4 The e-beam evaporation system used for GLAD in this thesis with its custom substrate holder. Samples are fixed to the plates in positions I, II, III and IV. 35

Figure 3.5 The SE measurement process. Linearly polarized light is reflected from the sample with an elliptical polarization. 36

Figure 3.6 Example of an optimization routine for TiN. 38

Figure 3.7 Four point probe measurement setup over a rectangular sample. . . . 40

Figure 4.1 Growth rate and resistivity of TiN as a function of plasma exposure time. Films were deposited at 380 °C, with a 300W hollow cathode plasma. 46

Figure 4.2 AFM phase maps of samples deposited using 100 W (a) and 300 W (b) of hollow cathode plasma. 48

Figure 4.3 Growth rate (a) and resistivity (b) of TiN as a function of substrate temperature. 48

Figure 4.4 Chlorine and oxygen concentration HC-PEALD films deposited at 130 °C, 255 °C and 380 °C and a thermal film deposited at 380 °C. 49
Figure 4.5 Ellipsometric model used for thickness and resistivity measurements of titanium nitride (TiN) processed by atomic layer deposition (ALD) and plasma enhanced atomic layer deposition (PEALD). 53
Figure 4.6 Resistivity as a function of thickness for TiN films deposited by HC-PEALDs. 54
Figure 4.7 Growth rate as a function of plasma pulse length for hollow cathode plasma (HCP) power between 150 W and 600 W. 55
Figure 4.8 Chlorine and oxygen concentration HC-PEALD films deposited with 15 s, 60 s and 99 s of plasma exposure time. 55
Figure 5.1 Scanning electron micrograph of a SiO_2 slanted columnar thin film taken prior to ALD functionalization. 59
Figure 5.2 Micrographs of a TiN-coated SiO_2 nanocolumn obtained by transmission electron microscopy. 61
Figure 5.3 (a) *p*- (left y-axis) and *s*-polarized (right y-axis) transmission spectra of a SiO_2 slanted columnar thin film coated with 500 cycles of TiN by ALD measured at three different angles. 62
Figure 5.4 Luminous transmittance (T_{lum}) as a function of incidence angle (θ) for SiO_2 SCTFs coated with, from left to right, 0, 400, 500 and 600 cycles of TiN using ALD. 63
Figure 5.5 Relative luminous angular selectivity ($T_u^{lum}(+60°)/T_u^{lum}(-60°)$) vs. maximum transmittance ($T_u^{lum}(+60°)$) of unpolarized light. 64
Figure 5.6 Core-shell SCTFs deposited with multiple SCTF thicknesses, glancing angles (α) and core thicknesses (number of cycles). 66
Figure 5.7 (a) Absolute AS as a function of positive angle transmission and wavelength for films of the first series. (b) Absolute AS as a function of positive angle transmission for all films of the second series. 67
Figure 5.8 Absolute angular selectivity as a function of positive angle transmission for films with shell thicknesses of (a) 300 cycles and (b) 500 cycles and SCTF thicknesses as indicated for each curve. 67
Figure A.1 Thickness of a TiN layer during deposition measured by in-situ SE over a period of 10 cycles. Noise reduction is done by averaging 10 consecutive measurements adjusted to begin at a thickness of 0 nm, hence the nominal thickness. Despite the averaging, data is too noisy to study process cycle dynamics. 86

LIST OF SYMBOLS AND ACRONYMS

ALD	Atomic layer deposition
AS	Angular selectivity
CMOS	Complementary metal-oxide-semiconductor
CVD	Chemical vapor deposition
CS-SCTF	Core-shell slanted columnar thin film
FCSEL	Functional coatings and surface engineering laboratory
FPP	Four point probe
GLAD	Glancing angle deposition
GPC	Growth per cycle
HCP	Hollow cathode plasma
HC-PEALD	Hollow cathode plasma enhanced atomic layer deposition
IBAD	Ion beam assisted deposition
ICP	Inductively coupled plasma
IC-PEALD	Inductively coupled plasma enhanced atomic layer deposition
IEE	Interference enhance ellipsometry
IR	Infrared
iSE	*In-situ* spectroscopic ellipsometry
LPCVD	Low pressure chemical vapour deposition
MFP	Mean free path
MSE	Mean squared error
NH_3	Ammonia
PEALD	Plasma enhanced atomic layer deposition
PLD	Pulsed laser deposition
PPL	Plasma pulse length
PVD	Physical vapor deposition
QCM	Quartz crystal microbalance
RBS	Rutherford backscattering
REALD	Radical enhanced atomic layer deposition
RF	Radio-frequency
SCTFs	Slanted columnar thin films
SE	Spectroscopic ellipsometry
SEM	Scanning electron microscopy
$TiCl_4$	Titanium tetrachloride

TiN	Titanium nitride
UHV	Ultra high vacuum
UV	Ultra-violet
VASE	Variable angle spectroscopic ellipsometry
XRR	X-ray reflectivity
α	Angle of the incident material flux in glancing angle deposition
β	Angle of columns in slanted columnar thin films
Δ	Phase change after reflection in ellipsometry
ΔT	Absolute angular selectivity
λ	Wavelength
Ψ	Tangeant of the ratio of reflected amplitudes in ellipsometry
S	Relative angular selectivity
θ	Incidence angle

LIST OF APPENDICES

Appendix A: High rate in-situ SE during PEALD of TiN 86

CHAPTER 1 INTRODUCTION

1.1 Foreword

For the past two decades, atomic layer deposition (ALD) has been a growing trend in thin film processing. The technique, a subset of chemical vapor deposition (CVD), saw significant development in the early 2000s for its potential at improving gate dielectrics in the nano-electronics industry, eventually culminating to its adoption by Intel corporation in 2007 [1]. As a result of this development, ALD garnered interest in many other fields for its ability to control thickness down to sub-angstrom levels while providing conformal deposition over even the most challenging substrate geometries. Consequently, the global ALD market is now expected to reach over 9 Billion $US by 2025 [2].

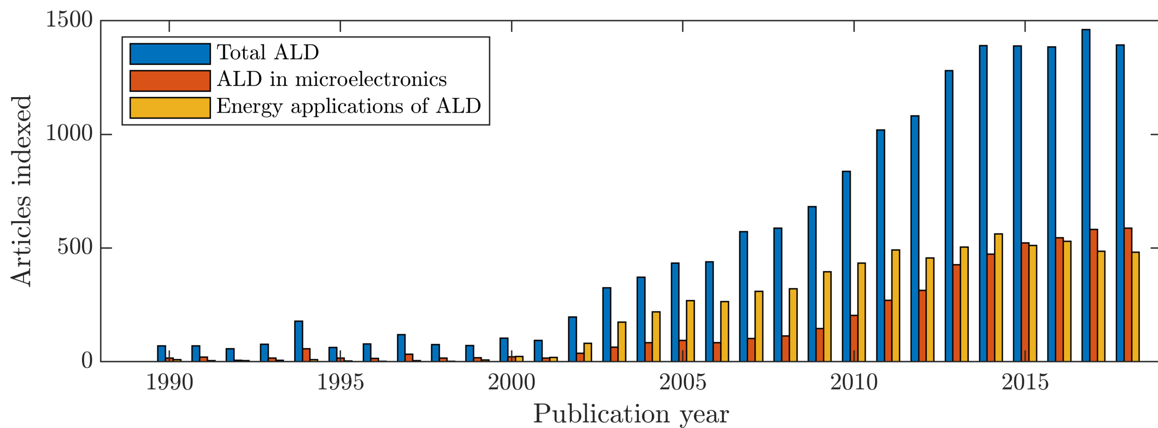

Figure 1.1 All articles indexed in Compendex on the topic of ALD for every year since 1990 as well as those pertaining to microelectronic and energy applications of ALD[1].

Nowadays energy applications are among the key drivers of ALD research, in part because the conformity of ALD over 3D structures can yield substantial improvements in anything from batteries [3] and fuel cells [4] to photovoltaics [5] and photocatalysis [6]. Most notably, due to its precise thickness control, the use of ALD over 3-dimensional optical metamaterials or over plasmonic structures can lead to precise tunability of optical properties [7–11]. Such tunable structures can have applications in energy efficient fenestration, solar energy, ophthalmic

[1]Data automatically compiled in Engineering Village for search terms : *("Atomic Layer Deposition" OR "Atomic Layer Epitaxy" OR "Molecular Layer Deposition") WN All Fields*. Microelectronic applications are associated to search terms : *("High-k" OR "gate dielectric"OR transistor OR capacitor OR "gate oxide") WN All fields*. Energy applications are associated to search terms : *(solar OR energy) WN All fields.*

lenses, and many other fields. As such, research on this topic is a growing trend in optical film processing.

The best examples of research concerning the tuning of optical properties by ALD involves the deposition of dielectrics like Al_2O_3 and TiO_2, which are both very typical ALD processes[2]. This is partly because, despite a constantly expanding selection of ALD processed materials, films of high optical quality are limited. This is especially the case for metal nitrides, which often suffer from very low deposition rates (typically 0.2 Å/ Cycle) [12], high levels of contamination (Namely H, Cl, O and C) [13], poor crystalline quality [14], and high resistivity [13] which in turn affect their optical performance. Since nitrides have many useful optical applications, much research is left to be done both on the processing of better metal nitride films and on their use for tuning 3-dimensional optical metamaterials. As some previous work has been done on dynamically tunable absorption in slanted columnar thin films (SCTFs) [15] at the Functional Coating and Surface Engineering Laboratory (FCSEL), using atomic layer deposition of a metal nitride to tailor the absorption of SCTFs is a natural continuation.

1.2 Titanium Nitride: a case for metal nitride ALD in optical thin films

Titanium nitride (TiN) was first deposited through ALD by Hiltunen et al. [16] in 1988 using titanium tetrachloride ($TiCl_4$) and ammonia (NH_3). Since then, it has become one of the most investigated ALD nitride processes [13]. In addition, the metalchloride/ammonia chemistry developed by these authors has been applied to many other metals, and is to date one of the most popular chemistries in nitride processing [12, 17, 18]. Accordingly, TiN is a good choice of materials for researching improvements in ALD nitride processing. TiN is also an important material in the field of optical thin films because of its high visible and infrared absorption [19], beautiful golden colour, high conductivity at low thickness [20, 21], and because of its good thermal stability [22] and mechanical properties [23]. It is especially promising as a replacement to noble metals in plasmonic applications [19, 23, 24] because of its tunable optical properties [21, 25] and compatibility with complementary metal-oxide-semiconductor (CMOS) technology [26].

As mentioned above, when processed by ALD, TiN films perform substantially worse than those made using deposition techniques such as sputtering[1]. The ALD films exhibit high

[2]In fact, over a third of publications mentioning “atomic layer deposition” in Compendex also mention alumina, Al_2O_3 or aluminum oxide.

[1]This will be shown in chapter 2.

resistivity [21, 27], low absorption and high levels of contamination [14, 21, 27] which change their colour from gold to a brownish purple. Indeed, the chloride/ammonia chemistry tends to lead to films with high chlorine content [12], as well with small crystallite sizes that make them susceptible to oxidation [14]. In addition, the deposition rates of this family of processes are so low that they restrict applications of nitride ALD to only very thin films (below 20 nm). Emerging metal-organic chemistries can be used to increase growth rates for these types of films. However, they tend to leave important amounts of carbon and hydrogen in the nitride films leading to amorphous or partially amorphous films with poor resistivity and poor optical performance.

In the past decade, plasma enhanced atomic layer deposition (PEALD) has established itself as a way to improve the properties of some ALD films. In the PEALD process of TiN and other nitrides, the same metal chloride precursor is used while the ammonia precursor is replaced by exposure to an $Ar/H_2/N_2$ plasma. This difference can lead to a dramatic increase in growth per cycle (GPC) [21]. Chlorine contamination in the films is also greatly diminished because the hydrogen and nitrogen metastables used in the plasma enhanced process are significantly more reactive than ammonia [18,21]. As a result, PEALD typically yields nitride films with greater crystallite sizes and lower resistivity. The additional energy provided by the plasma in PEALD also enables one to deposit films at much lower temperatures than are possible with conventional ALD [18]. While PEALD clearly can improve nitride processing over thermal ALD, the resulting films generally remain of poorer quality than those processed with more mature techniques such a sputtering (see table 2.2).

In most published cases, inductively coupled remote plasmas (ICPs) are employed in PEALD. Correspondingly, most commercial R&D PEALD systems also come equipped with these types of plasma sources [18]. However, hollow cathode plasma (HCP) sources have distinguished themselves as a possible replacement in the last few years [28]. Indeed, for other nitride films, much higher growth rates, crystallite sizes and lower contaminations have been reported when using an HCP [29–31]. These recent reports suggest that this type of plasma could greatly improve TiN films processed by PEALD.

1.3 Core-shell SCTFs : a case for tuning absorption in metamaterial films

As mentioned previously, FCSEL has a growing interest and expertise in angular selective SCTFs. These sculptured films are deposited using a technique called glancing angle deposition (GLAD), which has been extensively studied by the group in its efforts to develop low index transparent materials [32]. When SCTFs are made from absorbing materials, however, they exhibit angular selectivity (AS) [33] : low transmission at incidence angles perpendicular

to the columnar structure and high transmission at incidence angles parallel to it. This is because the columnar structure causes high absorption in one direction and low absorption in the other.

This anisotropic absorption has applications for energy efficient fenestrations, ophthalmic lenses and much more. However, GLAD-based angular selective coatings can be difficult to integrate into device fabrication [34] because film aspects such as columns angle, shape and density have great variability between materials and deposition conditions [35]. Indeed, the AS has to be reoptimised every time the colour or transmission of the films is tailored to a specific purpose because any change in material [36], thickness [37] or glancing angle also affects the columnar structure of the film. These challenges can be overcome by using ALD of metals or metal nitrides: By depositing a thin absorbing layer by ALD over a dielectric SCTF, it is possible to create core-shell SCTFs (CS-SCTFs) that behave like their metallic counterparts. The advantage of this method is that one can change the absorbing material, or the quantity of absorbing material, without changing the structure of the columnar film. In addition, this technique enables the fabrication of AS films from materials that cannot easily be used for GLAD, such as TiN. Both these advantages result in GLAD based AS films that are much simpler to tailor to specific applications.

1.4 Thesis objectives

The main objective of the present master's thesis is to advance knowledge in ALD of metal nitride optical films by improving the optical quality of ALD-processed TiN, and by applying it to the development of a novel nanostructured optical coating in which absorption is tailored using ALD. Specifically, the project aims at advancing the field by focusing on the following aspects:

1. Optimizing resistivity in TiN films obtained by ALD and PEALD for optical applications.
2. Investigating the use of an HCP source for improving the quality of TiN deposited by PEALD.
3. Obtaining angular selective CS-SCTFs from ALD of TiN over silica films fabricated by GLAD.
4. Demonstrating the AS of the fabricated CS-SCTFs and the advantages of the proposed method.

1.5 Patent, conferences and publications

As a result of the work presented in chapter 5.2 of this thesis, an international provisional patent has been filed in collaboration with Essilor International S.A :

Nanostructured thin film coating with angular selectivity, 2018.

In addition, the research in chapter 4 was presented at the 61st Annual Society of Vacuum Coaters Technical conference (SVC TechCon 2018) in April 2018 and subsequently published in the SVC TechCon proceedings. This conference paper will be presented in chapter 4.

S. Woodward, O. Zabeida, L. Martinu, B. Rayner, N. O'Toole, K. S. A. Butcher, *Plasma Enhanced Atomic Layer Deposition of High Purity Titanium Nitride: Comparison of Hollow Cathode and Inductively Coupled Discharges, 2018.*

The results in chapter 5.2 were also presented at the OSA Optical Interference Coatings Conference in June 2019, and published as a long-form abstract :

Sasha Woodward-Gagné, Nicolas Desjardins-Lecavalier, Bill Baloukas, Oleg Zabeida, Ludvik Martinu *Tuning absorption in angular selective slanted column thin films (SCTFs), 2019.*

In September 2019, the work presented in chapter 5 was accepted for publication in the OSA journal Optical Materials Express. The article will be included as a chapter in this thesis.

Sasha Woodward-Gagné, Nicolas Desjardins-Lecavalier, Bill Baloukas, Oleg Zabeida, and Ludvik Martinu, *Tailoring angular selectivity in SiO2 slanted columnar thin films using atomic layer deposition of titanium nitride,* Opt. Mater. Express 9, 4556-4563 (2019)

In addition to these conferences and publications, a collaboration was done on another conference paper :

Joe Brindley, Benoit Daniel, Victor Bellido-Gonzalez, Richard Potter, Benjamin Peek, Oleg Zabeida, Sasha Woodward-Gagne, Ludvik Martinu *A Remote Plasma Spectroscopy-Based Method for Monitoring of ALD Processes, 2018.*

1.6 Thesis outline

Following this introduction, a literature review is presented in chapter 2. This review focuses first on ALD and PEALD, the theory behind it and the advantages and limitations of both techniques. Afterwards, the processing of TiN by ALD and PEALD is reviewed and the potential of HCPs for improving nitride films processed by ALD is presented. The optical properties of TiN are then briefly discussed and the quality of films manufactured through multiple deposition techniques is compared. Subsequently, AS is introduced as well as how it is obtained in structured thin films. Finally, the literature pertaining to ALD over SCTFs is surveyed as well as how ALD has been used to tune optical properties in other structured films.

The third chapter exposes elements of the experimental methodology used in this work. Sample preparation will be presented including the substrates we used, the ALD and PEALD reactors and processes and the GLAD process and setup. Characterization tools will then be discussed, such as ellipsometry, spectrophotometry, four-point-probe, X-ray reflectometry and more.

In the fourth chapter a conference article is presented: *Plasma enhanced atomic layer deposition of high purity titanium nitride: comparison of hollow cathode and inductively coupled discharges*. Some additional results are presented afterwards which further answers some of the questions raised in the article.

In the fifth chapter, the central article of the thesis is presented : *Tailoring angular selectivity in SiO_2 slanted columnar thin films using atomic layer deposition of titanium nitride*, some additional work on the topic is then presented that was not included in the article.

Both chapters will then be briefly discussed followed by the final conclusion.

CHAPTER 2 LITERATURE REVIEW

2.1 Atomic layer deposition

2.1.1 Thermal atomic layer deposition

Theory

Atomic layer deposition is a type of CVD in which growth occurs through repeated deposition of atomic monolayers [1]. This is most often achieved by using a binary chemistry [38] whereby the sample is sequentially exposed to two different gaseous precursors separated by inert gas purges, as illustrated in figure 2.1. Each precursor then reacts only with the sample surface leaving reaction sites for the next precursor: this is called a half-reaction [1], or half-cycle. In order for growth to occur by atomic monolayers, each half-reaction must be self limiting [39], i.e. once all sites on the surface are occupied, the process ceases until the sample is exposed to the next precursor. In addition, each half-cycle must leave suitable reaction sites for the next one. This is represented in figure 2.1 where precursor A has a triangle head and a tetragon tail and Precursor B the opposite, leading to each block being only able to land on the other.

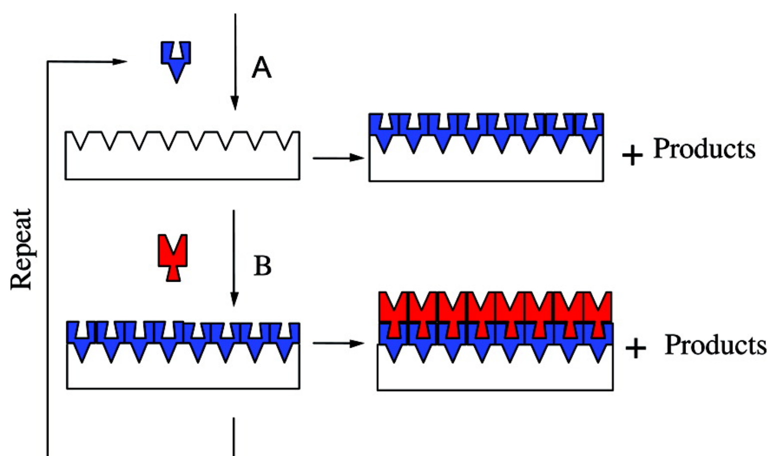

Figure 2.1 Schematic representation of a binary ALD process. Reprinted with permission from [38]. Copyright 2010, American Chemical Society.

In reality, this is typically achieved by using molecules with high symmetry as is illustrated in figure 2.2 with the case of tetragonal titanium chloride. In this half-cycle, once the $TiCl_4$ has reacted with all the hydroxyl sites, only Ti-Cl groups are left on the surface. Since the

only reacting gas present in the chamber is titanium chloride, no further reaction can occur at the process temperature.

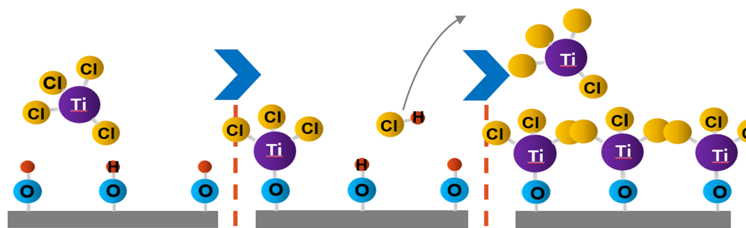

Figure 2.2 An ALD half-reaction of $TiCl_4$ with hydroxyl groups on a sample surface. Adapted from [40].

Indeed, the choice of processing temperature is critical for self-limiting growth [41]. For one, the system must provide enough energy for precursors A and B to react entirely together. Additionally, the temperature must be chosen so that neither of the precursor condenses on the surface, or goes through thermal self-decomposition. Finally, since growth rates by ALD are fairly low, any amount of re-evaporation of the film will significantly interfere with growth. In figure 2.3 the effect on the growth rate of each of these temperatures-related phenomena is presented. For most processes, we can define an *ALD temperature window* [1] in which self-limiting monolayer growth occurs.

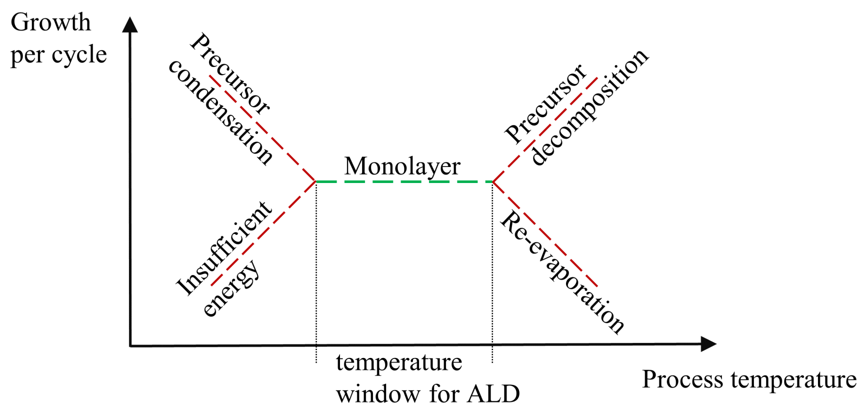

Figure 2.3 Defining the ALD temperature window for self-limiting growth. Adapted from [42].

While multiple reactor types exist for ALD, by far the most common types are viscous flow reactors [43]. These are designed to eliminate stagnant precursor pockets that cause parasitic CVD. A typical reactor is presented in figure 2.4 (a): Precursors A and B as well as inert purge gas are mixed in a shower head above the sample surface. These types of

reactors are operated at close to 130 Pa (1 Torr) with continual pumping. The pressure is maintained using large flows of inert gas. This flow is usually kept throughout the process while the gaseous chemical co-reactants are briefly introduced to the chamber one after the other using high-speed valves. The timings of this process are represented in 2.4 (b). Most often precursor exposures are in the order of 10 ms while purging times can last between 1 and 10 seconds. However, this varies greatly among deposition systems and as a function of process conditions. As such, cycle pulse times must be optimized for every new precursor chemistry and deposition chamber.

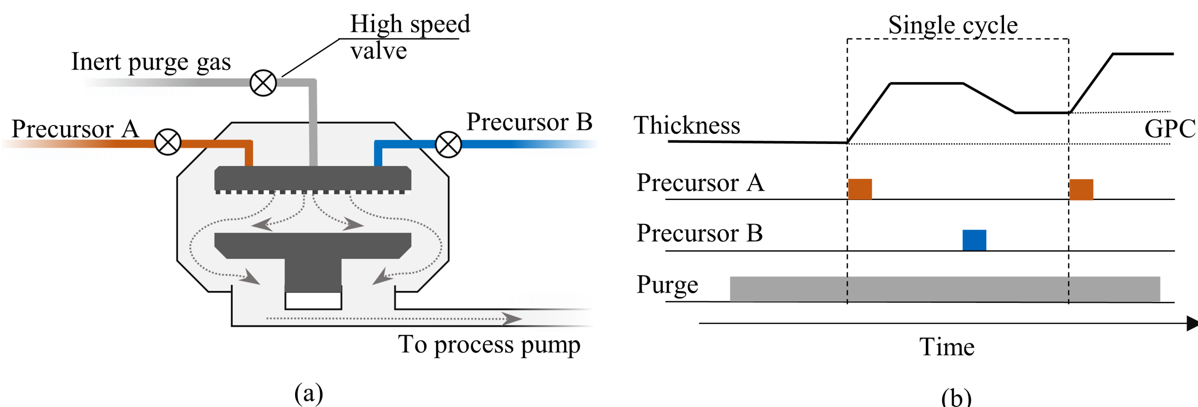

Figure 2.4 (a) A laminar flow reactor setup for ALD and (b) a typical ALD cycle. Precursors are fed into a shower head above the substrate and pulsed using high-speed valves. Continual flow of inert gas maintains a laminar flow. A single cycle includes exposure to both reactants as well as purging times. The GPC is defined as the thickness changes after a single cycle. Adapted from (a) [44] and (b) [45].

When a precursor exposure time is too short, the resulting half-reaction will be incomplete, i.e. the reacting gas will not chemisorb on all available surface sites. This will lead to preferential growth in zones with higher concentration of precursor. To avoid this, cycle timings are optimized as shown in figure 2.5 (a). Multiple samples are made using different exposure times and GPC is measured for each one. The optimal exposure time is generally accepted as the shortest pulse after which longer ones do not affect growth rate [41]. Indeed, after a full monolayer is deposited on the surface, continuing exposure to the precursor does not yield any growth because of the self-limiting nature of the reaction. When the pulse time is too short, however, the GPC diminishes due to incomplete monolayer deposition. In some cases, non-uniformity is used in addition to GPC, because uneven precursor concentration in the chamber can lead to sub-monolayer growth on the edges of a wafer while the centre exhibits ALD growth, or vice versa [41]. Similarly, if non-line of sight deposition is required,

it can be pertinent to increase pulsing times beyond the optimal value to ensure the saturated ALD occurs everywhere. Reacting gas exposures can also be optimized through their vapour

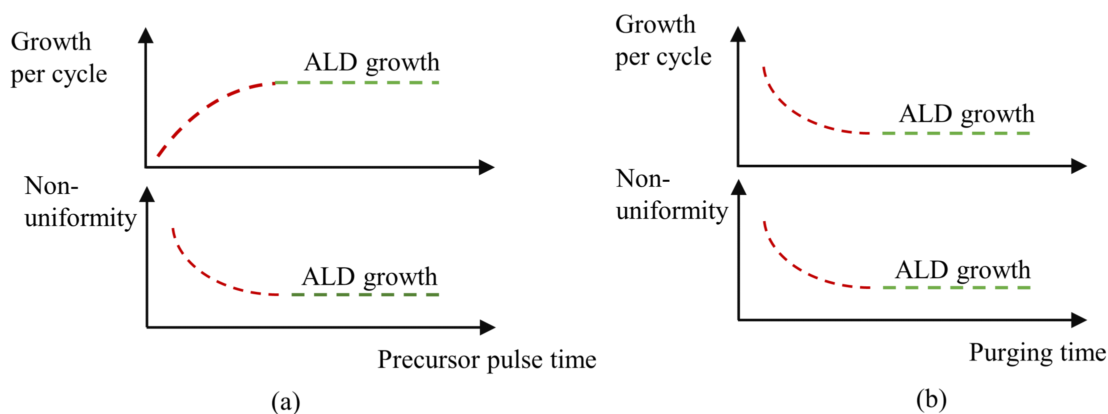

Figure 2.5 Optimization uptakes for (a) precursor exposure and (b) purging time. For mono-layer growth to occur, GPC must be saturated as a function of both reactant pulse times and purge times. Adapted from [39].

pressure (by heating) or mass flow, but these options offer less fine control, as such the final optimization step is usually done with pulse times. Purge optimization follows a similar process, as shown in figure 2.5 (b) when a steady state is achieved as a function of purging times the reaction is considered optimal. Purges that are too short will lead to the presence of both precursors in the chamber at the same time, leading to parasitic CVD [41], line of sight effects, multi-layer growth and in some cases gas-phase reaction and powder production. Considering that these uptakes are important for true ALD growth, they are often shown in articles presenting new precursor chemistries or improving existing ones.

Advantages and limitations

As indicated by its rapid adoption in multiple industries, ALD has many advantages over other vapour deposition techniques, the most important of which are fine thickness control and high conformity. Since the film thickness can be digitally controlled by the number of ALD cycles, it is reproducible down to angstrom levels [1]. In addition, the self-limiting nature of ALD means that the deposition rate is constant in every area of the substrate [46] as shown in figure 2.6. This allows for non-line-of-sight deposition and coating of high aspect ratio structures and has been demonstrated over spherical [47] and porous substrates [48–50, 50], deep trenches [51] and much more [52–54]with impressive results. These two advantages are the main interests for the present work. Other ones include, low roughness, intrinsic stress

and defect density and high uniformity [38] .

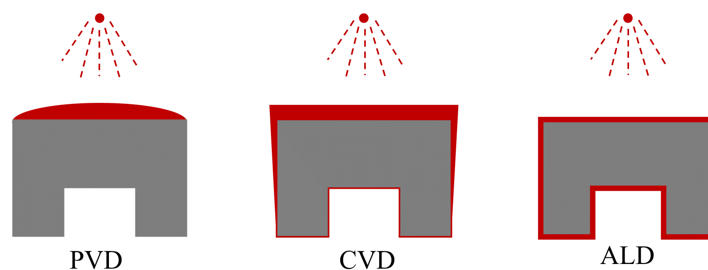

Figure 2.6 Comparing conformity in PVD, CVD and ALD. Adapted from [46].

ALD, however, has some important limitations. For one, throughput is very low, typically below 3 nm/min and often much slower. Consequently, the method is not viable for processing films thicker than a few tens of nanometres. In addition, ALD is mostly limited to the deposition of compounds due to the binary nature of the chemical reaction. This is especially limiting for optical applications where elemental metals are very important. Even among compounds, some important films cannot be fabricated by ALD because no suitable precursor chemistry has yet been found. Continual research on this topic is, however, constantly yielding new ALD-ready materials[1]. Contamination can also be a problem in ALD due to incorporation of reaction by-products, incomplete reactions and also because of the slow growth and relatively high processing pressures. Additionally, the temperature requirements of the process often prohibit deposition on polymers and devices with a strict thermal budget. The tight temperature window also can limit optimization possibilities especially for crystal structure. Some of these issues can be addressed by using PEALD.

2.1.2 Plasma enhanced atomic layer deposition

Theory

In thermal ALD, the substrate is exposed to two co-reactants. The first one, precursor A, is generally a metal precursor such as titanium chloride or trimethylaluminium (TMA) whereas the second one, precursor B, reacts with precursor A, typical examples are NH_3 and H_2O. In PEALD, introduction of the second reacting gas is replaced by a plasma exposure whose function is equivalent, mostly H_2, H_2/N_2 or O_2 plasmas [18]. Figure 2.7 compares the steps for both types of processes. Since only the second reactant is replaced, metal precursors used in ALD can often also be used for PEALD.

[1] An exhaustive database of ALD materials can be found at : `https://atomiclimits.com/alddatabase/`.

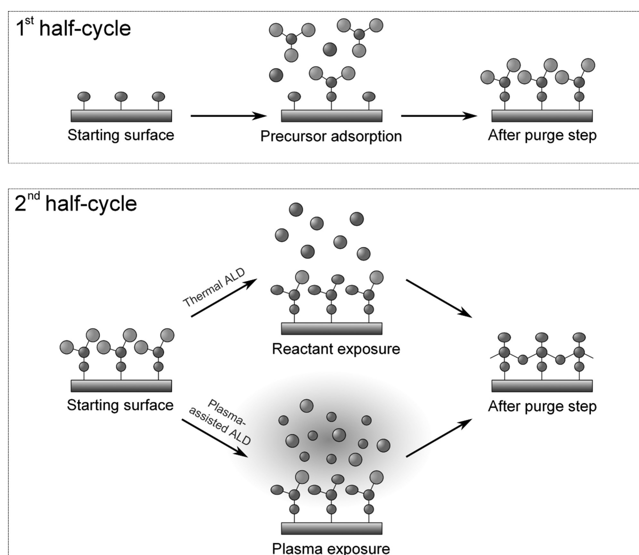

Figure 2.7 Comparing PEALD to thermal ALD. The second half-cycle is replaced by a plasma exposure. Reprinted with permission from [18].Copyright 2010, American Vacuum Society.

In their 2011 review of PEALD literature, Profijt et al. distinguish three main types of PEALD, as are shown in figure 2.8. In the first kind, presented in 2.8 (a), Microwave or RF plasma sources are fixed to an existing thermal ALD system. In these setups, the plasma is generally far away leading to fewer electrons and ions impinging on the sample surface. For this reason the method is referred to as radical enhanced atomic layer deposition (REALD). In the second kind, shown in 2.8 (b), the substrate is placed on a grounded electrode below the showerhead, a capacitively coupled plasma is then generated between it and a showerhead (variants of this setup exist that do not use a showerhead [38]), this is known as direct PEALD. In this type of PEALD, radical and ion fluxes on the substrate are very high, as such, care must be taken to avoid etching during the ALD process. Plasma damage from high energy photons can also be a problem with direct plasma ALD. This type of PEALD is common in industrial applications because of the simple design and scalability. Tailoring of material properties is, however, more challenging with these systems.

In the third type of PEALD (2.8 (c)), plasma generation takes place above the substrate. We call this remote PEALD. RF driven ICP sources are the most common for this type of PEALD, they consist of a conductor coiled around a dielectric tube in which the plasma is generated. The configuration differs from REALD in that the plasma reaches down to the substrate surface, thus more reactive species are involved in the reaction. Ion and electron densities are, however, much lower than in direct plasmas, which can help reduce etching and plasma damage. As such, the technique offers a good compromise between the two other

methods. In addition, plasma properties can be optimized independently from the substrate conditions, as the latter is not involved in plasma generation. This provides much more flexibility when optimizing deposition. It is in part for these reasons that remote plasmas are very popular in laboratory reactors and commercial R&D tools. However, the ICP sources involved in remote PEALD do not scale very well because they require high gas flows to prevent metallization of their dielectric tubes [28]. It has also been shown that the quartz often used in these tubes can cause oxygen contamination in processed films [55], with other materials such as sapphire and alumina also causing similar, but lesser, effects. As such, alternative plasma generation methods for PEALD are an emerging research topic.

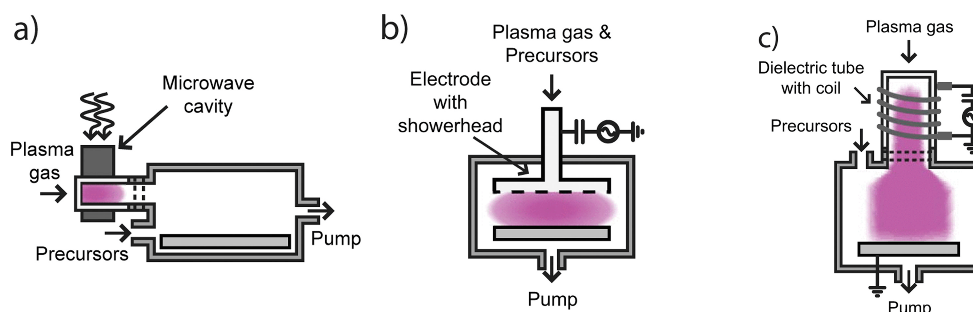

Figure 2.8 Three types of PEALD: (a) Radical enhanced ALD, (b) Direct PEALD and (c) Remote PEALD. Reprinted from [18].

Advantages and limitations over thermal atomic layer deposition

As previously mentioned, the use of plasma can remedy some of the shortcomings of ALD. First of all, it can significantly expand the ALD temperature window, making deposition possible at much lower temperatures [13, 18]. This is notably the case for TiN, that can be deposited at as low as 100 °C by PEALD [20] while no growth occurs below 300 °C [21] in the thermal process. This is an important benefit as it enables deposition on a variety of temperature sensitive substrates. Materials that normally inhibit the growth of certain chemistries can also be functionalized. For instance, H-terminated Si prevents growth from metal chloride ALD, but with PEALD, a thin layer of nitride or oxide is formed on the surface enabling deposition [20]. PEALD can also be used to obtain materials that can't be made by ALD, notably many elemental metal films [13]. In most cases, GPC is radically improved [18] because of the higher reactivity of the plasma [21], and due to diminished steric hindrance of the smaller metastables. This higher reactivity also leads to the processing of denser films with lower contamination [13] and better electrical properties [21] which is often the case for metal nitrides processed by PEALD. In addition, the greater number of

parameters involved [18], such as plasma characteristics (power, composition, pressure, flow, bias) and the increased temperature window, enable higher tunability of properties such as stoichiometry [18] and crystal structure [13] which in turn offers more control over electrical and optical properties.

While PEALD clearly has many benefits over thermal ALD, it does have some drawbacks. For one, conformality is typically greatly reduced [13] due to the line of sight effects of the plasma. This makes PEALD less suitable for applications that involve high aspect ratio structures. When it comes to metal nitride processing for optical quality films, PEALD still lags behind other deposition techniques in terms of film impurity content, stoichiometry and resistivity. The substrate temperatures required for PEALD are also often relatively high, especially when high film quality is required. This is notably the case for TiN which will be discussed in the following section.

2.1.3 Atomic layer deposition of titanium nitride

Comparing the thermal and plasma-enhanced processes

The deposition of TiN by ALD was pioneered by Hiltunen et al. in 1988 [16] alongside niobium, tantalum and molybdenum nitride. All three compounds were processed using a chloride-ammonia chemistry, which has now also been successfully used for aluminum [56], boron [57], silicon [58], gallium [59], rhenium [60]. Since then, TiN has become a very well-documented material in ALD literature. The material can be deposited by a variety of other chemistries, however, the chloride-ammonia chemistry is the most common and will be the sole focus of this section.

The reaction involved in the processing of TiN is presented in equation 2.1 along with the Gibbs free energy at 320 °C calculated by Elers et al. [21]. Equations 2.2 and 2.3, also from the same authors, present reactions involved in the plasma enhanced process. In the thermal reaction, $TiCl_4$ is used as a metal source and ammonia as a reducing agent and nitrogen source. In the plasma enhanced one, the ammonia exposure is replaced by an H_2/N_2 plasma. In many cases argon is also present in the plasma because it is used as an inert gas in viscous flow reactors.

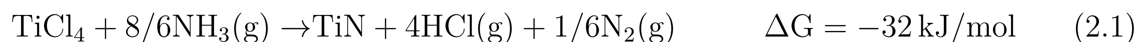

$$\mathrm{TiCl_4 + 8/6NH_3(g) \rightarrow TiN + 4HCl(g) + 1/6N_2(g)} \qquad \Delta\mathrm{G} = -32\,\mathrm{kJ/mol} \qquad (2.1)$$

$$\mathrm{TiCl_4 + N(g) + 4H(g) \rightarrow TiN + 4HCl(g)} \qquad \Delta\mathrm{G} = -1202\,\mathrm{kJ/mol} \qquad (2.2)$$

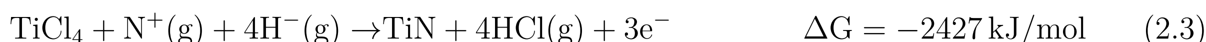

$$\mathrm{TiCl_4 + N^+(g) + 4H^-(g) \rightarrow TiN + 4HCl(g) + 3e^-} \qquad \Delta\mathrm{G} = -2427\,\mathrm{kJ/mol} \qquad (2.3)$$

As surmised, the use of plasma in this context yields much more favourable reactions. In fact, the authors compared thermal ALD and direct PEALD films and obtained a 100% increase in growth rate, and up to a 50% reduction of chlorine content with PEALD. They also found a substantial effect of plasma power and exposure times on chlorine concentration as presented in figure 2.9, presumably this would improve resistivity. In fact, the authors report resistivities below 200 µΩ cm and 150 µΩ cm for 30 nm films respectively processed by ALD at 400 °C and by PEALD at 320 °C.

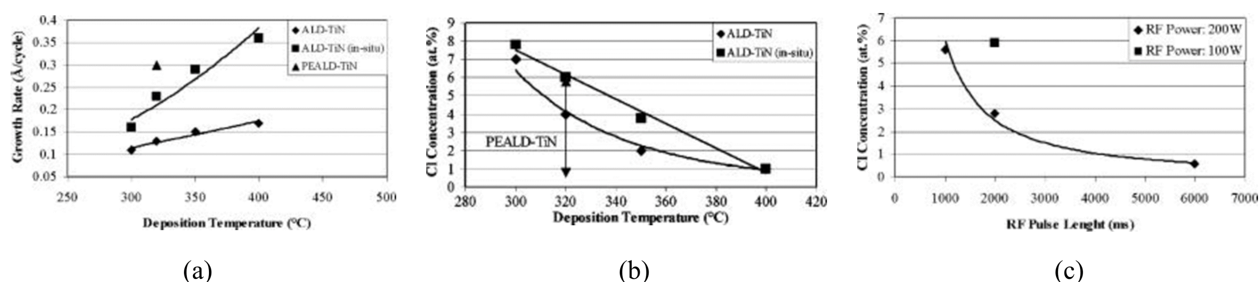

Figure 2.9 Key findings from Elers et al. when comparing TiN films obtained from ALD and PEALD. A third process (*in situ*) is also compared where metallic titanium is used as a catalyst for *in situ* reduction of the titanium chloride precursor. (a) Growth rate and (b) chlorine concentration at a given temperature are significantly improved when using PEALD as opposed to ALD. One can also significantly reduce chlorine concentration in PEALD with longer and higher power plasma exposures, as shown in (c). Reprinted with permission from [21]. Copyright 2005, Electrochemical Society.

In terms of the differences in resistivity and growth rate, the advantages of PEALD become overwhelming at lower temperatures. In the thermal process, growth occurs at rates from 0.11 0.17 Å/cycle between 300 and 500 °C (the ALD-temperature window) whereas GPC in PEALD varies from close to 0.6 Å/cycle at 400 °C to 0.3 Å/cycle at 100 °C [20]. As such, using plasma expands the ALD window down to much lower temperatures and triples the GPC when both processes are possible. In addition, resistivity is presented in figure 2.10 as a function of temperature both for a PEALD process [20] and a thermal one [61]. Resistivity typically decreases at higher temperatures as the more favourable reactions lead to films with higher density and lower impurity count [13].

One can see that a reasonably low resistivity is maintained even at lower temperatures in figure 2.10a. Moreover, PEALD films keep below 150 µΩ · cm between 300 °C and 400 °C whereas thermal films have resistivities up to almost 300 µΩ · cm at 350 °C. This difference is especially impressive when considering that the films from figure 2.10 (a) are between 23 nm

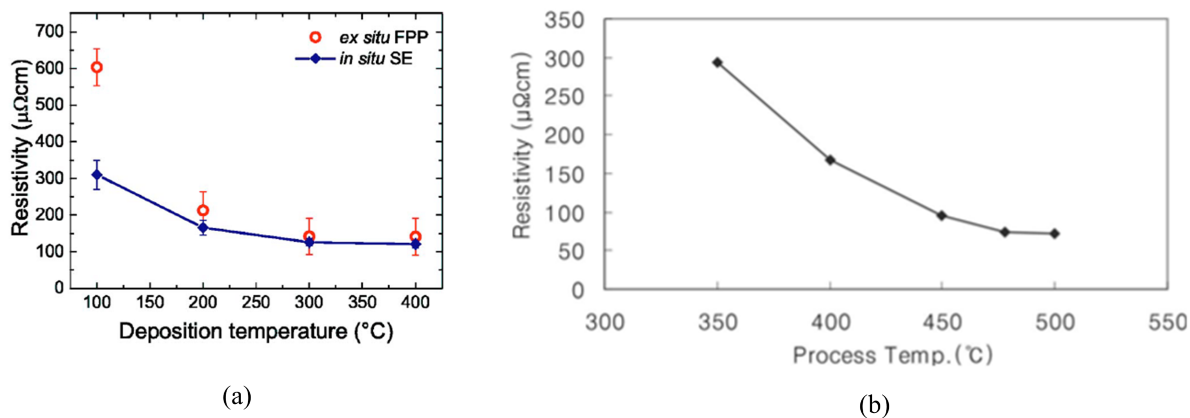

Figure 2.10 Comparing resistivity as a function of temperature for TiN films processed by PEALD and ALD. (a) TiN films deposited on thermally growth SiO_2 using 350 to 400 cycles of PEALD [20]. (b) 32 nm films of TiN deposited by ALD on Si. (a) Reprinted from [20], with the permission of AIP publishing. (b) Reprinted from [61] with permission from Springer.

and 10 nm while the films from 2.10b are all 32 nm thick. Indeed, for such ultra-thin films, the thickness has a large influence on the resistivity. This effect was measured by ellipsometry by Langereis et al. [20], their results are presented in figure 2.11. As a consequence, the impact of thickness on resistivity below 10 nm is very significant. Thus, it should always be taken into account when comparing resistivity.

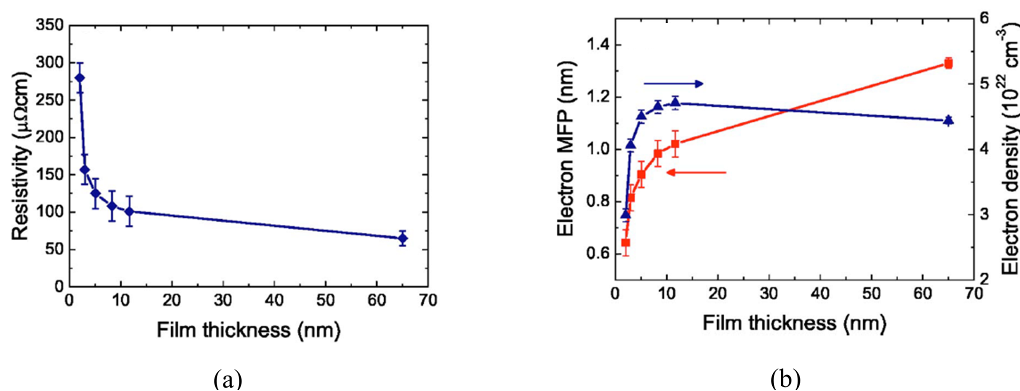

Figure 2.11 Resistivity (a) as well as (b) Electron mean free path (MFP) and density as a function of thickness for TiN films deposited by PEALD. Reprinted from [20], with the permission of AIP publishing.

These examples highlight the main advantages of PEALD for processing TiN from $TiCl_4$, mainly higher growth rates, lower resistivity and contamination and a larger temperature window. Adding to these advantages, the ability to tune stoichiometry has been reported [21],

as well as a sharp decrease in nucleation delay [20].

2.1.4 Uses of hollow cathode plasma in PEALD

The hollow cathode effect

A hollow cathode discharge occurs when two opposing cathodes are placed at a short distance, d, from one another at a given pressure, p, and voltage such that $d \cdot p = 1 - 13$ Pa·m ($1 - 10$ Torr·cm) depending on the gases used [62, 63]. While this effect can be achieved between two plates, cylindrical cavities are also often used, as is the case in this work, and previous work at FCSEL [64]. In this type of discharge, sequential reflection of electrons off the sheaths of the opposing cathodes, called the electron pendulum effect, promotes high plasma densities (over 10^{10}cm^{-3}) and high plasma currents, often orders of magnitude above what is normally achieved using a capacitively coupled system [62]. These high densities can enhance surface reactions in the PEALD process when compared to lower density discharges [28]. When operated under radio frequency (RF), the imbalance in responsiveness of ions and electrons to the changing electric field leads to the formation of a virtual anode [63] whereby the plasma acts as the anode of the system. Consequently, most high energy species are accelerated perpendicularly to the cathode surface and do not exit the hollow cathode toward the substrate [62]. In addition, because current is very low in HCPs, voltage is lower for a given power leading to less energetic ions than would otherwise be expected. These two properties are ideal for PEALD as they minimize etching and plasma damage.

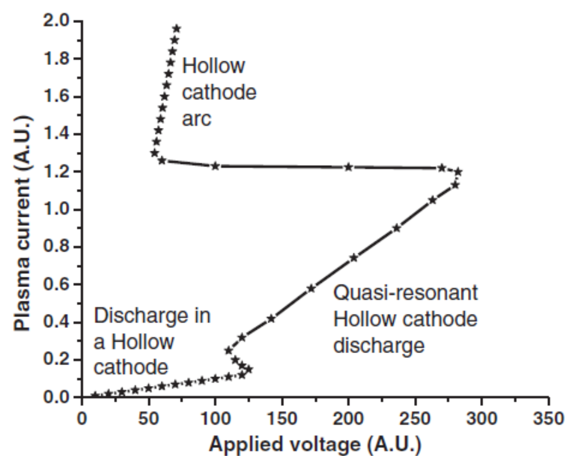

Figure 2.12 Typical I-V curve of a hollow cathode system exhibiting three regimes. Reprinted from [62], with permission from Elsevier.

As mentioned above, the hollow cathode effect only takes place for certain pressure, distance

and voltage values. When the pressure or voltage is too low, or when the distance is too large, a normal capacitively coupled discharge occurs, called *discharge in a hollow cathode* by Muhl and Perez, this is shown in figure 2.12 which presents I-V characteristics for a typical HCP along with three different regimes. Current and density for this regime are lower than what can be obtained in the quasi-resonant hollow cathode discharge regime. Conversely, when the applied power is too large or if the cathode is allowed to heat, the discharge develops into a hollow cathode arc. Optimal operation is done in the quasi-resonant hollow cathode discharge regime [28], as the highest densities and currents are achieved without the negative effects of the arc regime which include cathode sputtering.

Advantages of hollow cathode PEALD

When used in PEALD, the higher density of hollow cathode discharges together with the lower ion energies and the lower probability of ions impinging on the surface could improve growth rates by enhancing reactivity and reducing etching as compared to the ICPs mentioned above. The enhanced reactivity could also lead to lower levels of contamination such as chlorine and carbon and higher film mass densities by promoting more complete surface reactions even at much lower plasma powers. Oxygen contamination could also be lower in hollow cathode systems then in inductively coupled ones because they do not require dielectric components to be in contact with the plasma. For metal nitrides, this would in turn enhance crystal quality and electrical properties, as oxygen tends to segregate in grain boundaries, promote amorphous growth and decrease electron mean free path [14].

In their pioneering work on hollow cathode PEALD (HC-PEALD), Ozgit-Akgun et al. processed aluminum nitride (AlN) and gallium nitride (GaN) in a Fiji F200-LL reactor modified to accommodate a Meaglow Ltd. hollow cathode source [29]. They saw an important decrease in oxygen and carbon contamination in their films when compared to ones they had previously processed in similar conditions by inductively coupled PEALD (IC-PEALD). They also noticed increases in density and growth rate for AlN processed with the HCP source. Similar observations were made subsequently by other authors for both films [31, 65], these works are compiled in table 2.1 alongside several examples of said films deposited using ICP at similar temperatures and with identical precursors. Processing of good quality indium nitride films was also reported by HC-PEALD [31].

As surmised from table 2.1, AlN GPCs increase by 0.3-0.5 Å/cycle when using an HCP while density increases in GaN by close to $1\,\mathrm{cm}^{-3}$. Bulk carbon content also significantly diminished for HCP films. When it comes to oxygen contamination, improvements are harder to demonstrate because there is substantial variation among films for both types of processes.

Table 2.1 Comparing the quality of published nitride films obtained by HC-PEALD and IC-PEALD.

Mater.	Plasma Type	GPC [Å/cycle]	Density [cm^{-3}]	Contaminations in bulk [at.%]	Temp. [°C]	Precursors	Ref.
AlN	HCP	0.99-1.02	2.82	O <1, C: <1	200	$AlMe_3$ / NH_3	[29]
AlN	HCP	1.11	3.20	O: 5, C: <1	200	$AlMe_3$ / NH_3	[65]
AlN	ICP	0.7	–	O: 35, C: 30	200	$AlMe_3$ / NH_3	[66]
AlN	ICP	0.65	3.07	O: 9.1, C: 3.4	250	$AlMe_3$ / N_2-H_2	[67]
AlN	ICP	0.66	2.49	O: 1.5, C: 3.9	190	$AlMe_3$ / NH_3	[30]
GaN	HCP	0.23-0.26	5.86	O: <1, C: <1	200	$GaMe_3$ / NH_3	[29]
GaN	HCP	0.31 - 0.32	–	O: 3.2	200	$GaMe_3$ / NH_3	[31]
GaN	HCP	0.34 - 0.37	–	O: 3.9	200	$GaEt_3$ / NH_3	[31]
GaN	ICP	0.25	–	O: 13, C: <1	200	$GaEt_3$ / N_2-H_2	[68]
GaN	ICP	0.31	4.64	O: 21.5	185	$GaMe_3$ / NH_3	[30]
GaN	ICP	0.22	4.91	O: 4.7, C: 4.2	200	$GaMe_3$/ N_2-H_2	[30]

Indeed, while an HCP source can help decrease oxygen content, it cannot compensate for other sources of contamination such as system leak rates, insufficient pumping and precursor and purge gas purity. An improvement is seen. however, when comparing the films of Ozgit-Akgun et al. [29, 30] processed in the same system with identical conditions aside from the plasma type. Indeed, they saw a drop in oxygen content from 4.7 at. % and 1.5 at.% to below a detection limit of 1 at.% in their GaN and AlN films respectively. When comparing GPCs in the gallium nitride films, oxygen contamination must be considered, because oxygen content significantly increases GPC due to the high 0.5 Å/cycle [69] growth rate of Ga_2O_3 . This effect is seen in the table as films with higher oxidation have higher GPCs. With this in mind, one can notice that GPC increases by close to 50% in GaN films of similar oxygen content. As such, emerging research in HC-PEALD does indeed show improved growth rates, contamination and density. However most of the work has been done on metal-organic chemistries, these advantages have yet to be demonstrated in films processed with the metal chloride chemistry presented above for TiN.

On a further note, HCPs are also advantageous for industrial applications as compared to ICPs while retaining a higher flexibility than capacitively coupled direct plasmas. Indeed, their all-metal construction makes them more scalable as metallization of the cathode surface does not affect its operation, comparatively to metallization of dielectric quartz tubes in ICPs (i.e. increasing size does not require scaling of gas flows). Additionally, if very high purity is required HCP sources can be made of metals such as titanium or molybdenum for better process compatibility [28].

2.2 Optical properties of TiN

The dielectric constant of TiN can be modelled [19] using a Drude term with two additional Lorentz oscillators, as described in equation 2.4. It is often referred to using ϵ_1 and ϵ_2, respectively the real and imaginary parts of the dielectric constant.

$$\epsilon(\omega) = \epsilon_{\infty} - \frac{\omega_{pu}^2}{\omega^2 - i\Gamma_D\omega} + \sum_{j=1}^{2} \frac{f_j\omega_{0j}^2}{\omega_{0j}^2 - \omega_i^2\gamma_j\omega} = \epsilon_1 + i\epsilon_2 \tag{2.4}$$

The first term, σ_{∞} corresponds to contributions in the dielectric function that are out of the experimental range. The second term is the Drude oscillator, characterized by the unscreened plasma energy $E_{pu} = \hbar\omega_{pu}$ which relates to carrier density, resistivity and electron MFP. This term has increasing influence as wavelengths approach the infrared (IR) and is used to quantify the metallic character of the material. When optical measurements are unavailable, resistivity measurements such as by 4-point probe can be used to estimate the Drude term and to compare the metallic character of films. The third term is a sum of two Lorentz oscillators, typically centred around 3.5 eV and 5.2 eV in the ultra-violet (UV). These terms simulate the contributions of interband transitions. Figure 2.13 presents the optical properties of TiN

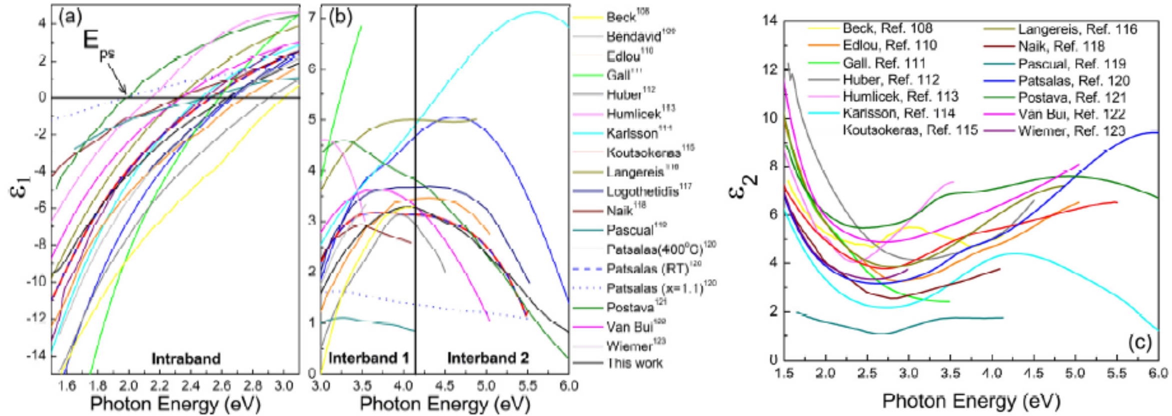

Figure 2.13 Experimentally determined dielectric constants of TiN in literature as compiled by Patsalas et al. Reprinted from [19].

as compiled by Patsalas et al. [19]. Films obtained by ALD (Langereis et al. and Van Bui et al.) find themselves in the middle of these lines. As notes, there is significant variability in the properties of TiN; this is because the material's optical constants are very sensitive to stoichiometry (N/Ti ratio), oxidation, chlorine contamination, grain size and density as these affect electron mean free path and electron density.

E_{ps} in figure 2.13a can be defined as the energy value at which ϵ_1 is null, it is referred to as the screened plasma energy. Its value is of great importance for plasmonic applications of TiN. As observed, E_{ps} varies significantly from one TiN film to another. In fact, it has been found by Kang et al. [25] to be a good predictor of stoichiometry in sputtered TiN films (see figure 2.14). A similar observation was later made by Langereis et al. pertaining to ALD films [20]. As seen in figure 2.14a E_{ps} is 2.65 eV when the nitride composition (Ni/Ti ratio) is 1. Logothetidis et al. [70] linked this value of unscreened plasma energy to the golden colour of TiN indicating the lower values of E_{ps} yielded a brownish-coloured film.

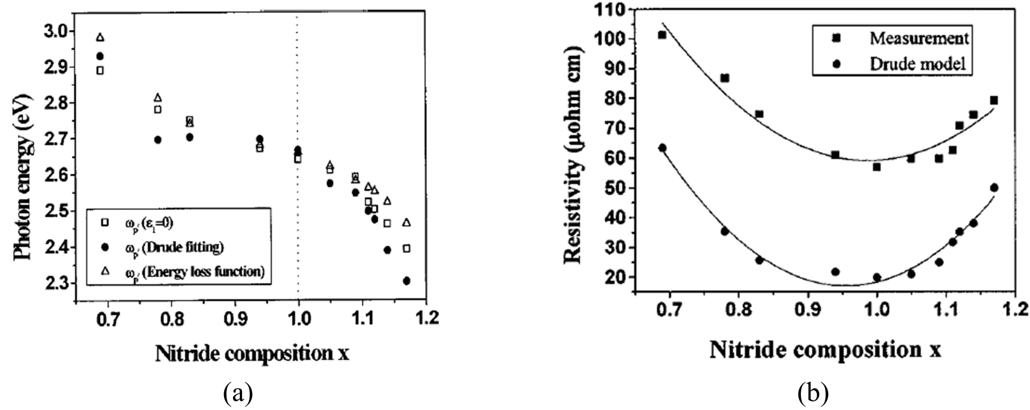

Figure 2.14 (a) E_{ps} and (b) resistivity as a function of N/Ti ratio in TiN. Reprinted from [25], with the permission of AIP Publishing.

In figure 2.14 (b) we also notice that resistivity is at its minimum for the same value of E_{ps} at which the TiN is stoichiometric. This is not only the case when studying stoichiometry in the films as determined by Patsalas et al. in their review. Indeed, E_{ps} stabilizes around 2.7 eV for higher value of unscreened plasma energy (E_{pu}) found in literature. Since resistivity is an inverse function of E_{pu}, the same argument can be made for lower values of resistivity. As such, resistivity is a good measure not only of the metallic character of the TiN films, but also of their colour, and plasmonic properties. It has also been linked to chlorine [21] and oxygen contaminations [71] in these films as well as crystallite size, making it the most important metric for comparing or optimizing the quality of TiN films.

For comparison, lowest resistivity of TiN films deposited using various techniques by multiple authors is compiled from literature in table 2.2. It can be seen there that PEALD typically results in TiN of higher quality than thermal ALD, low pressure chemical vapour deposition (LPCVD) and ion beam assisted deposition (IBAD). However magnetron sputtering can yield significantly better films at comparable thicknesses. Pulsed laser deposition (PLD) also yields similar quality film at much lower deposition temperatures. As such, improving

PEALD of TiN is critical for its adoption in optical film processing.

Table 2.2 Resistivity of TiN films found in literature for common types of thin film deposition techniques along with films thickness and resistivity measurement method. In articles with more than one sample, the film with lowest resistivity is chosen.

Deposition technique	Thickness [nm]	Resistivity [μΩ cm]	Measurement technique	Temp. [°C]	Reference
ALD	17	300	FPP	500	Cheng et al. [27]
ALD	32	83-87	FPP	500	Ahn et al. [61]
ALD	45	<200	FPP	400	Elers et al. [21]
PEALD	45	<150	FPP	320	Elers et al. [21]
PEALD	–	80	FPP	350	Kwon et al. [72]
PEALD	23	142	VASE	400	Langereis et al. [20]
PEALD	65.5	71	VASE	400	Heil et al. [73]
LPCVD	135	200	–	630	Mei et al. [74]
Magnet. Sput.	300-400	25	VASE	300	Kang et al. [25]
Magnet. Sput.	30	39	VASE	300	Naik et al [75]
IBAD	>300	133	SE	–	Humlicek et al. [76]
PLD	>100	116	VASE	20	Patsalas et al. [19]

2.3 Angular selective thin films

In the context of this work, we define angular selectivity (AS) as a difference in transmission between a given positive and negative angle of incidence. For instance, a film with high transmission at an incidence of 60° and low transmission at −60° exhibits AS. We will also refer to this property as anisotropic transmission throughout the text. The said property can have beneficial impacts in energy, optoelectronics, biomedical and other optical applications. In this work we focus mostly on AS in the visible spectrum, and AS as it is perceived by the human eye with intended applications in ophthalmics and architectural glass. AS can be used in ophthalmic lenses to focus the wearer's attention to certain areas of their field of view or to attenuate parasitic light sources coming from specific angles, for instance during night or day driving. It can also be used in architecture to maintaining clear visibility of the outdoor while avoiding excessive incident sunlight or to tune solar transmittance based on the sun's position in the sky. For example, to control lighting from dawn to sundown or to optimize passive heating for winter and summer.

In this work, two metrics are discussed for AS, namely relative AS, S, and absolute AS, ΔT, as seen in equation 2.5 and 2.6 respectively where $T(\lambda, +\theta)$ refers to transmission at a specific wavelength λ and incidence angle θ. Each metric is useful for different considerations such as

the signal-to-noise ratio or perceived transmission differences. Relative AS is used by Mbise et al. [33], and in other papers published by Claes-Göran Granqvist's research group, as such it is often used for comparisons with literature.

$$S(\lambda, \theta) = \frac{T(\lambda, +\theta)}{T(\lambda, -\theta)} \tag{2.5}$$

$$\Delta T(\lambda, \theta) = T(\lambda, +\theta) - T(\lambda, -\theta) \tag{2.6}$$

This type of AS can be obtained by using SCTFs, which will be the topic of the following sections.

2.3.1 Glancing angle deposition of SCTFs

Slanted columnar thin films are made using a technique called GLAD in which nanocolumn films are deposited by exploiting ballistic shadowing during physical vapor deposition [35]. In order to obtain this effect, the sample surface must be placed at a high angle respective to the incident material flux, called the glancing angle. The process by which columns are formed is shown in figure 2.15.

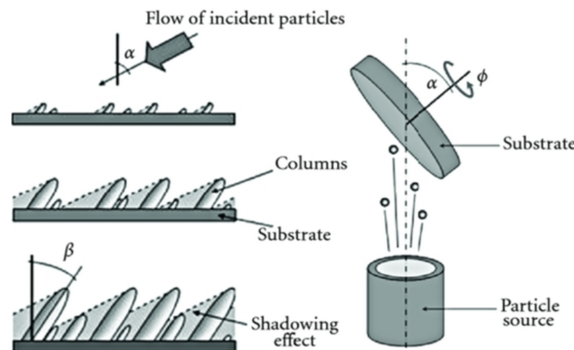

Figure 2.15 Column growth mechanism in GLAD and sample placement respective to the material source. Reprinted from [77].

Assuming conditions promote Volmer-Weber Growth [35], 3D islands form on the substrate during the initial phase of deposition. Because of the high angle, growth then continues preferentially on one side of the island while the other side is shielded from the incident material flux. Nanocolumns grow on the sample as a result of this shadowing. The angle of the columns, β, is proportional to the glancing angle used, α. The relation between the α and β,is often approximated by the tangent rule [35] shown in equation 2.7.

$$\tan(\alpha) = 2\tan(\beta) \tag{2.7}$$

An SiO_2 SCTF is presented in figure 2.16 showing distinct columns with a constant inclination throughout the film. Such films can be used to obtain angle dependent properties.

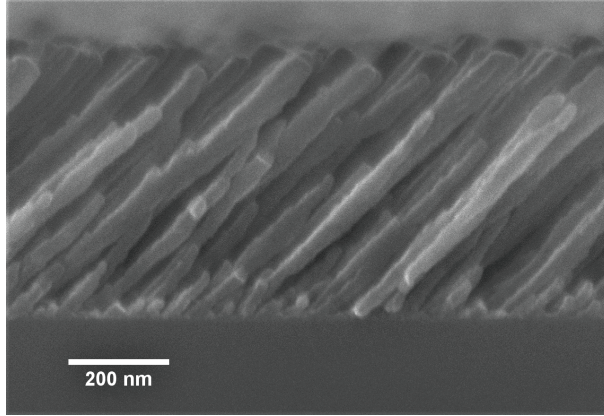

Figure 2.16 Scanning electron micrograph of a SiO_2 SCTFs made by GLAD.

Effective ballistic shadowing is essential to obtain such highly columnar structures. Consequently, ideal deposition conditions include a high mean free path of incident material and homogeneous and parallel incoming material flux. In order to meet the first requirement, ultra high vacuum (UHV) is required. The use of plasma such as in reactive evaporation or sputtering also significantly reduce the mean free path and SCTF quality. For the second condition, a large distance between the sample and the material source is required (throw distance) [35]. For all these reasons, non-reactive e-beam and thermal evaporation is typically the best choice for GLAD.

Aside from the columnar structure, these films have highly tunable porosity which is geometrically related to the glancing angle, α, as shown in equation 2.8, where ρ_{bulk} is bulk density and ρ_{SCTF} is films density

$$\rho_{\text{SCTF}} = \frac{2\cos(\alpha)}{1+\cos(\alpha)}\rho_{\text{bulk}} \tag{2.8}$$

Previous works at FCSEL investigated this property as a way of making ultra-low index materials [78]. In the present thesis, we concentrate on the AS of SCTFs.

2.3.2 Angular selectivity of SCTFs

When SCTFs are made of an absorbing material such as chromium, they have angular selective properties for p-polarized light. This is caused by the particular geometry of the structure leading to anisotropic absorption [33] as shown in figure 2.17. This can be understood by examining the extreme cases: when p-polarized light is incident perpendicular to the column (at a negative angle of θ) it interacts with the long section of the absorbing columns whereas when it is parallel to them (positive angle of θ) it interacts with the small axis of the columns. As shown in 2.17, this is only the case for p-polarization as s-polarization is not affected in this way.

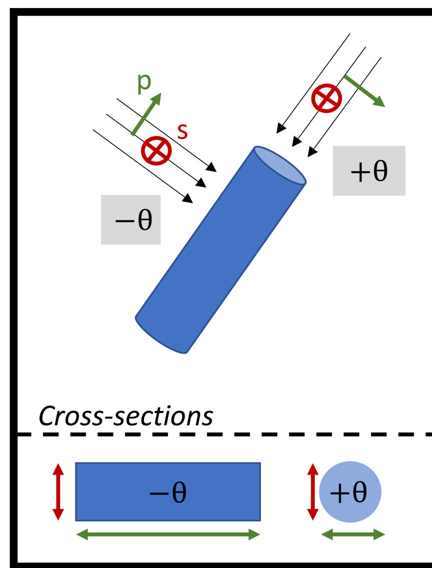

Figure 2.17 Understanding the cause of anisotropic absorption in SCTFs and how it relates to the geometry of the columns.

The spectra of such AS films are represented in figure 2.18 (a) for evaporated Cr SCTFs. A large difference in transmission of p-polarized light is seen between $\theta = +55°$ and $\theta = -55°$ whereas none is found for s-polarized light. For assessing the AS perceived by the human eye, it is useful to study luminous transmittance as a function of incidence angle, this is plotted in figure 2.18b for one of the most AS films found in literature. While s-polarized light is unaffected by the slanted columnar structure, the effect on p-polarized light is great enough to provide noticeable AS behaviour even with unpolarized light.

In their 1997 paper, Mbise et al. [33] developed an efficient representation for comparing multiple AS films. It is shown in figure 2.19 where relative AS at 60° is plotted as a function

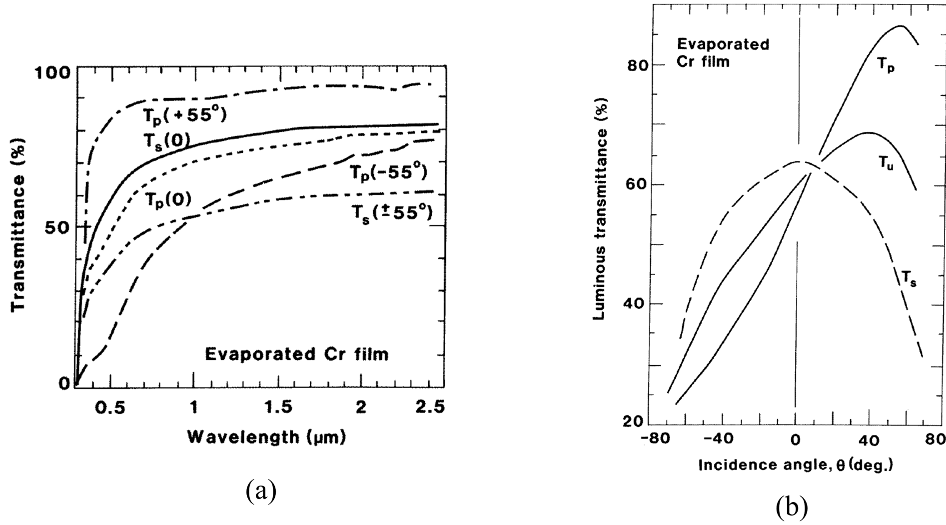

Figure 2.18 Angular selective properties of evaporated chromium SCTFs. (a) Transmittance for positive and negative angle incidences and *s*- and *p*-polarizations. (b) Luminous transmittance as a function of incidence angle. Each figure corresponds to a different film. Reprinted from [33] with the permission of IOP publishing.

of transmission at 60°. In most use-cases, optimal films should have high transmission at positive angles and high AS. As such, films trending towards the upper right corner of the figure are seen as better performing. One can see from figure 2.19 that sputtered SCTFs generally have poorer performance than evaporated ones and that the best films are made of evaporated chromium.

In an effort to better understand what affects the performance of these films J. Gagnon [15] made analytical simulations based on Bruggeman modelling of SCTFs his results are presented in figure 2.20. The porosity and thickness of the simulated films were varied and plotted in a representation similar to figure 2.19. Films with porosity between 70% and 80% exhibit the highest selectivity for a given thickness. Additionally, increasing thickness increases selectivity while reducing positive angle transmission. According to these simulations, it would seem that very thick films above 1000 nm with porosity above 85% would yield maximum performance. Some limitations of this simulation approach should, however, be taken into account.

First of all, the aspect ratio of the columns is maintained constant in these simulations meaning that the thicker films also have significantly wider columns. If one were to deposit SCTFs by GLAD, increasing film thickness would not affect column dimensions in the same way. Additionally, SCTFs thicker or even approaching 1000 nm tend to have a less well-defined

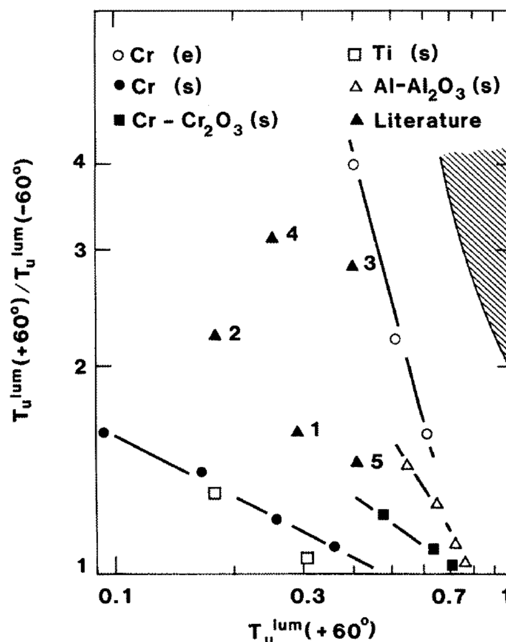

Figure 2.19 Relative unpolarised luminous angular selectivity at 60° as a function of unpolarised luminous transmission at 60° for films found in literature. Films noted (s) and (e) are respectively sputtered and evaporated. Reprinted from [33] with the permission of IOP publishing.

columnar structure because of broadening and extinction of the columns as a function of thickness [35]. Finally, the analytical anisotropic Bruggeman modelling used to approximate the columns cannot fully reproduce their geometry [50]. Indeed, while the simulations give a good general picture of how to optimize GLAD for certain desired optical properties, they cannot be used to predict them for a given process. This is well demonstrated by the difference between the modelled and measured AS presented in figure 2.20. In addition to the limitations of such simulation approaches, even predicting the columnar structure of SCTFs from given GLAD process parameters can be very challenging, this will be discussed in the following section.

2.3.3 Challenges in the fabrication of SCTFs

As was mentioned, optimizing and predicting the structural characteristics, and thus the optical properties, of GLAD-deposited SCTFs from deposition conditions is very challenging. Mainly, column angle, density and column shape each have a high dependence on substrate temperature, glancing angle, thickness and deposited material.

For instance, density is most often manipulated by changing the glancing angle, as was shown

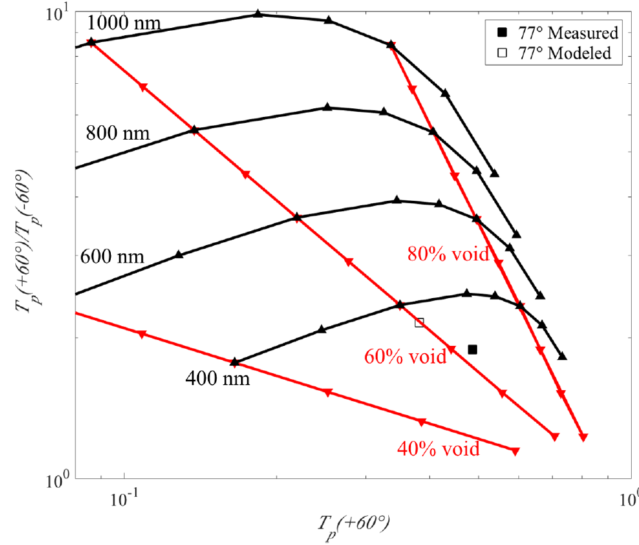

Figure 2.20 Relative p-polarized luminous angular selectivity at 60° as a function of p-polarized luminous transmission at 60°. Films are simulated from an anisotropic bruggeman effective medium approximation of WO_3 and void. Reprinted from [15].

in equation 2.8. This method would be used, for instance, to vary film porosity in figure 2.20 as a method of tuning AS. However, the glancing angle also directly affects the column angle, as seen in equation 2.7. This angle in turn affects AS by shifting the angular position of the transmission peak [33]. As a result, tuning AS through porosity is very difficult, especially if specific angular spectra are required. Some authors have proposed the use of textured seed layers to control the porosity of GLAD films [79] independently from columns angle. While such techniques are often successful, they add a complex and time consuming pattering step to the fabrication of devices, which makes their use less favourable for high throughput industrial applications. Changing SCTF thickness could be another way of tuning AS, as suggested in figure 2.20. However similar challenges appear. While studying density as a function of thickness, Asgharizadeh et al. [37] showed that SiO_2 coatings deposited at a glancing angle of 60° had a porosity of 40% at 18 nm while it dropped below 15% for films thicker than 100 nm. Evidently, if increasing thickness decreases porosity, then thickness cannot be used to independently tune AS.

The same authors also demonstrated that thickness and glancing angle affect the density profile of the columnar films as seen in figure 2.21. This could lead to further complications as changing either parameter would affect the reflectivity of the STCFs, and the shape of the columns which in turn would affect the transmission selectivity.

Furthermore, the relation between the glancing angle and porosity is dependent on the ma-

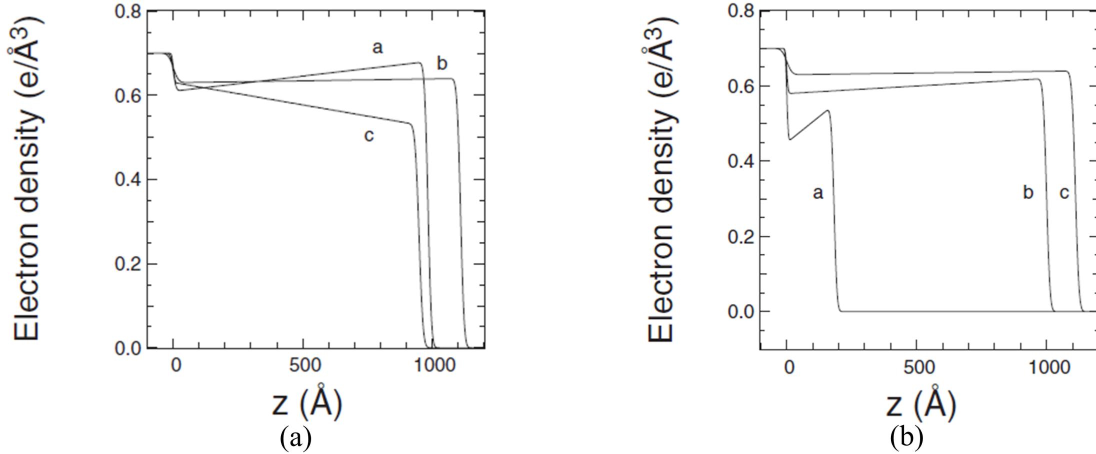

Figure 2.21 Density profiles determined by XRR as a function of (a) glancing angles of a: 40°, b: 60° and c: 70°; and (b) thicknesses of a: 18 nm. b: 100 nm and c: 110 nm. Reprinted with permission from [37] Copyright 2009 by the American Physical Society.

terial [80] as seen in figure 2.22 (a) where one can notice that identical angles do not yield identical density for different films, and even that trends can be very different from one material to the other. Similarly, in figure 2.22 (b), the relationship between column angle and glancing angle is heavily dependent on the film material and deposition temperature [36]. As a result, optimization of AS has to be redone for every new material. This is an important limitation as material interchangeability would otherwise enable easy tuning of AS to different spectral regions. In addition, since non-reactive evaporation yields the best AS films, the material selection from which SCTFs can be made is limited to materials that can be evaporated. For the reasons mentioned here, glancing angle deposition is too complex for most industrial applications because no general methodology can be developed to produce SCTFs of different nanostructures and materials [34] .

2.4 Core-shell SCTFs

Recent developments in the field of GLAD may provide a solution to the aforementioned limitations. It was found on multiple occasions that applying a thin conformal layer of a given material by ALD over an SCTF enables one to decouple a device's morphology and its material properties [81]. We will call these types of films core-shell SCTFs. In some cases, the shell layer is used to modify the surface chemistry of an SCTF. Using this method, applications relying on surface contact can benefit from the high surface area of SCTFs without the need to deposit the material implicated in the surface reaction by GLAD. This was done for ultrathin layer chromatography [49], nanorod based schottky photodiodes [82],

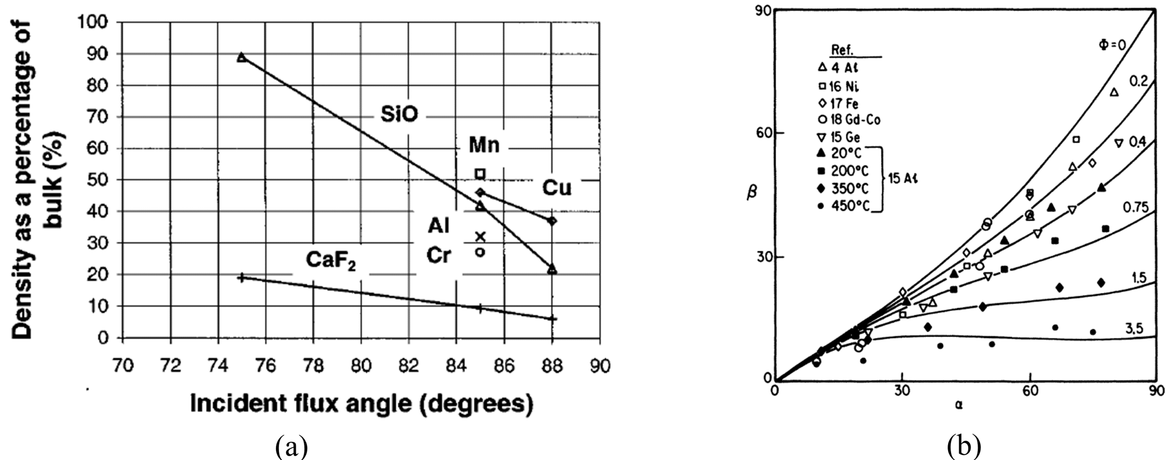

Figure 2.22 Density (a) and column angle, β, (b) as a function of glancing angle, α for different materials. (a) Reprinted with permission from [80]. Copyright 1997, American Vacuum Society. (b) Reprinted with permission from [36]. Copyright 1986 by the American Physical Society.

photocalalysis [81] and solid oxide fuel cells [10].

This same idea can be applied to create structures with angle dependent material properties. In one case, Fe_2O_3 was deposited over Si SCTFs to produce highly anisotropic magnetic films [83]. In the second part of this work, we will focus on the production and tuning of films exhibiting anisotropic transmission using a similar method.

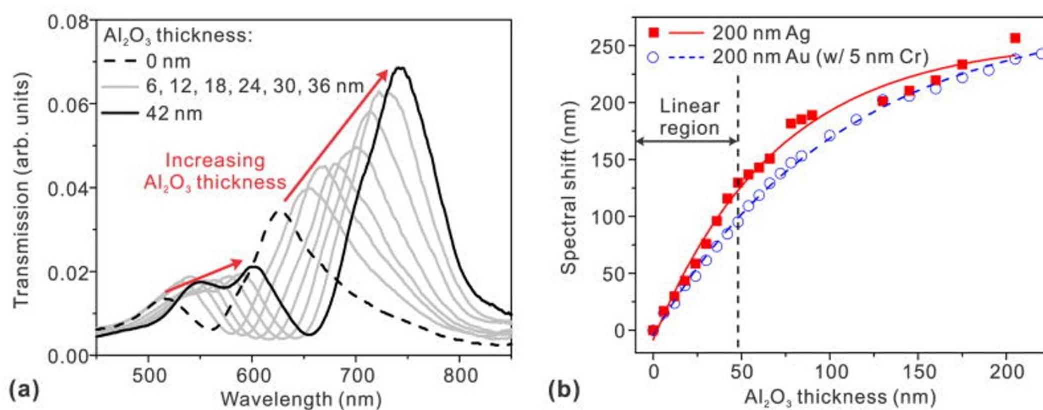

Figure 2.23 Tuning (a) transmission and (b) spectral shift in a nanohole-based SPR sensor as a function of the thickness of an ALD alumina overcoat. Reprinted with permission from [84]. Copyright 2010, American Chemical Society.

2.5 Tuning optical properties with ALD

ALD is also useful for deposition over many other types of nanostructures thanks to its high conformity. When doing so in optical metamaterials, one can achieve precise digital tuning of properties thanks to the fine thickness control of the deposition technique. For instance, Im et al. [84] showed they could tune the transmission and spectral shift of nanohole-based SPR sensors by fine-tuning of the effective ambient index using thin conformal layers of ALD made Al_2O_3, as shown in figure 2.23.

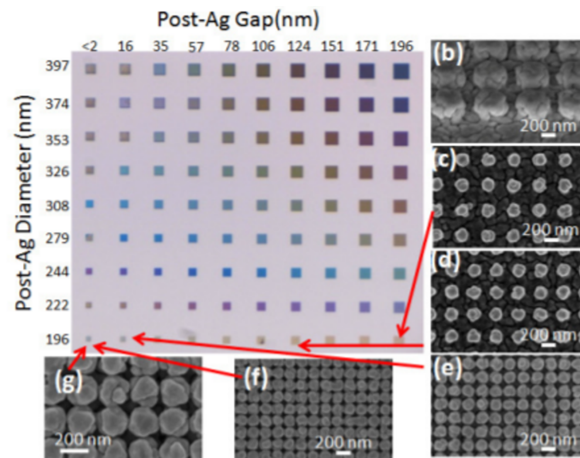

Figure 2.24 Optical reflection of Ag coated Si nanopillar arrays with varying diameter and interparticle gap. Reprinted from [11].

Similar tuning of optical properties was also achieved in: nanoporous gold using ALD of titania [7] and silver coated nanosphere arrays using Al_2O_3 [8]. Photonic band tuning was also demonstrated in silicon photonic crystals using ALD of titania [9] and hafnia [10]. As noted, most uses of ALD involve dielectric oxides as they are the most common ALD processes, but some research has also been done on the use of metals as shown in figure 2.24 where overcoating silicon nanopillars with silver by PEALD enables the creation of reproducible plasmonic nanopillar arrays and fine-tuning of interparticle gap. [11]. In the present work, AS selectivity will be tuned by varying the thickness of an absorbing TiN overcoat in SiO_2 SCTFs.

CHAPTER 3 METHODOLOGY

The following chapter details the methods used both for fabrication and analysis of our films. When optimizing ALD and PEALD processes, sample batches were made while varying deposition conditions such as temperature, exposure times and plasma characteristics. In each batch, three substrates were used: doped and high resistivity silicon as well as Si with 1 µm thick thermal oxide. The specific substrates were each geared towards certain characterization tools as will be discussed.

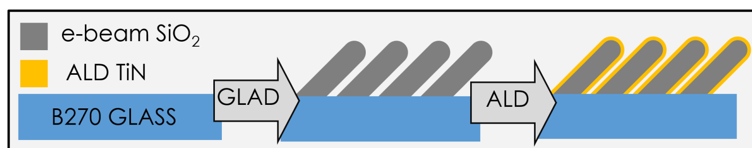

Figure 3.1 Making core-shell SCTFs through successive GLAD and ALD.

For the core-shell SCTFs, the columnar films were made by SiO_2 GLAD and subsequently covered by atomic layer deposition of TiN as shown in figure 3.1. These samples were made on glass and doped silicon substrates. Further details can be found in chapter 5.2.

3.1 Atomic layer deposition

3.1.1 Experimental setup

Sample depositions by ALD and PEALD were made in the *Kurt J. Lesker Co. ALD-150LX* system presented in figure 3.2 (a). The tool allows the simultaneous use of up to 4 chemical precursors in 4 sources like the ones in either edge of figure 3.2 (b), two of which can be used in a bubbler configuration for chemicals with insufficient vapour pressure. Each source supports rapid pulsing of the gaseous co-reactants using high-speed and low-leak ALD valves, the gases are then uniformly distributed over the substrate by a single common circular showerhead. An ICP source is fixed atop the chamber to enable PEALD in the *ALD-150LX*'s typical configuration. Our particular tool was customized to accommodate a *Meaglow Ltd.* hollow cathode plasma source, which is shaded in blue in figure 3.2 (b), instead of an ICP. Ellipsometry viewports are also integrated into the system for *in situ* real time monitoring during growth.

A more detailed schematic of the chamber is shown in figure 3.3. In this system, every part in contact with the reactants is heated to temperatures above 120 °C to prevent any

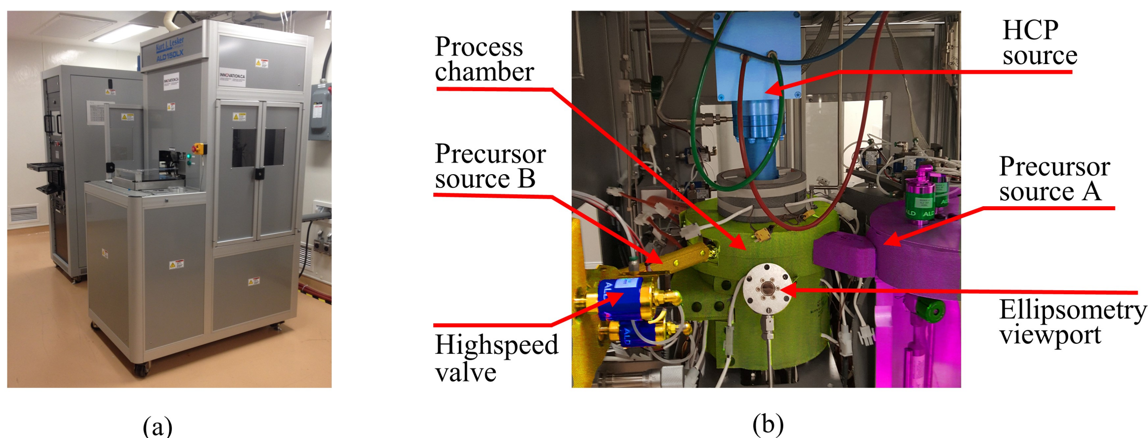

Figure 3.2 (a) The *Kurt J. Lesker Co. ALD-150LX* used in the current thesis, with the control unit (back) and depositions chamber (front). (b) Inside view of the system and its constituent parts.

condensation that would lead to parasitic CVD. This includes the chamber walls, precursor lines, valves, ellipsometry viewports, chamber top and bottom plates, the sample transfer port and the foreline. In a similar effort, inert gas flows are used in these areas as well as in the plasma source to minimize precursor residence time in the system [44]. In total, 1100 sccm of argon are used for this purpose leading to a processing pressure close to 1.4 torr maintained by continuous operation of a mechanical pump.

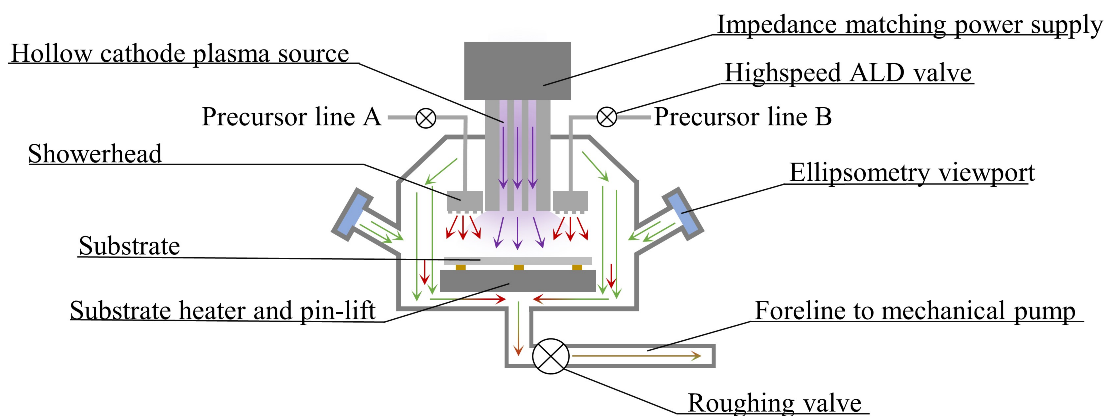

Figure 3.3 Schematic representation of the ALD system.

Substrates are heated by conduction with a heater capable of temperatures up to 500 °C,

equivalent to 380 °C at the sample surface. A pin lift is also integrated into the heater to facilitate transfers. Indeed, insertion and removal of the sample is done with an end effector and pin lift through a transfer port. During this process, the chamber is vented using argon gas, and kept at a positive pressure to minimize contamination. In some cases, the sample was cooled before extraction to limit rapid oxidation. However this was avoided when unnecessary as it can take up to 8 hours.

3.1.2 Thermal atomic layer deposition of TiN

Thermal atomic layer deposition of TiN was performed using the *ALD-150LX*. These depositions were made using 99.999% anhydrous ammonia and titanium tetrachloride kept a room temperature as the reducing agent and metal precursor respectively. Pulse and purge times were optimized for speed and saturated growth, as will be shown in chapter 4, using *in situ* ellipsometry. Anhydrous argon (99.999% with additional filtering) was used as an inert purge gas, with a total flow of 1150 sccm during deposition as recommended by the manufacturer to maintain laminar flow. Substrate temperature was varied between 200 and 380 °C in order to investigate its effect on film properties and GPC.

3.1.3 Plasma enhanced atomic layer deposition of TiN

Plasma enhanced ALD was also performed in the system. In this case, 99.999% anhydrous titanium tetrachloride was used as the metal source while reduction was done with an HCP. The gas flow through the plasma source was 100 sccm of the same argon used for purging in conjunction with 10 sccms of premixed 40% H_2/N_2. These flows were maintained throughout the process. The 40% H_2 concentration in the reactant gas mixture was found to be a minimum threshold for self-limiting ALD deposition of TiN [72], while also being low enough to avoid the need for a costly hydrogen-rated line and cabinet. The plasma was tuned to minimize reflected power using a *Seren IPS Inc.* impedance matching power supply set to manual. The automatic setting was found to be unreliable because of the rapid pulsing of the plasma required for ALD. Just like the thermal process, 1150 sccms of argon was kept flowing through the chamber during the entire deposition. The effects of RF power, cycle timing and substrate temperature were investigated and films were compared to ones made with and ICP source by another laboratory. Details of the second setup can be presented in chapter 4.

3.2 Glancing angle deposition

SiO_2 SCTFs were made by GLAD in a *Leybold Optix Boxer Pro* pilot scale evaporation system. A schematic representation is shown in figure 3.4.

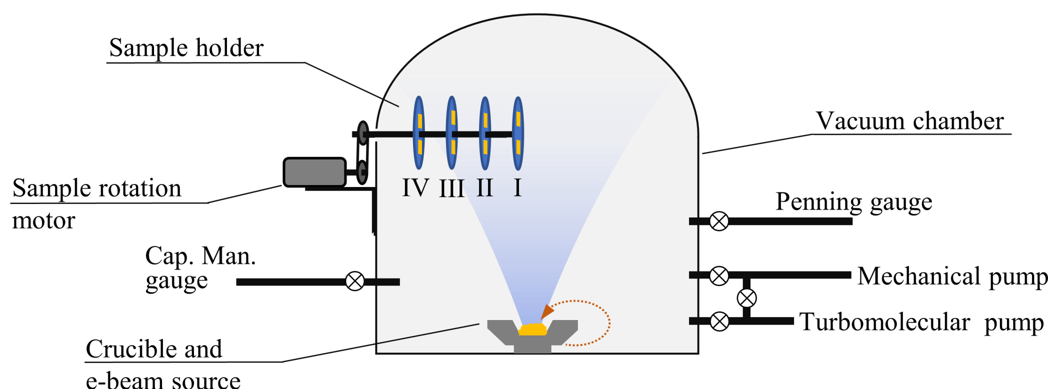

Figure 3.4 The e-beam evaporation system used for GLAD in this thesis with its custom substrate holder. Samples are fixed to the plates in positions I, II, III and IV.

The films were made from 1–5 mm pellets of 99.99% pure SiO_2 evaporated by e-beam. The glancing angle was obtained using a custom-made substrate holder [32] as shown in figure 3.4 where positions I,II,III and IV correspond respectively to angles of 87°, 77°, 68° and 60° [78]. No substrate rotation was used, although it can be done in the custom setup a via an additional motor, as seen in figure 3.4. Prior to deposition, the chamber was pumped down to a base pressure of 2.6x10^{-3} Pa (2x10^{-6} Torr) via a turbomolecular pump backed by a mechanical pump. Pressure in this system is determined using a Penning gauge in high vacuum and a capacitance manometer gauge in low vacuum. The amount of material deposited is measured *in situ* from a dense film grown on a quartz crystal microbalance (QCM). While this does not provide the thickness of the SCTFs, QCM setpoints can be used as targets to reproduce known SCTFs made in the same conditions. Thickness determination for the SCTFs is done *ex situ* by ellipsometry and other means that will be discussed.

3.3 Spectroscopic ellipsometry

Spectroscopic ellipsometry (SE) is extensively used with ALD made films [14, 20, 21, 29, 65–67, 85]. The technique can resolve the very small thicknesses associated with ALD and can be used to infer other important characteristics such as resistivity, roughness and composition

through analysis of a given film's optical properties [20]. SE is also useful for SCTFs [15, 50, 78, 86–90] as a means of measuring thickness, porosity, columns angle, aspect ratio and refractive index. Consequently, it is the primary method of characterization in both parts of this thesis.

In ellipsometry, the complex change in polarization, ρ, is measured. In a reflection configuration, this change emerges from differences in reflection of p-polarized, $\mathrm{R_p}$, and s-polarized, $\mathrm{R_s}$, light. ρ is most often described with the values Ψ and Δ which correspond respectively to the ratio of reflected amplitudes and the phase change after reflection. These parameters are shown in relation to each other in equation 3.1.

$$\rho = \frac{R_p}{R_s} = \tan(\Psi)e^{-i\Delta} \tag{3.1}$$

The process exploited in ellipsometry is shown in figure 3.5. A sample is illuminated with light of a known linear polarization oriented between the s- and p-plane. After interaction with the sample, the elliptically polarized reflected light travels though a rotating analyser which is used to measure its polarization state. ρ is then determined by comparing with the known state of the incident beam [91].

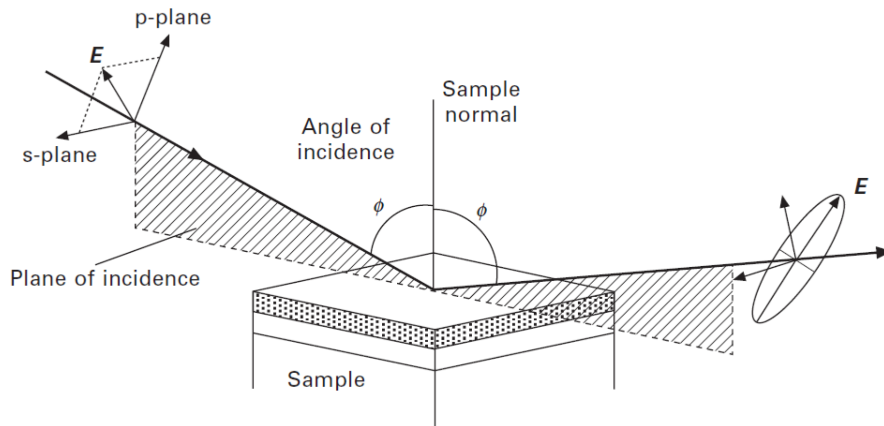

Figure 3.5 The SE measurement process. Linearly polarized light is reflected from the sample with an elliptical polarization. The change in polarization is then determined by comparing the reflected light polarization to the known polarization of the incident light. Reprinted from [92], copyright 2011, with permission from Elsevier.

In the case of samples with multiple interfaces, the polarization change of the reflected light contains contributions from each interface. Modelling is thus used to individually determine the characteristics of the superimposed films. In such models, the thickness and complex

refractive index, $N = n + ik$, of each layer are optimized to the values which minimize the mean square error (MSE) between the Ψ and Δ of the measured and simulated stacks.

For transparent coatings, for which k $\rightarrow$ 0, the true thickness and index can be quickly determined using this technique. However absorbing materials, such as TiN, are more challenging because the high correlation between thickness and optical parameters often leads to non-unique model solutions [93]. Hilfiker et al. [93] demonstrated that convergence can be improved for these films by using the following solutions:

- Optical constant parametrisation – Multiple solutions are avoided by constraining the possible material optical properties to realistic ones.
- Combined ellipsometry and transmission – The additions of a transmission spectrum to the SE data improves convergence by adding non-redundant information.
- *In situ* SE – If the thickness changes between measurements of the sample, it can be easily decorrelated from the optical constants, assuming they do not change much themselves.
- Interference enhanced ellipsometry (IEE) – Using a thick transparent layer underneath the absorbing film increases sensitivity to its thickness since fringes are present in the Ψ and Δ spectra.

Indeed, to ensure more physically accurate convergence, parametric oscillators are often used to constrain the possible values of refractive index for a given material. They include, Drude, Lorentz and Gaussian oscillators and much more. Our TiN model included one Drude and two Lorentz oscillators, as discussed in section 2.2. In this case, it was possible to calculate resistivity from the characteristics of of the Drude term. Characteristics such as porosity, roughness and columnar structure can also be accounted for by using effective medium approximations (EMA) such as Bruggeman or Maxwel-Garnett models. This strategy was used both for TiN films and for SCTFs. Thickness, resistivity and roughness were determined by SE for TiN samples, while thickness and porosity were measured in SCTFs. The specificities of the models used will be presented in the following chapters.

Furthermore, most TiN samples referenced in this thesis are deposited onto a 1 µm silicon thermal oxide layer to improve SE measurement accuracy by IEE. *In situ* spectroscopic ellipsometry (iSE) is also routinely used as will be further discussed in the following section. The use of transmission spectra for ellipsometry modelling was however forgone because most samples were deposited onto silicon wafers.

3.3.1 *In situ* SE

As previously mentioned, iSE was used throughout this project. The method was used to improve the measurement accuracy of the thin absorbing films, but also to speed up optimization and to characterize samples prior to *ex situ* oxidation. The measurements were made using a *M2000* ellipsometer from *J.A. Woolam*, fastened to the *ALD-150LX* viewports (shown in figure 3.2). This setup provided an incidence angle of 70° with a wavelength range of 400-1000 nm limited by the viewport window material. After installations on the ALD system, the ellipsometer was calibrated using a 20 nm SiO_2/Si calibration wafer to compensate for window anisotropy and to determine the precise angle of incidence. Alignment was then redone for every new sample.

The method for optimizing an ALD process is presented in section 2.1: samples are typically made using multiple deposition conditions; their growth rate is then measured *ex situ* and compiled into a dataset like the one represented in figure 2.5. For TiN, a minimum layer thickness of about 20 nm is required for accurate GPC determination by *ex situ* ellipsometry to minimize the effects of nucleation delay [20] and oxidation [14] and because the optical properties of TiN vary greatly at lower thicknesses [20, 21]. Depending on the complexity of the optimization, and the purge and pulsing times involved, this process can thus take between two weeks and a month. When using *in situ* SE however, conditions can be varied during a continuous deposition as shown in figure 3.6. This drastically reduces the time required for optimization because only a few nanometres need to be deposited for each process condition in order to measure the associated GPC. High frequency iSE can also be used to accelerate the process (See appendix 7) although this was not possible for the present project.

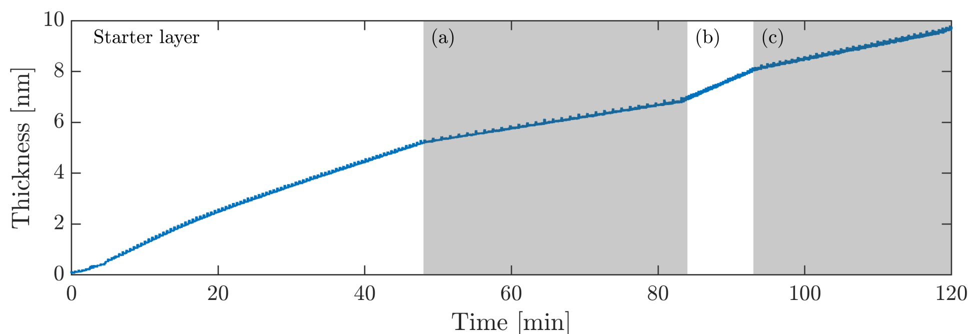

Figure 3.6 Example of an optimization routine for TiN. 100 cycles are deposited as a starter layer followed by 30 cycles with (a)90 s, (b)10 s and (c)60 s of plasma exposure time.

iSE is thus used for process optimization in this thesis. A starter layer of 100 cycles is used for stabilization of the growth rate followed by a sequence of 30 cycles for each set of deposition

parameters. The first set is repeated in the middle and at the end of the process in order to ensure that results are reproducible.

3.3.2 *Ex situ* SE

Ex situ ellipsometry was also used to characterize both TiN samples and SCTFs. In this case, measurements were performed on an *RC2* ellipsometer from *J.A. Woolam*. These measurements had the added benefit of a wider wavelength range (from 200 nm to 1700 nm) and a variable incidence angle: 45,55, 65 and 75° was consistently used in this thesis. For the anisotropic samples, the full Mueller matrix was acquired whereas standard Ψ and Δ were determined for the TiN films. The SCTFs characterized in this setup were deposited on silicon rather than glass to provide better contrast between the layer and substrate. TiN samples were measured both on 1 µm of SiO_2 and directly on silicon.

3.4 Sample characterization

Alongside ellipsometry, many other characterization techniques were used to determine optical properties, thickness and structure as well as composition of the samples. They will be briefly discussed in the present section.

3.4.1 Optical properties

Variable Angle Spectrophotometry

Spectrophotometry measurements were carried out in a *Cary 7000 universal measurement spectrophotometer* from *Agilent*. Transmission and reflection measurement can be taken in this system for p- and *s*-polarized light at incidence angles ranging from $-80°$ to $80°$ in the ultraviolet, visible and near infrared.

Thanks to the ability to measure at positive and negative incidence, it was possible to measure angular selectivity using this spectrophotometer. Indeed, the *s*- and *p*-polarized transmission spectra of the core-shell SCTFs were acquired for angles (θ) from $-70°$ to $70°$ at $10°$ intervals. These measurements were taken between wavelengths (λ) of 300 and 800 nm to minimize acquisition time and the measured samples were deposited onto *SCHOTT advanced optics' B270* glass which is transparent in the visible. The unpolarized transmission was also calculated from a wavelength-by-wavelength averaging of both polarized spectra.

In order to facilitate comparisons with literature and among samples, angular luminous transmission, $T_{lum}(\theta)$, was calculated from every spectrum. This enabled the association

of each to a single value: transmission intensity perceived by the human eye at a given incidence angle. Equation 3.2 presents the calculation of T_{lum} [94] where $T(\lambda, \theta)$ is the sample's transmission, $\bar{y}$ is the CIE 1931 standard observer [95] corresponding the sensitivity of cones in the human eye and $I(\lambda)$ is the CIE E equal energy standard illuminant.

$$T_{lum} = \frac{\Sigma_\lambda T(\lambda,\theta)\bar{y}(\lambda)I(\lambda)}{\Sigma_\lambda \bar{y}(\lambda)I(\lambda)} \tag{3.2}$$

Both raw spectra and T_{lum} values are shown for multiple samples in chapter 5.2.

Four-point probe

As mentioned in section 2.2, resistivity is a good measure of the metallic character and optical quality of TiN. As such, it was a major focus when optimizing TiN growth by ALD. Along with ellipsometry, four-point probe (FPP) was found to be an effective way of measuring it. A typical FPP setup is shown in figure 3.7. The sample is probed by four collinear electrodes separated by an equal distance s. A current, I, is applied between the points on both extremities and potential, V, is measured between the two centre points. The use of a separate set of probes for applying current and measurement voltage eliminates the contribution of contact resistance as opposed to 2-probe setups.

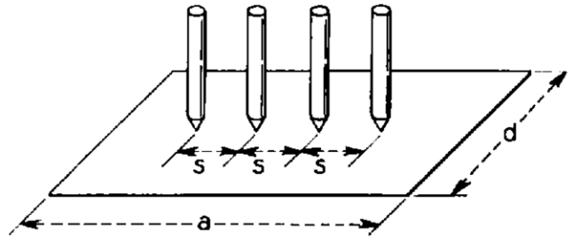

Figure 3.7 Four point probe measurement setup over a rectangular sample. Reprinted from [96].

Sheet resistance, ρ_s, can then be calculated from equation 3.3 where $C\left(\frac{a}{d}, \frac{d}{s}\right)$ is a factor calculated from the dimensions of the sample and probe. Its value can vary from below 1 when $\frac{d}{s} \rightarrow 1$ to $\frac{\pi}{\ln 2}$ for an infinite substrate.

$$\rho_s = \frac{V}{I} C \left(\frac{a}{d}, \frac{d}{s} \right) \tag{3.3}$$

$$\rho = w \rho_s \tag{3.4}$$

The resistivity, ρ, can then be calculated from the sheet resistance and thickness, w, using equation 3.4. For accurate determination of the layer resistivity, it is important to avoid conduction through the substrate. Consequently, the films measured by FPP in this work were either deposited onto a 1 µm thick silicon oxide layer or directly onto Si wafers with low dopant concentration. In many cases, small rectangular samples were used and their sheet resistance corrected using values of $C\left(\frac{a}{d}, \frac{d}{s}\right)$ published by F. M. Smits [96]. Finally, thickness, w, measured by ellipsometry was used for calculations of resistivity from sheet resistance.

3.4.2 Thickness and structure

X-ray Reflectometry

As previously mentioned, thickness measurements by SE for thin TiN films can be challenging. In this work, X-ray reflectivity (XRR) was used to confirm them. Thicknesses determined by XRR for single layer films are usually very accurate considering they can be directly calculated from angular fringes in the reflectance curve. The technique is, however, only sensitive to films between around 10 and 200 nm as fringes will be either too far apart to be detected in the possible measurement range or too close to be resolved.

Measurements were carried out in a *Bruker D8 ADVANCE* X-ray diffractometer at a wavelength of 1.54 Å(Cu K_α). The measurement procedure published by Scott A. Speakman [97] for this system was used. Analysis of the reflectance curves for thickness determination was done in the open-source *GenX* software [98]. The results are shown in chapter 4. While XRR worked well for flat TiN films. SCTFs could not be measured with the technique because of their high surface roughness and thickness.

Scanning electron microscopy

Scanning electron microscopy (SEM) was used to determine both the thickness, and the column angle of the SCTFs. These measurements were performed on uncoated columns in a *JEOL JSM 840A* scanning electron microscope operated at a 10 kV. The SCTFs were prepared on a doped silicon substrate rather than glass to minimize charging effects. The

micrographs were made over a freshly cleaved edge. SEM was also performed on TiN sample cross-sections as a third way of validating thickness measurements, doped silicon substrates were also used for this.

Transmission electron microscopy

Transmission electron microscopy (TEM) was used to confirm the presence of core-shell columns in the TiN coated SCTFs. The details of these measurements are presented in section 5.2.3.

3.4.3 Composition

Core-shell SCTFs

During TEM measurements, energy dispersive x-ray spectroscopy (EDS) mappings were made over single core-shell columns providing elemental counts of Si, Ti, O and N. Ratios of one element to the other could not be determined as the measurement was not calibrated. However, zones of higher and lower concentration could be distinguished for a given element. By using these measurements alongside selected area electron diffractograms, it was possible to determine the composition of the core and shell.

TiN films

Composition was measured for the TiN samples using two different methodologies. First of all, oxygen and chlorine concentration depth profiles were acquired by time of flight secondary ion mass spectroscopy (TOF-SIMS) using 1 kV cesium ions. These concentrations were calibrated to the known composition of one of the samples, previously determined by elastic recoil detection (ERD).

X-ray photoelectron spectroscopy (XPS) was also performed on two samples made using different plasma sources. Oxygen concentrations as well as Ti/N ratios were measured and are compared in chapter 4. These measurements were made by a co-author at Pennsylvania State University.

CHAPTER 4 ARTICLE 1: PLASMA ENHANCED ATOMIC LAYER DEPOSITION OF HIGH PURITY TITANIUM NITRIDE: COMPARISON OF HOLLOW CATHODE AND INDUCTIVELY COUPLED DISCHARGES

S. Woodward, O. Zabeida, B. Rayner, N. O'Toole, K. S. A. Butcher and L. Martinu

4.1 Foreword

In this chapter, a conference article is presented on the subject of improving the quality of PEALD processed TiN using an HCP source, it was published in the 2018 Society of Vacuum Coaters TechCon proceedings. Afterwords, some additional results are presented that support some of the conclusions found in the article and further our understanding of the method.

4.2 Article : Plasma enhanced atomic layer deposition of high purity titanium nitride: comparison of hollow cathode and inductively coupled discharges

4.2.1 Abstract

Inductively coupled plasma (ICP) sources are routinely used for plasma enhanced atomic layer deposition (ALD) processing. While these sources are adequate for obtaining quality metal oxides, high purity metal nitrides present a greater challenge due to oxygen contamination from etching of the ICP's dielectric tube, as well as atmosphere permeation through elastomer seals. It is thus important to consider alternative types of plasmas for processing metal nitrides by ALD. The all-metal construction of hollow cathode plasma (HCP) sources overcomes these challenges. However, direct exposure of the metallic electrode to energetic ions can provide another film contamination source. In this study, we compare HCP and ICP sources for titanium nitride growth by plasma enhanced ALD (PEALD) using $TiCl_4$ and $Ar/N_2/H_2$ plasma. Films deposited using HCP are first optimized for growth rate and resistivity. Afterwards, two films, one obtained using each type of discharge, are compared for oxygen and chlorine concentration, resistivity, uniformity and growth per cycle. Our results indicate a significantly higher growth rates of 0.05 nm/cycle when using an HCP source as compared to an ICP (0.029 nm/cycle). The film deposited with an ICP, however, has lower resistivity and oxygen contamination. Considering that conditions were not identical for the two films, these results are preliminary. This work presents the results of our optimization

and comparisons, discusses the scope of our results and the steps to be taken in further analysis.

4.2.2 Introduction

Atomic Layer Deposition (ALD) presents many advantages over other thin film deposition techniques. Two of its greatest assets are its high conformity over 3D structures, and its highly reproducible atomic scale thickness control [1].

In the past two decades, much of the research on ALD has been focused on dielectrics like Al_2O_3, HfO_2, TiO_2 for nanoelectronics applications [1]. However, other materials like pure metals and metal nitrides deposited by ALD are gaining momentum. In this case plasma enhanced atomic layer deposition (PEALD) is often used as it generally provides better material properties and enables the deposition of a larger selection of materials [18].

Most often, inductively coupled plasma (ICP) sources are used in PEALD. While these sources are adequate for obtaining quality metal oxides, high purity metal nitrides present a greater challenge due to oxygen contamination from etching of the ICP's dielectric tube, as well as atmosphere permeation through elastomer seals typically used to create a vacuum seal around this tube. Consequently, it becomes important to explore other types of plasmas that might improve the quality of these films.

Hollow cathode plasma (HCP) sources may help overcome the oxidation problems mentioned above. The source's all metal construction eliminates the need for elastomeric seals and eliminates the possibility of oxygen incorporation when etching occurs around the plasma. In fact, works have shown that the source promotes high growth per cycle when depositing AlN and InN and improves crystal quality in GaN and AlN [29, 31]. Silicon nitride has also been deposited with low leakage current and oxygen content using this source [99, 100].

In this work, we investigate the use of the HCP source and its impact on the quality of titanium nitride (TiN) deposited by PEALD. In the first part, the hollow cathode PEALD (HC-PEALD) processing of TiN is optimized for growth rate and resistivity. In the second part, films obtained from HC-PEALD, inductively coupled plasma PEALD (IC-PEALD) and thermal ALD are compared for film resistivity, composition, growth per cycle and uniformity.

4.2.3 Experimental

In part 1, all films were deposited in a laboratory scale KJLC ALD-150LX PEALD system. The metal source used for the deposition of the titanium nitride was titanium tetrachloride

($TiCl_4$). For thermal ALD of TiN, ammonia (NH3) was used as a reducing agent. Exposure times to the two precursors were 60 ms for titanium chloride and 20 ms for ammonia separated by 5 s of argon purge. For the PEALD deposition of TiN, reduction and nitrogen incorporation was done using a $H_2/N_2/Ar$ plasma generated by a hollow cathode plasma source purposefully installed onto our ALD system. The purge times and the titanium chloride exposure time used were identical to the thermal process while the plasma exposure time was optimized as part of the experiment presented here. The gas mixture flowing through the plasma source during the deposition was a mixture of 110 sccm of argon, 6 sccm of nitrogen and 4 sccm of hydrogen; similar N_2/H_2 ratios were shown to enable ALD deposition in other works, although with a much lower relative argon flow [72]. Depositions were done at an operating pressure of 1.6 Torr provided by 1150 sccm of continuous 5N argon flow. To compensate for the lack of load lock on our ALD system, all films were cooled to 130 °C prior to *ex situ* exposure.

In part 2, one film was deposited using an HCP source in LaRFIS at Polytechnique Montreal using the conditions described above. The film prepared using an ICP source was made at the Kurt J. Lesker Co. Lab, also using an ALD-150LX PEALD system. While many conditions were similar in both processes, some were not; specifically, it is important to note that the ALD system at KJLC was equipped with a load lock. Table 4.1 presents an overview of the conditions used for both experiments.

Table 4.1 Comparing deposition parameters for films deposited in part 2.

	LaRFIS	**KJLC**
Plasma Source	HCP	ICP
Titanium precursor	$TiCl_4$	$TiCl_4$
Purge gas	Ar	Ar
Process temperature [°C]	380	380
Plasma power [W]	300	975
H_2 flow [sccm]	4	6
N_2 flow [sccm]	6	3
Ar flow [sccm]	1150	1150
Operating pressure [Torr]	1.6	1.2
Plasma pulse time [s]	60	9

4.2.4 Results and discussion

Part 1: Optimizing Deposition with the HCP

In this first part of experiments, TiN films are deposited using hollow cathode plasma and optimized for resistivity and growth per cycle. Growth rate and resistivity values are compared to reported values from IC-PEALD TiN films as well as experimental values for the thermal ALD process of TiN.

Effect of plasma exposure time

In order to demonstrate growth rate saturation to plasma exposure time, growth per cycle (GPC) was determined for films deposited with plasma exposure times between 5 and 99 seconds. As can be seen in Figure 4.1, saturation is achieved beyond 60 s of HCP plasma exposure. The saturated growth rate of 0.05 nm/cycle is also consistent with published values for this temperature in IC-PEALD [20]. However, resistivity still decreases after that point, indicating that plasma exposure times may also affect the crystallinity and roughness of the films beyond saturation.

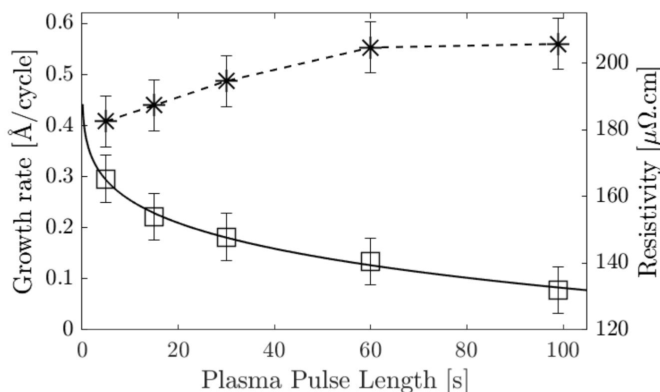

Figure 4.1 Growth rate and resistivity of TiN as a function of plasma exposure time. Films were deposited at 380 °C, with a 300W hollow cathode plasma.

Chlorine and oxygen concentrations were also measured by time of flight secondary ion mass spectrometry (TOF-SIMS) for films deposited using different plasma exposure times. In all cases, the chlorine concentration was below the detection limit of 0.01 at.% . In addition, the oxygen concentration of (5 ± 1) at.% did not significantly vary beyond the saturation point indicating that the variation in resistivity beyond this point is not caused by a variation in composition.

Following this experiment, all subsequent depositions are made using 60 s plasma exposure times, which was determined to be the growth saturation point.

Effect of RF power

The effect of power on film quality and growth rate was investigated by comparing films deposited using RF powers of 100 W and 300 W, the results are compiled in Table 4.2. A power of 300 W was determined to be the upper limit of the setup.

Table 4.2 Thickness, growth per cycle, roughness, resistivity and contamination for films deposited using 100 W and 300 W hollow cathode plasmas.

	100 W	**300 W**
Thickness [nm]	44 ± 3	52 ± 5
GPC [Å/cycle]	0.44 ± 0.03	0.52 ± 0.05
Roughness [nm]	5 ± 2	6 ± 2
Resistivity [$\mu\Omega \cdot$ cm]	121 ± 8	104 ± 7
Bulk Cl content [at.%]	<0.01	<0.01
Bulk O content [at.%]	3 ± 1	4 ± 1

As can be seen in Table 4.2, the higher plasma power increases growth rate by 18% and decreases resistivity by 10 %. Seeing how the roughness and composition of both films are within their respective error intervals, this difference in resistivity is likely the result of larger grains size. As indicated in Figure 4.2, the grain size of the films deposited at higher power are indeed larger at (55 ± 6) nm compared to (39 ± 4) nm. While higher hollow cathode power did increase growth rate and lower resistivity, the values obtained for both are not superior to values published for films made using ICP plasma [20].

Effect of deposition temperature

Depositions were done at temperatures between 130 °C and 380 °C with both the thermal and HC-PEALD processes. Figure 4.3 presents the growth rate and resistivity of these films as well as published values for ICP films prepared under similar conditions [20].

As shown in Figure 4.3, growth rates of up to 0.8 Å/cycle are achieved at lower deposition temperatures using the HCP source setup. This is significantly higher than reported values for TiN. However, resistivity for these films is higher than the resistivity of films deposited at similar temperatures using an ICP source. A probable explanation for the higher growth rate and resistivity of these films is higher oxygen incorporation in the films during deposition, as is shown later.

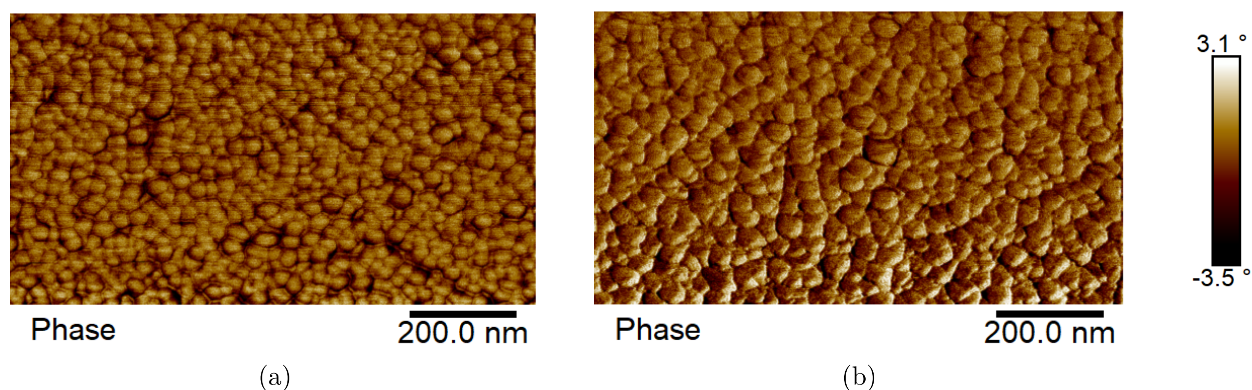

Figure 4.2 AFM phase maps of samples deposited using 100 W (a) and 300 W (b) of hollow cathode plasma.

It is also noteworthy that the use of PEALD (both HC-PEALD and IC-PEALD) for the deposition of TiN results in lower resistivity films than thermal ALD. As can be seen in Figure 4.3, the resistivity of films decreases by close to 50% when using PEALD as opposed to thermal ALD at a given temperature. PEALD also enables deposition at much lower temperatures than its thermal counterpart. Indeed, no deposition occurs from the thermal process for the temperatures below 330 °C.

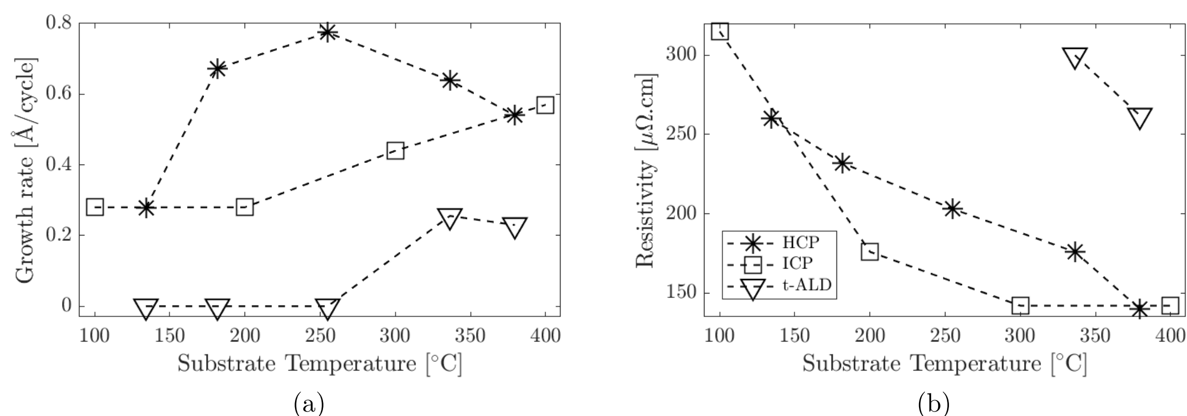

Figure 4.3 Growth rate (a) and resistivity (b) of TiN as a function of substrate temperature. HCP films were deposited using a 300 W hollow cathode plasma. Values for ICP films were taken from Langereis et al. [20].

Composition analysis was done by TOF-SIMS on HCP films for 3 different temperatures (130 °C, 255 °C and 380 °C) and a thermal ALD film deposited at 380 °C. Figure 4.4 presents the composition depth profile of these samples. One can notice that chlorine contamination

in the thermal films is two orders of magnitude higher than that of the HC-PEALD films. Deposition temperature also has a noticeable impact on chlorine content, with the higher temperature process providing a ten-fold decrease in concentration. However, the amount of chlorine at low temperature is significantly lower than reported value in other works [20]. This low chlorine content is thought to be achieved because of the long plasma exposure times used in our HC-PEALD process [21].

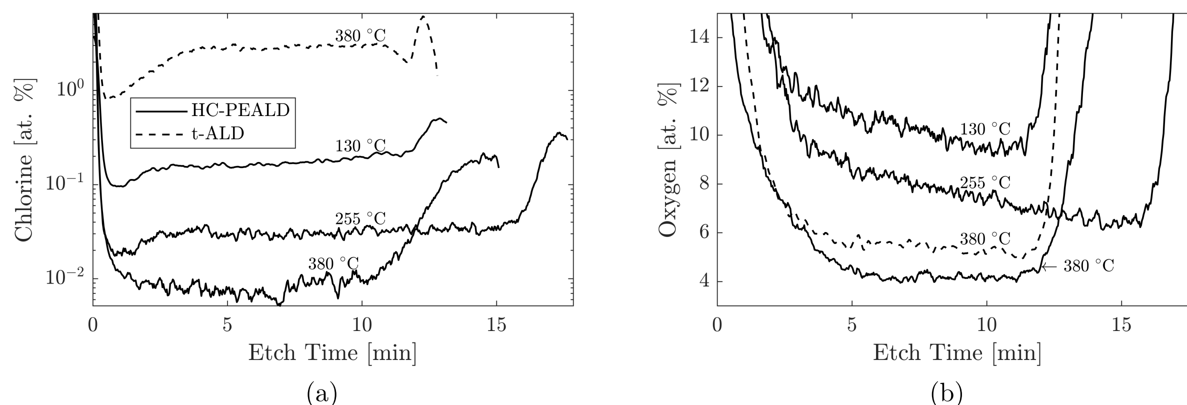

Figure 4.4 Chlorine and oxygen concentration HC-PEALD films deposited at 130 °C, 255 °C and 380 °C and a thermal film deposited at 380 °C. All profiles are measured by time-of-flight secondary ion mass spectrometry (TOF-SIMS).

Deposition temperature also has a significant impact on the oxidation of the films, with the low temperature deposition yielding heavily oxidized films. It can also be noticed that the thermal process yields films with comparable, if not slightly lower, oxygen contamination with respect to the HC-PEALD process. This hints at the possibility that oxidation is not limited by the process and may come from *ex situ* exposure or excess amounts of oxygen and water in the deposition chamber. The gradient in oxygen content observed in the low temperature films is also consistent with *ex situ* oxidation [14]. This oxidation problem is most likely due the fact that the ALD system used in these experiments is not equipped with a load-lock resulting in high temperature extraction of the films and frequent venting of the deposition chamber.

Part 2: Comparing Optimized Films Deposited Using Inductively Coupled Plasma and Hollow Cathode Plasma

In this part of the work, two films of identical thickness (50 nm) were prepared, one using the ICP source and the other one using the HCP source. The films were deposited using methods independently optimized for each source.

Growth rate, resistivity, composition and morphology

The films were compared for growth rate, uniformity, resistivity and composition, these results are compiled in Table 4.3.

As can be seen, growth per cycle is 55% lower for the film deposited with ICP plasma. The ICP process growth rate is, however, also significantly lower than other reported values for TiN deposited with an ICP in similar conditions. The overall throughput is, however, higher for the ICP process because the optimized plasma exposure times vary significantly from one process to another: the exposure times were 9 s for the ICP process and 60 s for the HCP process. These differences may come down to differences in the plasma density and temperature; indeed, the RF power used was 300 W for HCP and 975 W for ICP, but they could also be the result of differences in optimization methodologies

Table 4.3 Material properties of TiN films deposited on native oxide using hollow cathode (HCP) and inductively coupled (ICP) discharges. Thicknesses are measured by *ex situ* scanning electron microscope. Resistivity, growth per cycle and throughput are measured by *in situ* ellipsometry using a Drude-Lorentz parameterization [20]. Thickness and resistivity non-uniformity is calculated from the standard deviation of a 69-point *ex situ* ellipsometric map over 100 mm wafers. Chlorine concentration is measured by depth profile TOF-SIMS calibrated to Rutherford backscattering measurements. Bulk oxygen concentration and N/Ti ratio are determined from depth profile X-ray photoelectron spectroscopy (XPS) measurements.

	HCP	**ICP**
Thickness [nm]	50 ± 3	50 ± 3
Thickness non-uniformity [%]	4.2	2.3
GPC [Å/cycle]	0.52	0.29
Throughput [Å/min]	0.45	1.01
Roughness [nm]	6 ± 2	2 ± 2
Resistivity [$\mu\Omega \cdot$ cm]	104 ± 8	73 ± 7
Resistivity non-uniformity [%]	5.5	2.9
Bulk Cl content [at.%]	<0.01	0.5
Bulk O content [at.%]	6 ± 2	1 ± 1
Bulk N/Ti ratio	1.08	1.04

Notable is also the fact that the HCP film contains 6 times more oxygen than the ICP film. This result again supports the conclusion that oxygen contamination in the HCP process was caused by the absence of load-lock on the system. Differences in the plasma exposure time in the two processes may also contribute to the difference in oxygen contamination as oxygen

would have more time to incorporate in the slower reaction. This higher level of oxidation also may explain the higher roughness of the HCP film. The ICP film is also more uniform than the HCP film both in thickness and resistivity; this is most likely because thickness non-uniformity was taken into account when optimizing the ICP film.

The HCP film, however, contains a much smaller quantity of chlorine. As mentioned in Part 1, this difference is not accounted for by the difference in plasma exposure time. Further comparison will help determine whether this is a benefit of the HCP source.

In addition, despite its significantly higher oxygen contamination the HCP films exhibit a rather good resistivity of about 100 µΩ cm.

4.2.5 Conclusions

The deposition of TiN by PEALD using a hollow cathode source was investigated by varying plasma exposure time, power and temperature. Growth rate saturated to increasing plasma exposure time after 60 s. However, resistivity continued to decrease with longer exposure times. Increasing RF power and deposition temperature was shown to improve both growth rate and resistivity. Observed growth rates at temperatures lower than 350 °C were very high when using the HCP source; whether this is caused by the source or by other parameters is still to be determined.

When comparing a film deposited with an HCP to a film deposited with an ICP in another depositions system, significant differences were measured in the growth rate, resistivity, uniformity and composition. However, these differences are most likely due to differences in oxygen incorporation during and after the deposition caused by the fact that one of the deposition systems was not equipped with a load lock. Further comparison of these sources in identical deposition systems with identical conditions will help provide a more complete comparison. In concluding, we note that the properties of the films produced with both the HCP and ICP sources are both well within the range of values published for good quality TiN produced by PEALD.

4.2.6 Acknowledgements

The authors wish to acknowledge Mr. Francis Turcot, Mr. Sébastien Chénard and Mr. Francis Boutet for their technical support as well as Dr. Bill Baloukas, Dr. Simon Loquai, Dr. Thomas Schmitt and Mr. Jacques Lengaigne, for invaluable discussions, advice and training. This work was funded by the Natural Sciences and Engineering Research council

of Canada (NSERC). Society of Vacuum Coaters (SVC) provided a financial assistance to S.W. (SVC student sponsorship) to participate in this meeting.

4.3 Further work on atomic layer deposition of TiN

Other experiments were done in the preparation of this article that were not included in the final draft. The results of these experiments can, however, be useful in furthering our understanding of the subject. As such, they are presented in the following sections.

4.3.1 Thermal atomic layer deposition of TiN

Films obtained by thermal ALD are referenced in this article and compared to PEALD coatings. These films were previously optimized with 1.2 s purge times and 20 ms exposures to both titanium chloride and ammonia reactants for a total cycle time of 2.44 s. The saturated growth rate was lower than PEALD processes at 0.12 Å/cycle. Nonetheless throughput was much higher due to the short cycle times.

4.3.2 *In situ* and *ex situ* spectroscopic ellipsometry of TiN

In section 3.3.1, we present the use of iSE for rapid optimization of ALD process parameters. In addition to this, iSE is useful for understanding the evolution of film parameters like resistivity during deposition. The article presented in this chapter heavily relies on iSE to evaluate thickness and resistivity prior to *ex situ* exposure. As ellipsometric measurements can sometimes be unreliable, this section discusses the model used and compares its results to measurements made using other methods.

The ellipsometric model used in this chapter is presented in figure 4.5, it is based on Langereis et al.'s parametrisation of PEALD-grown TiN [20]. The bold parameters are fitted to every sample as they vary significantly with thickness or composition.

To validate ellipsometric thickness and resistivity measurements on TiN, a representative sample from each process (HC-PEALD, IC-PEALD and ALD) was assessed using iSE, variable angle SE (VASE), XRR, SEM and FPP (see table 4.4). For all three samples, thickness measurements from ellipsometry match with SEM measurements within error intervals. In the case of XRR, the measured thickness is 7 nm lower than other measurements for the HCP film because XRR is insensitive to the thin oxidized layer on the surface. A similar observation can be made for the ICP film. Measurements from all three techniques give very consistent results for the ICP film, whereas error and incertitudes increase for the more

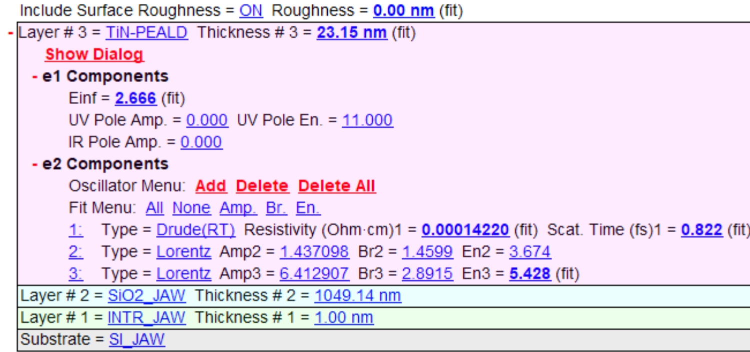

Figure 4.5 Ellipsometric model used for thickness and resistivity measurements of TiN processed by ALD and PEALD.

Table 4.4 Comparing TiN film thickness and resistivity measured by *In situ* spectroscopic ellipsometry, variable angle spectroscopic ellipsometry, x-ray reflectivity, scanning electron microscopy and four point probe.

	Thickness [nm]				Resistivity [$\mu\Omega \cdot cm$]		
	iSE	VASE	XRR	SEM	iSE	VASE	FPP
ICP	56 ± 2	56 ± 3	51 ± 1	50 ± 3	72 ± 5	72 ± 5	73 ± 5
HCP	52 ± 3	50 ± 4	43 ± 1	50 ± 3	101 ± 10	114 ± 9	104 ± 10
Thermal	23 ± 2		23 ± 1	N.A.	262 ± 30		

resistive films. Given the higher resistivity is largely caused by oxidation in this case :

- Inconsistencies between iSE and variable angle spectroscopic ellipsometry (VASE) are caused by oxidation during *ex situ* exposure.
- Inconsistencies between ellipsometry and four point probe (FPP) are caused by oxidation in grain boundaries.
- Higher incertitude of ellipsometric measurements is caused by an inadequacy of the model to account for a shift of optical properties due to oxidation.

In addition, accuracy decreases for thinner films. As discussed in section 2.1.3, for films below 10 nm VASE resistivity increases sharply as the electron mean-free path is constrained by the thickness, this is also seen in figure 4.6. For FPP resistivity, discontinuities in the thinner films add to this causing the increasing discrepancy observed in films thinner than 20 nm. To maintain consistency between resistivity determined from direct measurement and from ellipsometry, films should be thicker than 20 nm and have a resistivity below 200 $\mu\Omega \cdot cm$.

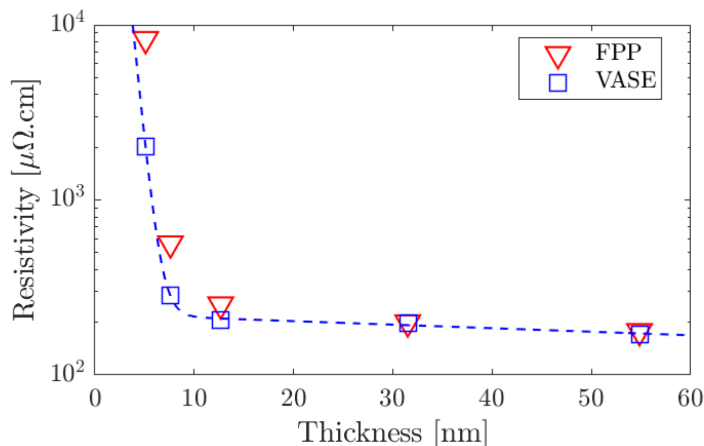

Figure 4.6 Resistivity as a function of thickness for TiN films deposited by HC-PEALDs. Resistivity measured by variable angle spectroscopic ellipsometry is comparable to that measured by four point probe for films over 10 nm.

Measurements that do not meet the second criteria are, however, useful for comparison and optimization.

4.3.3 Plasma exposure time

In the present chapter, a comparison is made between films processed with an inductively coupled plasma (ICP) and HCP. In this comparison, ICP films were exposed to a 975 W plasma for 9 s whereas HCP films were exposed to 300 W for 60 s. The differences in optimal plasma pulse length (PPL) are probably due to the different powers used for both sources. This can be seen in figure 4.7 where growth rates are presented in relation to PPL for 4 different HCP powers. For a 300 W plasma, saturated growth is achieved beyond 60 s, whereas 600 W lead to a PPL of 30 s. For 10 s exposures, growth rate is 80 % of the saturated value for 300 W and 90 % for 600 W. Using higher power thus decreases the optimal PPL. In the case of our HCP source, however, powers over 300 W cause the production of powders during deposition.

In the article, a question is raised: whether the differences in chlorine and oxidation between sources are caused by the differences in PPL. Namely, whether continuous parasitic oxidation of the films is favoured by the slower pulses of the HCP process and whether the longer exposures favour more a complete chlorine reaction.

As seen in figure 4.8a, this is not the case. The effect of PPL on bulk oxygen content in the films is marginal and cannot explain the 5 % difference between plasma sources. However the thickness of surface oxidation increases with decreasing PPL with a 4 nm oxide layer for

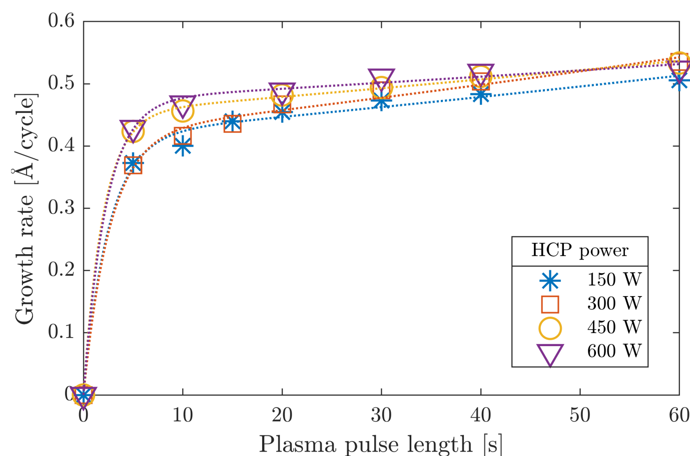

Figure 4.7 Growth rate as a function of plasma pulse length for HCP power between 150 W and 600 W. GPC is determined by *In situ* spectroscopic ellipsometry at a deposition temperature of 500 °C. Dotted lines are fits to the data.

15 s PPL compared to a 1 nm layer for 60 and 99 s PPL. As the surface oxide is caused by *ex situ* oxidation, this indicates a higher density of discontinuities or higher roughness in films processed with a shorter PPL. When comparing the two plasma sources, the differences in oxidation are most probably linked to the lack of load-lock in the HC-PEALD system requiring hot extraction of the samples.

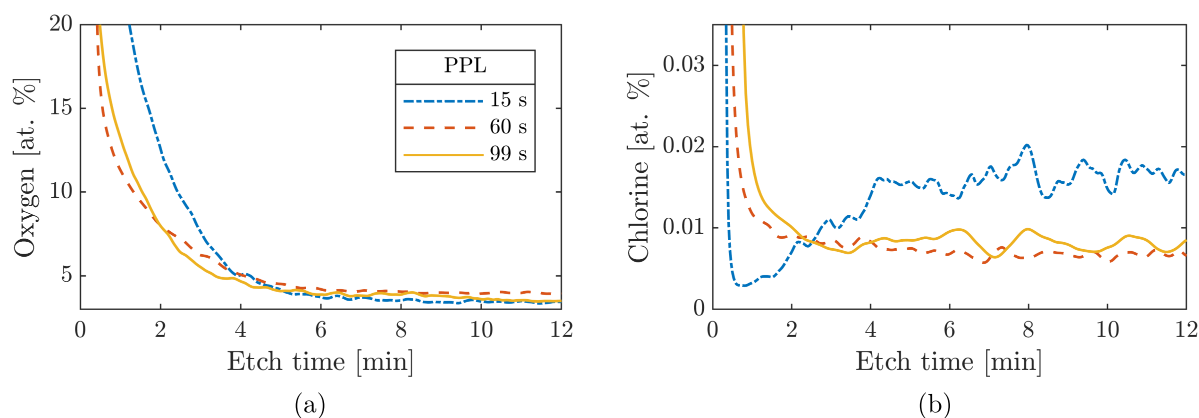

Figure 4.8 Chlorine and oxygen concentration HC-PEALD films deposited with 15 s, 60 s and 99 s of plasma exposure time. All profiles are measured by time-of-flight secondary ion mass spectrometry (TOF-SIMS) on films processed at 300 W with a substrate temperature of 380 °C.

When in comes to chlorine contamination, the longer pulsing times do affect its presence in the films, as seen in figure 4.8. Bulk chlorine content is 1.5 to 2 time greater for the shortest

pulse length. This increase however cannot explain the difference in Cl content between films from either source as it is close to two orders of magnitude. As such the likely conclusion is that the use of HCP plasma drastically diminished chlorine contamination in TiN films processed by ALD.

4.4 Concluding remarks

Good quality TiN is obtained by PEALD in this chapter by the use of an HCP source. When compared to IC-PEALD, HC-PEALD seems to reduce chlorine contamination and increase growth rate. While oxidation is a problem in the current HC-PEALD setup, this can be improved by means unrelated to the plasma source. Given the low Cl content of the films, such a process may indeed lead to improvements in PEALD processing of TiN and other metal chloride based processes.

Given the low powers used in our HC-PEALD, throughput was orders of magnitude lower than thermal ALD as per the long PPLs required to achieve saturation. In the next chapter, the high temperature thermal ALD films discussed in this chapter will be used to tailor angular selectivity in SCTFs.

CHAPTER 5 ARTICLE 2: TAILORING ANGULAR SELECTIVITY IN SiO_2 SLANTED COLUMNAR THIN FILMS USING ATOMIC LAYER DEPOSITION OF TITANIUM NITRIDE

Sasha Woodward-Gagné, Nicolas Desjardins-Lecavalier, Bill Baloukas, Oleg Zabeida and Ludvik Martinu

Published in **Optical Materials Express 9, 4556-4563 (2019).**

5.1 Foreword

This chapter presents the central article of the thesis pertaining to the tailoring of absorption in angular selective films using our TiN process. Following the article, some additional results are presented which further our understanding of the method.

5.2 Article: Tailoring angular selectivity in SiO_2 slanted columnar thin films using atomic layer deposition of titanium nitride

5.2.1 Abstract

Core-shell slanted nanocolumnar thin films (SCTFs) were produced by e-beam glancing angle deposition of SiO_2 and subsequent atomic layer deposition (ALD) of TiN. Conformity of the ALD film over the slanted columns was confirmed by transmission electron microscopy and energy dispersive X-ray spectroscopy mappings. Angle resolved spectrophotometry characterization revealed angle-dependent transmission of the films, akin to their fully metallic counterparts. We found that such inclined core-shell nanocolumn films enable tailoring of the angular selectivity independently from the SCTF thickness and density.

5.2.2 Introduction

Thin films with angle-selective (AS) transmission can yield significant improvements in optical performance suitable for applications such as ophthalmics, fenestration, as well as optoelectronic technologies. For instance, such films can be used to correct certain visual impairments, to tune solar transmission based on the sun's position in the sky [101], or to attenuate parasitic light sources coming from specific angles.

Slanted columnar thin films (SCTFs) fabricated through glancing angle deposition (GLAD) are an effective means of obtaining AS optical properties [33, 35, 86, 102–105]. Most notably, metal SCTFs have been shown to exhibit high optical transmission when incident light is parallel to the metal columns, and low transmission when it is perpendicular to them [33,101]. As an example, Mbise et al. reported evaporated chromium SCTFs with 52 % luminous transmittance at a positive angle of 60°, and 24 % at the negative angle equivalent [33]. For selected wavelengths and *p*-polarised light, the transmission of such films can reach values ten times higher at positive angles then at negative angles [33].

The observed angular selectivity results from the geometry of the optically absorbing columns which leads to a higher absorption in one direction and lower absorption in the other. Precise properties of GLAD-based SCTFs can, however, be difficult to predict solely from deposition parameters. Indeed, in GLAD coatings, the columns' inclination is adjusted by varying the angle of the incident material flux; the latter , however, also affects the film density and growth rate [35]. In addition, even with identical glancing angles, film porosities and column angles vary significantly for different materials [36], substrate temperatures, deposition rates [35] and other parameters. The density of SCTFs also depends on their thickness, due to broadening and extinction of the columns during their growth [35, 37]. As a result, manufacturing GLAD-based AS coatings is a major challenge if independent tailoring of either the angle of the columns, the opacity and/or the film color is required.

Additionally, GLAD SCTFs are limited to materials that can be deposited by physical vapor deposition (PVD) [35]. In fact, the most AS SCTFs are obtained through evaporation [33] as it combines long throw distances and mean free paths [35]. As the evaporated materials are limited, this discourages the use of certain optically important materials for manufacturing AS films. Most notably, this includes titanium nitride (TiN), which is of interest for its plasmonic properties [19, 23, 24], high thermal stability [22], good mechanical properties [23], and compatibility with CMOS technology [26].

In this paper, AS optical coatings are made by depositing conformal ALD layers of TiN over optically transparent SiO_2 SCTFs. Since selectivity is mainly absorption-based, the combination of GLAD and ALD provides an additional degree of freedom to independently adjust the microstructural and optical characteristics, leading to tunable angular selectivity. ALD functionalization of SCTFs has been reported in the literature for passivation of functional columns [50, 87, 88], decoupling of device microstructure and surface chemistry [49, 81], and for the fabrication of tubular magnetic nanostructures [83]. To our knowledge, we present the first application of this technique that adds optical functionality to existing SCTFs. Consequently, we compare the AS performance of these films to conventionally fabricated SCTFs

and discuss the advantages of the proposed approach.

5.2.3 Experimental methodology

GLAD deposition of the SiO_2 cores

SiO_2 SCTFs were prepared on B270 glass substrates using electron beam evaporation in a pilot scale Leybold Optics box coater (Boxer Pro). SiO_2 1-5 mm pellets of 99.99 % purity were used as source material. Prior to deposition, the process chamber was pumped down to a base pressure of 2×10^{-6} Torr. The angle of the columns was subsequently characterized by scanning electron microscopy (SEM) of the film cross-section (see Fig. 5.1). The measured column angle was then used in conjunction with variable angle spectroscopic ellipsometry measurements using a J.A. Woollam Co. RC2-XI and subsequent Bruggeman modeling [89] to determine the thickness, porosity and refractive index of the films (see table 5.1).

Table 5.1 SiO_2 SCTF characteristics prior to ALD functionalization. Thickness, porosity and refractive index were determined by ellipsometry whereas column angle was measured by SEM imaging.

Glancing angle [°]	Thickness [nm]	Porosity [% void]	n @ 550 nm	Column angle [°]
87	490	82	1.07	44

Deposition of TiN shells by ALD

The SiO_2 GLAD films were subsequently functionalized with different thicknesses of titanium nitride using titanium tetrachloride ($TiCl_4$) and ammonia (NH_3) precursors [21] in an ALD-

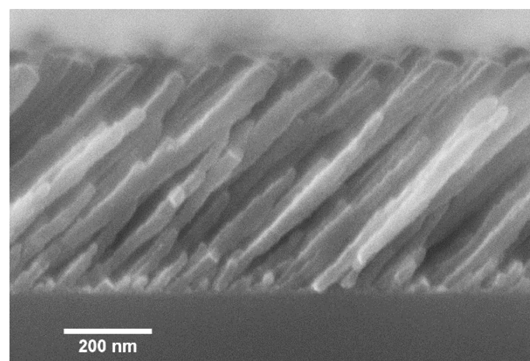

Figure 5.1 Scanning electron micrograph of a SiO_2 slanted columnar thin film taken prior to ALD functionalization.

150LX system from Kurt J. Lesker Company. The exposure times for both $TiCl_4$ and NH_3 were previously optimized to yield saturated ALD growth for a sample surface temperature of 335 °C.

Three different samples were made using 400, 500 and 600 cycles of ALD. The thicknesses were predicted to be of (5 ± 1) nm, (6 ± 1) nm and (7 ± 1) nm, respectively, using the known growth per cycle (GPC) of the process ((0.12 ± 0.02) Å/cycle). This GPC was calculated from the thickness of a 500-cycle sample deposited an Si wafer with a 1050 nm thermal oxide [20] known to improve thickness measurements for thin absorbing films by interference-enhancement during ellipsometric modeling [93].

Characterization

Transmission electron microscopy (TEM) measurements were taken over a core-shell columns using a JEOL JEM-2100F microscope operated at 200 keV.

Spectral angular transmittance values, T_p and T_s, were assessed for polarizations parallel (p) and perpendicular (s) to the incidence plane, respectively using an Agilent Cary 7000 Universal Measurement Spectrophotometer (UMS) in which film columns were oriented parallel to the incidence plane. Subsequently, the luminous transmittance (T_p^{lum}, T_s^{lum}, T_u^{lum}, where u indicates unpolarized light) was obtained for each incidence angle and polarization from an average of the spectral transmittance weighted to the CIE 1931 2° standard observer and CIE E standard illuminant [33, 95].

5.2.4 Results and discussion

TEM analysis of shell conformity

While ALD is known for conformal deposition, results can vary significantly with subtle differences in substrate surface chemistry [26] and process conditions. In this section, we demonstrate the presence of distinct TiN shells and SiO_2 cores in our core-shell SCTFs using TEM. As can be seen in Fig. 5.2 (a) from the TEM micrographs of a representative TiN-coated nanocolumn, a clear and distinct dark shell of TiN is visible around the SiO_2 nanocolumn. The thickness of the shell was estimated to be (7 ± 1) nm for the 600-cycle sample, and (4 ± 1) nm nm for the 500-cycle sample. In both cases, no significant variation of the shell thickness was observed along the column length. The measured thicknesses are within the range predicted by the known growth rate of the ALD process ((7 ± 1) nm and (6 ± 1) nm , respectively), indicating that optimal ALD growth occurred conformally around the SiO_2 columns. The slightly lower thickness for the 500-cycle shell may indicate

a longer nucleation delay [20] on the SiO_2 columns than on the thermal oxide used for GPC determination or the presence of deposition within the columns. In Figure 5.2 (c) and (d),

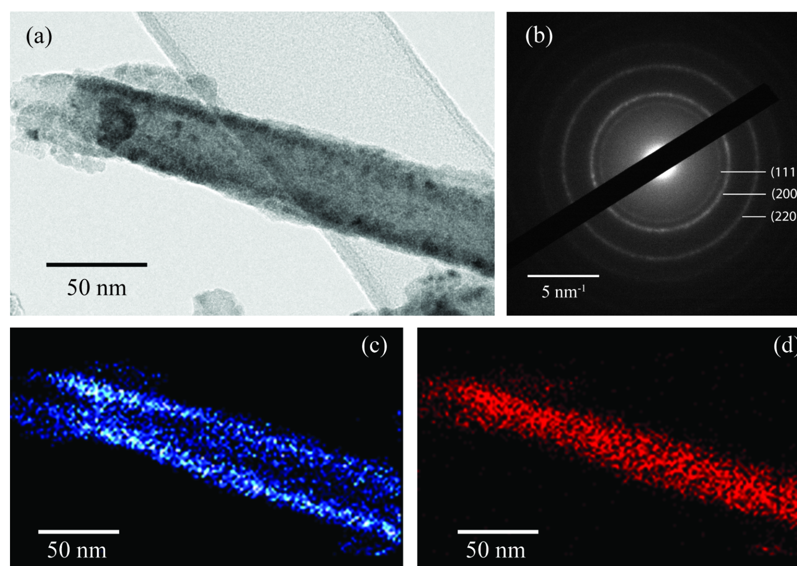

Figure 5.2 Micrographs of a TiN-coated SiO_2 nanocolumn obtained by transmission electron microscopy. (a) TEM bright field nanocolumn image used for measuring the TiN shell thickness. (b) Selected-area electron diffractogram taken over the TiN-coated SiO_2 nanocolumn shown in (a). Mappings of (c) titanium and (d) silicon EDS counts over the nanocolumn shown in (a).

EDS mappings confirm that the shell observed in Fig. 5.2 (a) is composed of titanium, or of a titanium compound. As can be seen, the counts of the titanium element are concentrated on the edges of the nanocolumn, whereas the counts of the silicon element are concentrated in the center, suggesting the presence of a distinct core and shell.

The crystalline structure of the shell was assessed by a selected-area diffraction measurement (SAED) (see Fig. 5.2 (b)). The presence of rings suggests that the darker region appearing in Fig. 5.2 (a) is caused by the presence of a polycrystalline layer of titanium nitride enveloping the SiO_2 column: on the edges of the column, multiple grains diffract the incident electrons, leading to darker edges. Dark spots can also be seen in the center of the column, corresponding to random diffracting grains present on the surface or on the bottom of the columns.The interplanar distances associated with the first three rings of the diffractogram are 2.39 Å, 2.08 Å, 1.48 Å. These distances correspond to the (111), (200) and (220) planes of cubic TiN [106] albeit the observed offset likely be caused by oxidation [17] and/or a non-stoichiometric Ti/N ratio [107, 108]. Considering these results, it is concluded that the ALD deposited TiN envelops the SiO_2 columns leading to the formation of core-shell SCTFs.

Angular selectivity

While SiO_2 SCTFs normally do not exhibit AS in the visible spectrum, the presence of an absorbing TiN shell in the core-shell SCTFs results in angular selective behaviour. As an example, the spectral transmission in the visible region for the 500-cycle sample is shown in Fig. 5.3 (a) for three angles of incidence: 0°, 60° and −60°. One can see that $T_p(+60°) > T_p(0°) > T_p(-60°)$ for all wavelengths. Such asymmetric behaviour is true for all angles of incidence but for p-polarization only, while for s-polarization $T_s(\theta) = T_s(-\theta)$. The angular selectivity can be defined in two ways: a) the ratio of transmitted light at a positive and negative angle which gives the relative AS: $S(\theta) = T(+\theta)/T(-\theta)$, and b) the difference in transmitted light at a positive and negative angle which gives the absolute AS: $\Delta T(\theta) = T(+\theta) - T(-\theta)$. Relative AS is useful for predicting signal to noise ratios, in opto-electronic applications for instance, whereas absolute AS is useful for indicating differences in perceived light intensity, or differences in transmitted solar energy, for ophthalmic and energy applications.

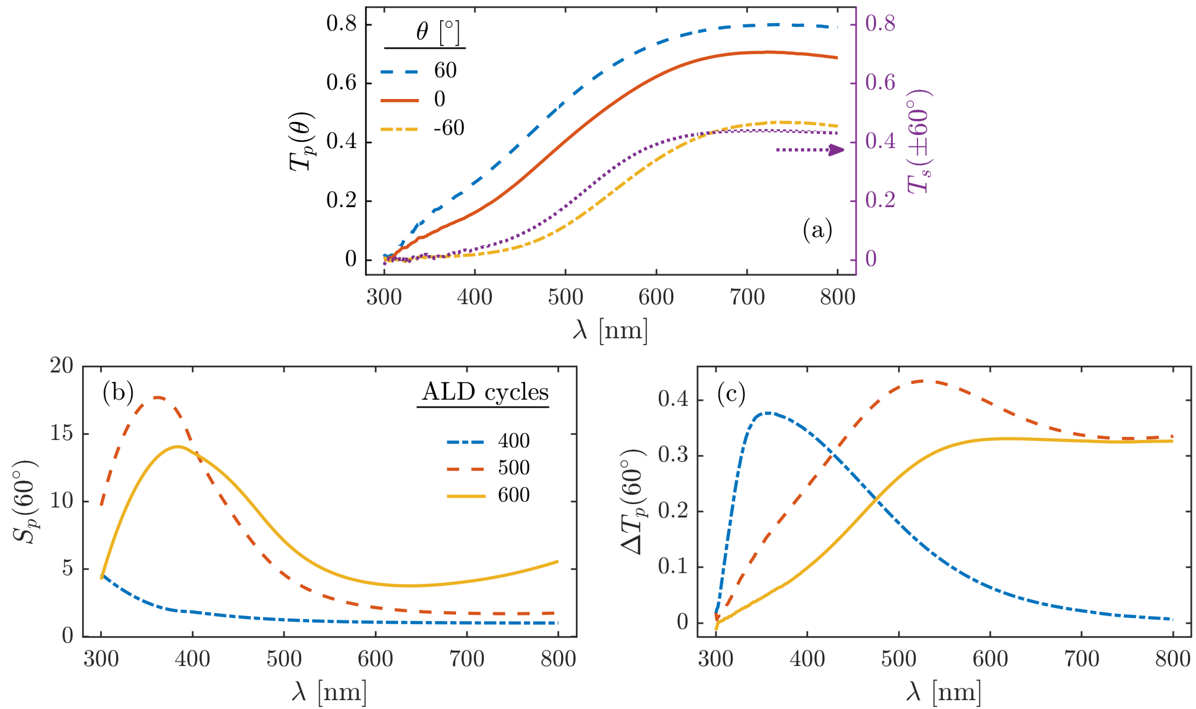

Figure 5.3 (a) p- (left y-axis) and s-polarized (right y-axis) transmission spectra of a SiO_2 slanted columnar thin film coated with 500 cycles of TiN by ALD measured at three different angles. Transmission at positive and negative angles are identical for s-polarized light; (b) relative AS and (c) absolute AS at 60° and -60° for core-shell SCTFs with 400, 500 and 600 cycles of ALD.

$S_p(60°)$ and $\Delta T_p(60°)$ are plotted in Fig. 5.3(b) and 5.3(c) for the 400-, 500- and 600-cycle samples as a function of wavelength. Taking the 500-cycle sample as an example, it can be seen that both these values vary significantly as documented by the peaks at 360 nm and 520 nm, respectively. A high transmission region above 500 nm corresponds to rather low values of S_p, but to relatively high $\Delta T_p > 0.4$. The gradually increasing TiN absorption [12] at shorter wavelengths leads to a lower transmission and hence to a decrease of ΔT_p. Meanwhile, S_p rises sharply, up to a maximum value of 17. Depending on the application, the balance between these two values for a fixed wavelength can be adjusted by the thickness of the absorbing shell.

Similar observations are true for the overall luminous selectivity of SCTFs, as it can be seen in Fig. 5.4 where polarized and unpolarized angular luminous transmittance T_{lum}, are presented for all three shell thicknesses as well as for an uncoated SCTF. As expected, the uncoated film exhibits no observable difference in transmission between positive and negative angles. However, the angular transmission of the coated GLAD SiO_2 films is asymmetrical for *p*-

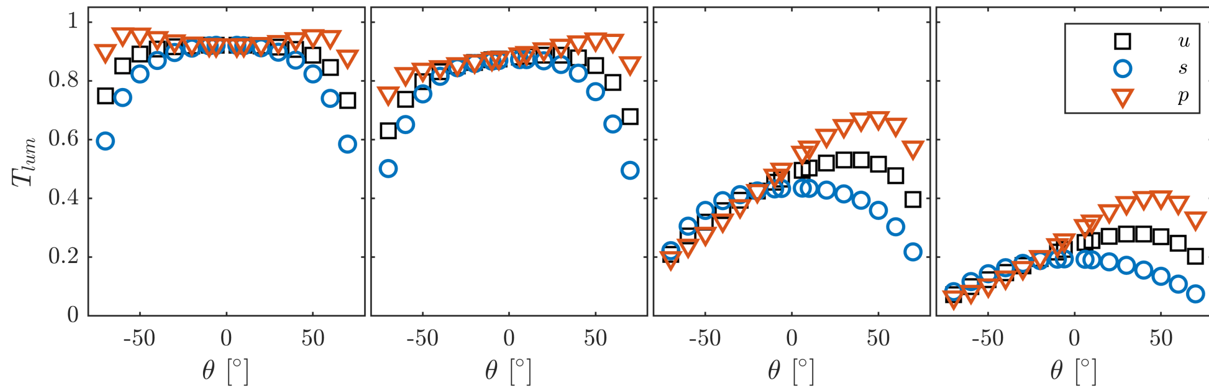

Figure 5.4 Luminous transmittance (T_{lum}) as a function of incidence angle (θ) for SiO_2 SCTFs coated with, from left to right, 0, 400, 500 and 600 cycles of TiN using ALD. The curves present *s*- and *p*-polarizations as well as unpolarized light (u).

polarization and symmetrical for *s*-polarization. For the coatings with 500 and 600 cycles of TiN, the angular position of the unpolarized light transmission maximum is measured at 50°, which is in close agreement with the 44° angle of the columns' inclination and consistent with the observations of metal SCTFs [33].

The measured $S_u^{lum}(60°)$ (i.e. $(T_u^{lum}(+60°))/(T_u^{lum}(-60°)\ ))$ values are 1.08, 1.75, 2.48, respectively, for 400, 500 and 600 cycles of ALD. Therefore, it is deduced that increasing the thickness of the shell leads to higher measured S_u^{lum} and lower measured ΔT_u^{lum}, similarly to the effect of increasing the thickness of a pure metal SCTF [33]. Contrarily to the latter, however, increasing the shell thickness does not significantly affect the size and shape of the

columns. Thus, core-shell SCTFs can have different selectivity with an identical morphology. In addition, metallic nanocolumnar angular selective coatings are typically limited to below 100 nm, as higher thicknesses lead to very low visible transmission [2]. This is not the case for the core-shell coatings studied here since longer columns can be compensated for by reducing the thickness of the absorbing shell. This offers an opportunity to control the interference in the film and other thickness-related effects, as the film thickness and absorption can be independently adjusted. In our case, this allows one to tailor the spectral response of the films. Indeed, the high values of $\Delta T_p > 0.3$ are reached at shorter wavelengths for the 400 cycles sample, in the middle of the visible for the 500 cycles one, and in longer wavelengths for the 600 cycles (see Fig. 5.3). This tunability is achieved without a significant loss in overall angular selective performance.

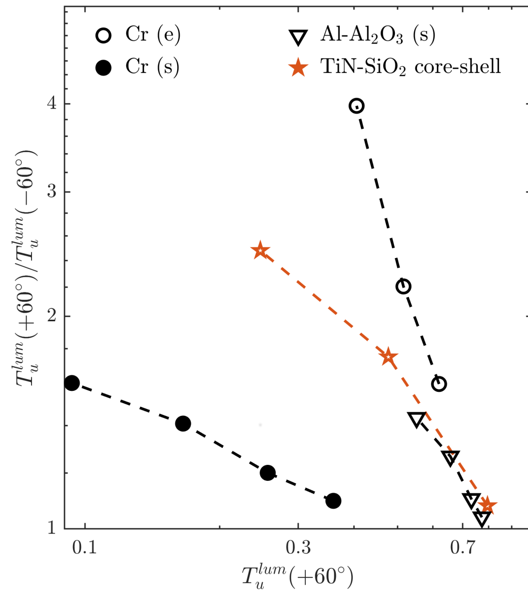

Figure 5.5 Relative luminous angular selectivity ($T_u^{lum}(+60°)/T_u^{lum}(-60°)$) vs. maximum transmittance ($T_u^{lum}(+60°)$) of unpolarized light. TiN-SiO_2 core-shell SCTFs values are compared with data published by Mbise et. al. for evaporated (e) and sputtered (s) Cr SCTFs as well as reactive DC sputtered Al_2O_3 SCTFs with metallic Al inclusions.

The overall AS performance of our samples is, in fact, comparable to the best results (highest $S^{lum}(60°)$ at given $T^{lum}(60°)$), known in the literature. Indeed, figure 5.5 shows a comparison between our core-shell films and selected results from other authors. Films offering high $T^{lum}(60°)$, in conjunction with high $S^{lum}(60°)$, are most desirable for AS applications, thus films trending towards the upper right part of the figure offer a better performance. As seen in the figure, the core-shell samples are similar in performance to evaporated Cr films and perform substantially better than sputtered Cr SCTFs, due to the structure they inherit from

evaporated SiO_2 SCTFs.

Indeed, this exemplifies another key advantage of the core-shell SCTF technique: while evaporation of good quality AS TiN SCTFs is technically challenging, the core-shell method enables one to incorporate the optical properties and temperature- and corrosion-resistant qualities of a material such as TiN into a AS film while leveraging the structure of a well established SCTF material such as SiO_2.

5.2.5 Conclusions

In conclusion, conformal deposition of TiN shells was achieved over SiO_2 SCTFs by ALD. The resulting core-shell films presented pronounced AS properties, similar to metal SCTFs. Contrarily to the latter, absorption and thus angular selectivity can be tailored independently from the column length. Furthermore, the use of ALD to deposit absorbing shells enables one to use new materials, such as durable metal nitrides, in the fabrication of GLAD-based AS coatings.

5.2.6 Acknowledgements

This work was supported by the Natural Sciences and Engineering Research Council of Canada (NSERC) through the Multisectorial Industrial Research Chair in Coatings and Surface Engineering (MIC-CSE) program, and by Essilor International who provided evaporation deposition equipment. The authors also thank Mr. Sébastien Chénard and Mr. Francis Turcot for their technical assistance, Julien Gagnon for assisting with GLAD deposition and Dr. Richard Vernhes for stimulating discussions.

5.3 Further work on core-shell SCTFs

Following the results in this article, a second series of core-shell films were deposited to investigate how the thickness and porosity of SCTFs affect their overall performance. Films of three different thicknesses and two glancing angles were deposited and covered with 300 and 500 cycles of ALD. Their luminous AS is presented in figure 5.6 in relation to their luminous transmission at +60°. Thicker SCTFs have higher surface area leading to more deposition of TiN, thus increasing AS for an identical shell thickness. This leads to a sharper drop in transmission and increase in selectivity when shell material is added over them as compared to thinner SCTFs (see green and red circles in Fig. 5.6). Thus when tuning the CS-SCTFs , smaller shell thickness increments should be used on thicker SCTFs.

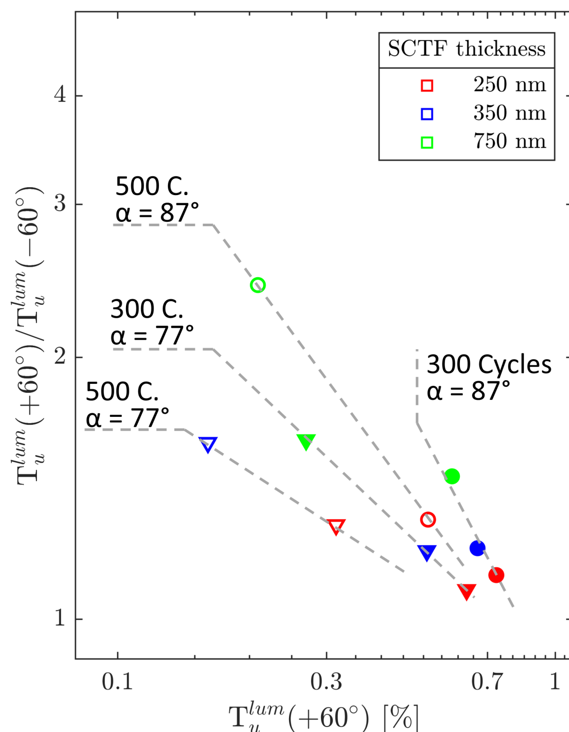

Figure 5.6 Core-shell SCTFs deposited with multiple SCTF thicknesses, glancing angles (α) and core thicknesses (number of cycles).

Lower glancing angle SCTFs ($\alpha = 77°$ in figure 5.6), also exhibit lower transmission and lower AS for identical shell thickness. This may be cause by their higher density. On these denser films, however, increasing shell thickness leads to a similar reduction in transmission and increase in selectivity as higher porosity SCTFs (See triangles in figure 5.6). Thus to obtain the best AS and transmission compromise, one should strive to make the most porous and thickest SCTFs possible just as is predicted in figure 2.20 by Julien Gagnon [15]. The key benefit of using ALD in this case in that the SCTF material can be chosen exclusively as a function of whichever produces the most porous and thick columnar films.

In efforts to understand how AS could further be improved in the core-shell films it is pertinent to consider how shell and SCTF thicknesses affect the spectral AS. A shown in figure 5.7 (a), the film we found to have the best performance (the 500 cycle film) also happens to have the higher absolute AS in the green region, which is also the region with the most importance when calculating luminous AS.

Furthermore, wavelength from 600 nm to 800 nm also have very similar high AS and positive angle transmission for this film. Conversely, the two other films either have too high or too

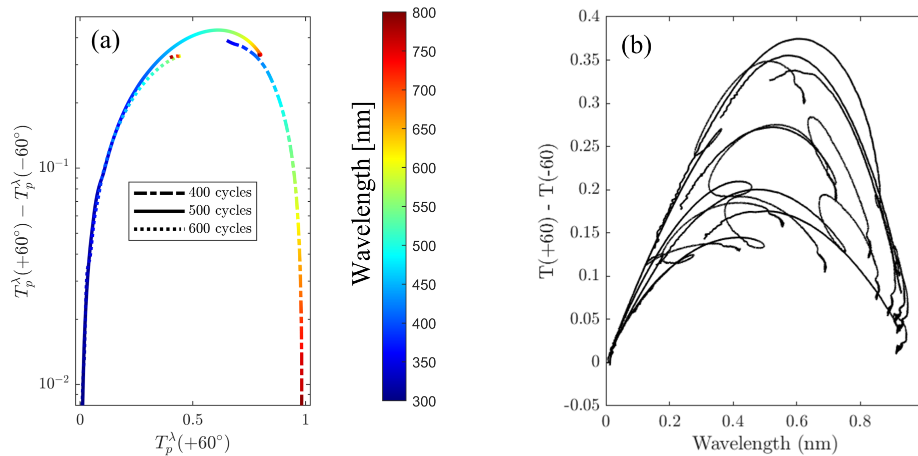

Figure 5.7 (a) Absolute AS as a function of positive angle transmission and wavelength for films of the first series. (b) Absolute AS as a function of positive angle transmission for all films of the second series.

low transmission at the expense of their overall performance. Interestingly, though, the curves in figure 5.7 (a) all seem to follow the same general aspect, with the selectivity maximum centred above a positive angle transmission of 50%. This is confirmed in figure 2 where all data from the second series in compiled in a similar representation.

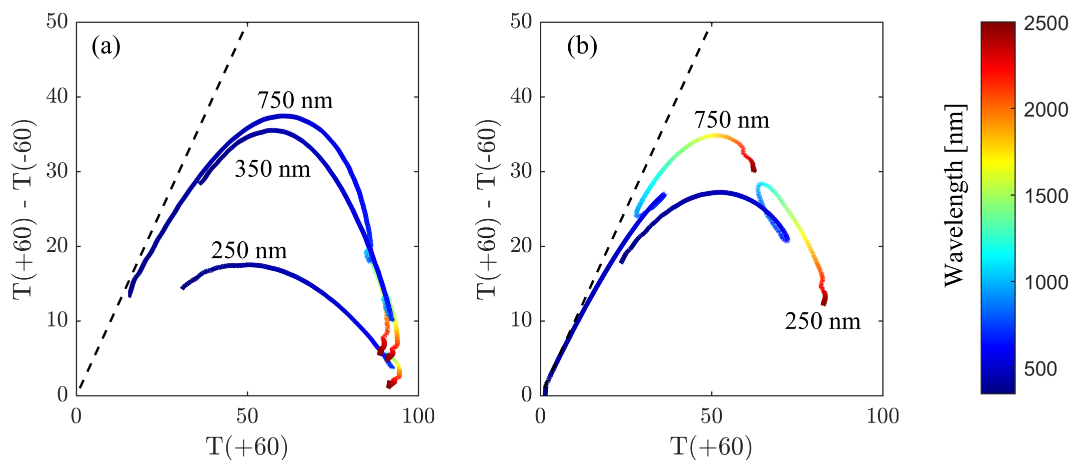

Figure 5.8 Absolute angular selectivity as a function of positive angle transmission for films with shell thicknesses of (a) 300 cycles and (b) 500 cycles and SCTF thicknesses as indicated for each curve.

Further insight regarding how to move about the curve is gained from figure 5.8. The maximum AS in the film increases with column thickness whereas shell thickness can either increase of decrease the maximum AS. One can also notice that changing the shell thickness

significantly changes the spectral position of the AS maximum. This is caused by the varying absorption of the TiN as a function of wavelength. When optimizing for luminous AS, one should thus aim to have close to 50% transmission in the entire visible spectrum by using shell materials with constant absorption. Conversely, when using shells with varying spectral optical properties, spectral AS can be tuned by changing the shell thickness.

5.4 Concluding remarks

As a result of this work, tunable angular selective core-shell SCTFs were made with silica cores and TiN shells. These films give similar performance as known metallic SCTFs with the added benefit of simple tunability which could encourage industrial adoption of such coatings. These tunable sculptured films provide a compelling example of how tailoring absorption with ALD can be used to improve existing processes.

CHAPTER 6 GENERAL DISCUSSION

The work presented in chapter 4 shows that hollow cathode plasma can be used to improve some aspects of titanium nitride PEALD for optical applications. Namely, HC-PEALD leads to a ten-fold reduction in chlorine contamination and close to double the growth rate when compared to our IC-PEALD. Table 6.1 compiles the GPCs, Cl and O concentrations, resistivity, and processing temperatures of the films deposited with our HC-PEALD and IC-PEALD processes as well as published values by other authors.

Table 6.1 Comparing the properties of our IC-PEALD and HC-PEALD coatings to selected results from other authors.

Authors	Plasma type	GPC [Å/cycle]	PPL [s]	Contamination [at. %]	Resistivity [$\mu\Omega \cdot$ cm]	Temp. [°C]
This Work	HCP	0.52	60	Cl: <0.01 O: 3–6	104	380
This Work	ICP	0.29	9	Cl: 0.5 O: 1	73	380
E. Langereis et al. [20]	ICP	0.57	15	Cl: 0.3 O: 1.6	<140	400
K.-E. Elers et al. [21]	CCP	0.3	3	Cl: ∼0.5	<150	320
J.-D. Kwon and J.-S. Park [72]	CCP	0.46	10	Cl: ∼0.5	80	350

The GPCs obtained through HC-PEALD are among the highest. This is especially true at low temperatures where GPCs up to 0.8 Å/cycle are reached. Throughput, however, is lower because the PPL needed to achieve self-limiting growth is 60 s. This exposure time is much longer than in the other PEALD processes, with <3 s [21] and 10 s [72] PPLs reported for direct PEALD and 15 s [20] and 9 s PPLs used in IC-PEALD. The trends presented in figure 4.7 however indicate that shorter PPL could be achieved by using higher plasma power than was possible with our system. For instance, 90% of saturated GPC is achieved after a 10 s PPL at 600 W. With shorter PPLs in a high-power setup, the high GPCs of HC-PEALD could be used to increase throughput over ICPs. This is especially true when depositing at low temperatures where GPC can be as much as 250% greater in HC-PEALD. This could be an important advantage for optical film processing since temperature sensitive polymer substrates are ubiquitous in ophthalmic lenses and many other optics.

Oxygen contamination was higher in the films made by HC-PEALD (3–6 at.%) as compared to our IC-PEALD (1 at.%) and to other published results (See Table 6.1). This was likely caused by the differing experimental conditions, especially the lack of load lock in our system. The much lower chlorine contamination observed in our HC-PEALD films, however, hints that HCP could indeed improve resistivity in TiN films if oxidation sources were reduced. Future upgrades to FCSEL's *ALD-150LX* will undoubtedly yield better results.

Nevertheless, the work presented in chapter 4 fulfils the second objective of this thesis by providing a detailed overview of TiN PEALD using a hollow cathode source. Since only very few materials have been deposited using a similar setup, the work will undoubtedly contribute to the understanding of HC-PEALD.

Table 6.2 Comparing the three deposition methods presented in chapter 4.

Process	GPC [Å/cycle]	Throughput [Å/min]	Resistivity [$\mu\Omega \cdot$ cm]	Cl at.%	Low temp. GPC Å/cycle
HC-PEALD	0.52	∼0.5	104	0.01	∼0.8
IC-PEALD	0.29	∼1.6	73	∼0.5	∼0.3
ALD	0.17	∼4.1	200	∼2	no deposition

The optimization of conductivity and GPC in films made with both ALD and HC-PEALD processes fulfils the first objective: to minimize resistivity in TiN films obtained by ALD and PEALD for optical applications. When comparing them to ALD, both PEALD processes yield films with lower resistivity and impurity count while having higher GPCs and a wider temperature window. Table 6.2 summarizes these results. The better properties of the PEALD films are, however, achieved at the expense of throughput because of the long plasma exposures. Hence PEALD should be reserved for application in which films are very thin and must be of high quality, for instance transparent conductive films or the tuning of absorption in SCTFs.

Indeed, angle-selective CS-SCTFs were obtained from conformal ALD of absorbing TiN over SiO_2 SCTFs in chapter 5.2. TEM images showed unambiguously that the TiN layer formed a shell around the columns and AS of the coatings was confirmed by angle-resolved spectrophotometry in accordance with the third objective of the thesis: to obtain AS in CS-SCTFs through successive GLAD and ALD of SiO_2 and TiN.

As per the fourth and final objective, the advantages of the fabrication method are demonstrated: The tailoring of AS in CS-SCTFs gives a compelling example of how ALD can be used for tuning absorption in nanostructured optical coatings. Furthermore, the proposed method has many advantages over traditional GLAD based fabrication of angular selective metal SCTFs. Namely, the structural and material properties of such coatings can be decoupled which enables independent tuning of either to specific applications. As an example, TiN was used in the core-shell films while obtaining TiN SCTFs through evaporation alone would be challenging both in terms of the quality of the material and its structure. This flexibility is especially important given that material optical properties have a large impact on the spectral distribution of the AS in SCTFs.

The ability to tailor coating performance without changing the SCTF structure also has important implications for industrial manufacturing of AS films. As process control in GLAD is often found to be too complex if any flexibility is required in terms of coating properties [34].

The current core-shell films underperform when comparing their luminous AS to other metal SCTFs. Indeed, the highest luminous relative AS, $S_{lum}(60°)$, of our CS-SCTFs was measured at 2.48 whereas evaporated Cr films have been reported with $S_{lum}(60°)$ at an equal positive angle transmission. However further improvement to CS-SCTFs will undoubtedly lead to more pronounced AS. For instance, different shell materials more geared toward this specific application will increase the AS of such films. A higher quality shell material such as one obtained by HC-PEALD may also increase the AS. Furthermore, given improvements in throughput, PEALD films should preferably be used in the context of tuning absorption in nanostructured optical films as only small amounts of material are deposited and lower quality films will result in less desirable colours, necessitate thicker ALD films and be more susceptible to environmental degradation.

CHAPTER 7 CONCLUSION

The results of this thesis show that optical quality titanium nitride films can be obtained from ALD, and that such films can be used for fine tailoring of optical properties in nanostructured coatings such as SCTFs.

TiN was deposited by ALD and PEALD and was optimized for optical applications. The TiN PEALD process was further developed by using a hollow cathode plasma source as a means of improving the material's quality. Since HC-PEALD deposition of TiN had never been attempted, great attention was given to characterize the process and how various parameters such as PPL, temperature and power affected it. HC-PEALD was found to provide benefits to PEALD of TiN namely by doubling low temperature growth rates and reducing contamination by chlorine tenfold. Oxidation sources in the chamber however limited the quality of the processed films and the ability to determine what effect the source had on oxygen content.

TiN was then conformaly deposited by ALD over silica SCTFs to produce angular selective coatings in which the AS and transmission could be tuned in by changing only the thickness of the shell. In addition to tuning luminous transmission, we found that specific shell thicknesses could be used to obtain maximum selectivity in specific spectral regions. As such, the method provides a simple way of tailoring optical properties in angular selective SCTFs. The work also provides a compelling example of how ALD of metal nitrides can be used to tune optical absorption in nanostructured coatings.

Future research at FCSEL should further investigate how angular selectivity is tuned in core-shell SCTFs. For instance, FDTD modelling of different columns and shell dimensions could yield better understanding on how to tailor the coatings to specific needs. Using other shell materials such as silver or chromium would also help to determine how different materials affect the properties of the core-shell coatings and would further demonstrate the discussed advantages of the technique. Further CS-SCTF experiments should also use high-quality materials obtained by PEALD or HC-PEALD for best results.

REFERENCES

[1] R. W. Johnson, A. Hultqvist, and S. F. Bent, “A brief review of atomic layer deposition: from fundamentals to applications,” *Materials Today*, vol. 17, no. 5, pp. 236–246, Jun. 2014. [Online]. Available: http://www.sciencedirect.com/science/article/pii/S1369702114001436

[2] “Global atomic layer deposition (ald) market by type (aluminium oxide (al2o3) ald, catalytic ald, metal ald, ald on polymers, others), application, region, global industry analysis, market size, share, growth, trends, and forecast 2018 to 2025,” https://www.fiormarkets.com/report/global-atomic-layer-deposition-ald-market-by-type-362185.html#description (2019/11/17), Jan 2019.

[3] X. Meng, “Towards high-energy and durable lithium-ion batteries via atomic layer deposition: elegantly atomic-scale material design and surface modification,” *Nanotechnology*, vol. 26, no. 2, p. 020501, dec 2014. [Online]. Available: https://doi.org/10.1088%2F0957-4484%2F26%2F2%2F020501

[4] N. Cheng, Y. Shao, J. Liu, and X. Sun, “Electrocatalysts by atomic layer deposition for fuel cell applications,” *Nano Energy*, vol. 29, pp. 220 – 242, 2016. [Online]. Available: https://doi.org/10.1016/j.nanoen.2016.01.016

[5] W. Niu, X. Li, S. K. Karuturi, D. W. Fam, H. Fan, S. Shrestha, L. H. Wong, and A. I. Y. Tok, “Applications of atomic layer deposition in solar cells,” *Nanotechnology*, vol. 26, no. 6, p. 064001, jan 2015. [Online]. Available: https://doi.org/10.1088%2F0957-4484%2F26%2F6%2F064001

[6] N. K. R. Eswar, S. A. Singh, and J. Heo, “Atomic layer deposited photocatalysts: comprehensive review on viable fabrication routes and reactor design approaches for photo-mediated redox reactions,” *J. Mater. Chem. A*, vol. 7, pp. 17 703–17 734, 2019. [Online]. Available: https://doi.org/10.1039/C9TA04780H

[7] L. Qian, B. Shen, G. W. Qin, and B. Das, “Widely tuning optical properties of nanoporous gold-titania core-shells,” *The Journal of Chemical Physics*, vol. 134, no. 1, p. 014707, Jan. 2011. [Online]. Available: https://aip.scitation.org/doi/10.1063/1.3523644

[8] S. S. Masango, R. A. Hackler, N. Large, A.-I. Henry, M. O. McAnally, G. C. Schatz, P. C. Stair, and R. P. Van Duyne, “High-Resolution Distance Dependence

Study of Surface-Enhanced Raman Scattering Enabled by Atomic Layer Deposition," *Nano Letters*, vol. 16, no. 7, pp. 4251–4259, Jul. 2016. [Online]. Available: https://doi.org/10.1021/acs.nanolett.6b01276

[9] E. Graugnard, D. P. Gaillot, S. N. Dunham, C. W. Neff, T. Yamashita, and C. J. Summers, "Photonic band tuning in two-dimensional photonic crystal slab waveguides by atomic layer deposition," *Applied Physics Letters*, vol. 89, no. 18, p. 181108, Oct. 2006. [Online]. Available: https://aip.scitation.org/doi/10.1063/1.2360236

[10] X. Yang, C. J. Chen, C. A. Husko, and C. W. Wong, "Digital resonance tuning of high-q/vm silicon photonic crystal nanocavities by atomic layer deposition," *Applied Physics Letters*, vol. 91, no. 16, p. 161114, Oct. 2007. [Online]. Available: https://aip.scitation.org/doi/10.1063/1.2800312

[11] J. D. Caldwell, O. J. Glembocki, F. J. Bezares, M. I. Kariniemi, J. T. Niinistö, T. T. Hatanpää, R. W. Rendell, M. Ukaegbu, M. K. Ritala, S. M. Prokes, C. M. Hosten, M. A. Leskelä, and R. Kasica, "Large-area plasmonic hot-spot arrays: sub-2 nm interparticle separations with plasma-enhanced atomic layer deposition of Ag on periodic arrays of Si nanopillars," *Optics Express*, vol. 19, no. 27, pp. 26 056–26 064, Dec. 2011. [Online]. Available: https://www.osapublishing.org/oe/abstract.cfm?uri=oe-19-27-26056

[12] M. Leskelä and M. Ritala, "Atomic layer deposition (ALD): from precursors to thin film structures," *Thin Solid Films*, vol. 409, no. 1, pp. 138–146, Apr. 2002. [Online]. Available: http://www.sciencedirect.com/science/article/pii/S0040609002001177

[13] V. Miikkulainen, M. Leskelä, M. Ritala, and R. L. Puurunen, "Crystallinity of inorganic films grown by atomic layer deposition: Overview and general trends," *Journal of Applied Physics*, vol. 113, no. 2, p. 021301, Jan. 2013. [Online]. Available: https://aip.scitation.org/doi/10.1063/1.4757907

[14] H. V. Bui, A. W. Groenland, A. a. I. Aarnink, R. a. M. Wolters, J. Schmitz, and A. Y. Kovalgin, "Growth Kinetics and Oxidation Mechanism of ALD TiN Thin Films Monitored by In Situ Spectroscopic Ellipsometry," *Journal of The Electrochemical Society*, vol. 158, no. 3, pp. H214–H220, Mar. 2011. [Online]. Available: http://jes.ecsdl.org/content/158/3/H214

[15] J. Gagnon, "Dépôt de couches minces de WO_3 à incidence rasante pour un électrochromisme stable e la sélectivité angulaire," Master's thesis, École polytechnique de Montréal, 2018.

[16] L. Hiltunen, M. Leskelä, M. Mäkelä, L. Niinistö, E. Nykänen, and P. Soininen, "Nitrides of titanium, niobium, tantalum and molybdenum grown as thin films by the atomic layer epitaxy method," *Thin Solid Films*, vol. 166, pp. 149–154, Dec. 1988. [Online]. Available: http://www.sciencedirect.com/science/article/pii/0040609088903756

[17] M. Radecka, E. Pamula, A. Trenczek-Zajac, K. Zakrzewska, A. Brudnik, E. Kusior, N.-T. Kim-Ngan, and A. Balogh, "Chemical composition, crystallographic structure and impedance spectroscopy of titanium oxynitride TiNxOy thin films," *Solid State Ionics*, vol. 192, no. 1, pp. 693–698, Jun. 2011. [Online]. Available: https://linkinghub.elsevier.com/retrieve/pii/S0167273810004194

[18] H. B. Profijt, S. E. Potts, M. C. M. van de Sanden, and W. M. M. Kessels, "Plasma-Assisted Atomic Layer Deposition: Basics, Opportunities, and Challenges," *Journal of Vacuum Science & Technology A*, vol. 29, no. 5, p. 050801, Aug. 2011. [Online]. Available: https://avs.scitation.org/doi/10.1116/1.3609974

[19] P. Patsalas, N. Kalfagiannis, and S. Kassavetis, "Optical Properties and Plasmonic Performance of Titanium Nitride," *Materials*, vol. 8, no. 6, pp. 3128–3154, Jun. 2015. [Online]. Available: https://www.mdpi.com/1996-1944/8/6/3128

[20] E. Langereis, S. B. S. Heil, M. C. M. van de Sanden, and W. M. M. Kessels, "In situ spectroscopic ellipsometry study on the growth of ultrathin TiN films by plasma-assisted atomic layer deposition," *Journal of Applied Physics*, vol. 100, no. 2, p. 023534, Jul. 2006. [Online]. Available: https://aip.scitation.org/doi/10.1063/1.2214438

[21] K.-E. Elers, J. Winkler, K. Weeks, and S. Marcus, "TiCl4 as a Precursor in the TiN Deposition by ALD and PEALD," *Journal of The Electrochemical Society*, vol. 152, no. 8, pp. G589–G593, Aug. 2005. [Online]. Available: http://jes.ecsdl.org/content/152/8/G589

[22] W. Li, U. Guler, N. Kinsey, G. V. Naik, A. Boltasseva, J. Guan, V. M. Shalaev, and A. V. Kildishev, "Refractory Plasmonics with Titanium Nitride: Broadband Metamaterial Absorber," *Advanced Materials*, vol. 26, no. 47, pp. 7959–7965, Dec. 2014. [Online]. Available: https://onlinelibrary.wiley.com/doi/abs/10.1002/adma.201401874

[23] L. Martinu, O. Zabeida, and J. E. Klemberg-Sapieha, "Chapter 9 - Plasma-Enhanced Chemical Vapor Deposition of Functional Coatings," in *Handbook of Deposition Technologies for Films and Coatings (Third Edition)*, third edition ed., P. M. Martin, Ed. Boston: William Andrew Publishing, 2010, pp. 392 – 465. [Online]. Available: http://www.sciencedirect.com/science/article/pii/B9780815520313000090

[24] G. V. Naik, V. M. Shalaev, and A. Boltasseva, “Alternative Plasmonic Materials: Beyond Gold and Silver,” *Advanced Materials*, vol. 25, no. 24, pp. 3264–3294, 2013. [Online]. Available: https://onlinelibrary.wiley.com/doi/abs/10.1002/adma.201205076

[25] J. H. Kang and K. J. Kim, “Structural, optical, and electronic properties of cubic TiNx compounds,” *Journal of Applied Physics*, vol. 86, no. 1, pp. 346–350, Jun. 1999. [Online]. Available: https://aip.scitation.org/doi/10.1063/1.370736

[26] U. Guler, A. V. Kildishev, A. Boltasseva, and V. M. Shalaev, “Plasmonics on the slope of enlightenment: the role of transition metal nitrides,” *Faraday Discussions*, vol. 178, no. 0, pp. 71–86, May 2015. [Online]. Available: https://pubs.rsc.org/en/content/articlelanding/2015/fd/c4fd00208c

[27] H. E. Cheng and W. J. Lee, “Properties of TiN films grown by atomic-layer chemical vapor deposition with a modified gaseous-pulse sequence,” *Materials Chemistry and Physics*, vol. 97, no. 2-3, pp. 315–320, 2006.

[28] K. S. A. Butcher, “Hollow cathode plasma sources for plasma enhanced ald and pecvd: Properties and advantages.” Available at http://www.meaglow.com/technical-notes/ (2019/11/17), 2018.

[29] C. Ozgit-Akgun, E. Goldenberg, A. K. Okyay, and N. Biyikli, “Hollow cathode plasma-assisted atomic layer deposition of crystalline aln, gan and ax$_x$ga$_{1-xN}$ thin films at low temperatures,” *Journal of Materials Chemistry C*, vol. 2, no. 12, pp. 2123–2136, Feb. 2014. [Online]. Available: https://pubs.rsc.org/en/content/articlelanding/2014/tc/c3tc32418d

[30] C. Ozgit-Akgun, I. Donmez, and N. Biyikli, “(Invited) Plasma-Enhanced Atomic Layer Deposition of III-Nitride Thin Films,” *ECS Transactions*, vol. 58, no. 10, pp. 289–297, Aug. 2013. [Online]. Available: http://ecst.ecsdl.org/content/58/10/289

[31] A. Haider, S. Kizir, and N. Biyikli, “Low-temperature self-limiting atomic layer deposition of wurtzite InN on Si(100),” *AIP Advances*, vol. 6, no. 4, p. 045203, Apr. 2016. [Online]. Available: https://aip.scitation.org/doi/10.1063/1.4946786

[32] W. Trottier-Lapointe, “Nouveaux matériaux à indice de réfraction ultra faible pour applications ophtalmiques,” Master’s thesis, École polytechnique de Montréal, 2015.

[33] G. Mbise, G. B. Smith, G. A. Niklasson, and C. G. Granqvist, “Angular Selective Window Coatings: Theory and Experiment,” *Journal of Physics D: Applied Physics*, vol. 30, no. 15, pp. 2103–2122, 1997.

[34] A. Barranco, A. Borras, A. R. Gonzalez-Elipe, and A. Palmero, "Perspectives on oblique angle deposition of thin films: From fundamentals to devices," *Progress in Materials Science*, vol. 76, pp. 59–153, Mar. 2016. [Online]. Available: http://www.sciencedirect.com/science/article/pii/S0079642515000705

[35] M. M. Hawkeye and M. J. Brett, "Glancing angle deposition: Fabrication, properties, and applications of micro- and nanostructured thin films," *Journal of Vacuum Science & Technology A*, vol. 25, no. 5, p. 1317, 2007. [Online]. Available: http://avs.scitation.org/toc/jva/25/5

[36] S. Lichter and J. Chen, "Model for Columnar Microstructure of Thin Solid Films," *Physical Review Letters*, vol. 56, no. 13, pp. 1396–1399, Mar. 1986. [Online]. Available: https://link.aps.org/doi/10.1103/PhysRevLett.56.1396

[37] S. Asgharizadeh, M. Sutton, K. Robbie, and T. Brown, "X-ray reflectometry characterization of porous silicon films prepared by a glancing-angle deposition method," *Physical Review B*, vol. 79, no. 12, Mar. 2009. [Online]. Available: https://link.aps.org/doi/10.1103/PhysRevB.79.125405

[38] S. M. George, "Atomic Layer Deposition: An Overview," *Chemical Reviews*, vol. 110, no. 1, pp. 111–131, Jan. 2010. [Online]. Available: https://doi.org/10.1021/cr900056b

[39] C. L. Dezelah, *Atomic Layer Deposition*. Dordrecht: Springer Netherlands, 2012, pp. 161–171. [Online]. Available: https://doi.org/10.1007/978-90-481-9751-4_372

[40] B. Van Hao, "Atomic layer deposition of tin films : growth and electrical behavior down to sub-nanometer scale," Ph.D. dissertation, University of Twente, Netherlands, 1 2013.

[41] M. Vos, "Atomic layer deposition process development - 10 steps to successfully develop, optimize and characterize ald recipes," Available at https://www.atomiclimits.com/2019/02/12 (2019/11/17), Feb 2019.

[42] M. R. Saleem, R. Ali, M. B. Khan, S. Honkanen, and J. Turunen, "Impact of atomic layer deposition to nanophotonic structures and devices," *Frontiers in Materials*, vol. 1, p. 18, 2014. [Online]. Available: https://www.frontiersin.org/article/10.3389/fmats.2014.00018

[43] P. O. Oviroh, R. Akbarzadeh, D. Pan, R. A. M. Coetzee, and T.-C. Jen, "New development of atomic layer deposition: processes, methods and applications," *Science*

and Technology of Advanced Materials, vol. 20, no. 1, pp. 465–496, May 2019. [Online]. Available: https://www.ncbi.nlm.nih.gov/pmc/articles/PMC6534251/

[44] Kurt J. Lesker Co., "KJLC awarded a patent for its atomic layer deposition system and process," Nov 2017. [Online]. Available: https://www.lesker.com/newweb/blog/post.cfm/kjlc-awarded-a-patent-for-its-atomic-layer-deposition-system-and-process

[45] "Illustrations atomic layer etching (alet) process." [Online]. Available: http://www.nanomanufacturing.nl/ALE/

[46] S. K. Panda and H. Shin, *Step Coverage in ALD.* John Wiley & Sons, Ltd, 2012, ch. 2, pp. 23–40. [Online]. Available: https://onlinelibrary.wiley.com/doi/abs/10.1002/9783527639915.ch2

[47] S. Kondruweit-Reinema, "Precision work: defect-free coatings for silicon spheres," Available at https://www.fraunhofer.de/en/press/research-news/ (2019/11/17), Jul 2017.

[48] Z. Golrokhi, S. Chalker, C. J. Sutcliffe, and R. J. Potter, "Self-limiting atomic layer deposition of conformal nanostructured silver films," *Applied Surface Science*, vol. 364, pp. 789 – 797, 2016.

[49] S. R. Jim, A. Foroughi-Abari, K. M. Krause, P. Li, M. Kupsta, M. T. Taschuk, K. C. Cadien, and M. J. Brett, "Ultrathin-layer chromatography nanostructures modified by atomic layer deposition," *Journal of Chromatography A*, vol. 1299, pp. 118–125, 2013. [Online]. Available: https://ac.els-cdn.com/S0021967313008182/1-s2.0-S0021967313008182-main.pdf?_tid=fd8a5994-c64d-11e7-8596-00000aab0f27&acdnat=1510342573_3ea72149e6e282c2d785e10c92a0fdba

[50] D. Schmidt, "Characterization of highly anisotropic three-dimensionally nanostructured surfaces," *Thin Solid Films*, vol. 571, no. 3, pp. 364–370, 2014. [Online]. Available: https://www.sciencedirect.com/science/article/pii/S0040609013017306?via%3Dihub

[51] J. W. Elam, *Coatings on High Aspect Ratio Structures.* John Wiley & Sons, Ltd, 2012, ch. 10, pp. 227–249. [Online]. Available: https://onlinelibrary.wiley.com/doi/abs/10.1002/9783527639915.ch10

[52] H. J. Fan and K. Nielsch, *Coatings of Nanoparticles and Nanowires.* John Wiley & Sons, Ltd, 2012, ch. 11, pp. 251–270. [Online]. Available: https://onlinelibrary.wiley.com/doi/abs/10.1002/9783527639915.ch11

[53] C. Marichy, A. Pucci, M.-G. Willinger, and N. Pinna, *Coating of Carbon Nanotubes.* John Wiley & Sons, Ltd, 2012, ch. 14, pp. 327–343. [Online]. Available: https://onlinelibrary.wiley.com/doi/abs/10.1002/9783527639915.ch14

[54] D. P. Gaillot and C. J. Summers, *Inverse Opal Photonics.* John Wiley & Sons, Ltd, 2012, ch. 15, pp. 345–376. [Online]. Available: https://onlinelibrary.wiley.com/doi/abs/10.1002/9783527639915.ch15

[55] N. M. Johnson, J. Walker, C. M. Doland, K. Winer, and R. A. Street, "Hydrogen incorporation in silicon thin films deposited with a remote hydrogen plasma," *Applied Physics Letters*, vol. 54, no. 19, pp. 1872–1874, 1989. [Online]. Available: https://doi.org/10.1063/1.101264

[56] J. Jokinen, P. Haussalo, J. Keinonen, M. Ritala, D. Riihelä, and M. Leskelä, "Analysis of aln thin films by combining tof-erda and nrb techniques," *Thin Solid Films*, vol. 289, no. 1, pp. 159 – 165, 1996. [Online]. Available: http://www.sciencedirect.com/science/article/pii/S0040609096089274

[57] J. Ferguson, A. Weimer, and S. George, "Atomic layer deposition of boron nitride using sequential exposures of BCl_3 and NH_3," *Thin Solid Films*, vol. 413, no. 1, pp. 16 – 25, 2002. [Online]. Available: http://www.sciencedirect.com/science/article/pii/S0040609002004315

[58] K. Park, W.-D. Yun, B.-J. Choi, H.-D. Kim, W.-J. Lee, S.-K. Rha, and C. O. Park, "Growth studies and characterization of silicon nitride thin films deposited by alternating exposures to si2cl6 and nh3," *Thin Solid Films*, vol. 517, no. 14, pp. 3975 – 3978, 2009, the proceedings of the 1st International Conference on Microelectronics and Plasma Technology (ICMAP 2008). [Online]. Available: http://www.sciencedirect.com/science/article/pii/S0040609009001904

[59] H. Tsuchiya, M. Akamatsu, M. Ishida, and F. Hasegawa, "Layer-by-layer growth of GaN on GaAs substrates by alternate supply of $\bf GaCl_{3}$ and $\bf NH_{3}$," *Japanese Journal of Applied Physics*, vol. 35, no. Part 2, No. 6B, pp. L748–L750, jun 1996. [Online]. Available: https://doi.org/10.1143%2Fjjap.35.l748

[60] J. Hämäläinen, K. Mizohata, K. Meinander, M. Mattinen, M. Vehkamäki, J. Räisänen, M. Ritala, and M. Leskelä, "Rhenium metal and rhenium nitride thin films grown by atomic layer deposition," *Angewandte Chemie International Edition*, vol. 57, no. 44, pp. 14 538–14 542, 2018. [Online]. Available: https://onlinelibrary.wiley.com/doi/abs/10.1002/anie.201806985

[61] C. H. Ahn, S. G. Cho, H. J. Lee, K. H. Park, and S. H. Jeong, "Characteristics of TiN thin films grown by ALD using TiCl4 and NH3," *Metals and Materials International*, vol. 7, no. 6, pp. 621–625, Nov. 2001. [Online]. Available: https://doi.org/10.1007/BF03179261

[62] S. Muhl and A. Pérez, "The use of hollow cathodes in deposition processes: A critical review," *Thin Solid Films*, vol. 579, pp. 174–198, Mar. 2015. [Online]. Available: http://www.sciencedirect.com/science/article/pii/S0040609015001947

[63] L. Bárdoš, "Radio frequency hollow cathodes for the plasma processing technology," *Surface and Coatings Technology*, vol. 86-87, pp. 648–656, Dec. 1996. [Online]. Available: http://www.sciencedirect.com/science/article/pii/S0257897296030563

[64] A. Kilicaslan, O. Zabeida, E. Bousser, T. Schmitt, J. Klemberg-Sapieha, and L. Martinu, "Hard titanium nitride coating deposition inside narrow tubes using pulsed dc pecvd processes," *Surface and Coatings Technology*, vol. 377, p. 124894, 2019. [Online]. Available: http://www.sciencedirect.com/science/article/pii/S0257897219308667

[65] A. Mohammad, D. Shukla, S. Ilhom, B. Willis, B. Johs, A. K. Okyay, and N. Biyikli, "Real-time in situ ellipsometric monitoring of aluminum nitride film growth via hollow-cathode plasma-assisted atomic layer deposition," *Journal of Vacuum Science & Technology A*, vol. 37, no. 2, p. 020927, Feb. 2019. [Online]. Available: https://avs.scitation.org/doi/10.1116/1.5085341

[66] N. Nepal, S. B. Qadri, J. K. Hite, N. A. Mahadik, M. A. Mastro, and C. R. Eddy, "Epitaxial growth of AlN films via plasma-assisted atomic layer epitaxy," *Applied Physics Letters*, vol. 103, no. 8, p. 082110, Aug. 2013. [Online]. Available: https://aip.scitation.org/doi/10.1063/1.4818792

[67] P. Motamedi and K. Cadien, "Structural and optical characterization of low-temperature ALD crystalline AlN," *Journal of Crystal Growth*, vol. 421, pp. 45–52, Jul. 2015. [Online]. Available: http://www.sciencedirect.com/science/article/pii/S0022024815002924

[68] H.-Y. Shih, M.-C. Lin, L.-Y. Chen, and M.-J. Chen, "Uniform GaN thin films grown on (100) silicon by remote plasma atomic layer deposition," *Nanotechnology*, vol. 26, no. 1, p. 014002, Dec. 2014. [Online]. Available: https://doi.org/10.1088%2F0957-4484%2F26%2F1%2F014002

[69] I. Donmez, C. Ozgit-Akgun, and N. Biyikli, “Low temperature deposition of Ga2o3 thin films using trimethylgallium and oxygen plasma,” *Journal of Vacuum Science & Technology A*, vol. 31, no. 1, p. 01A110, Oct. 2012. [Online]. Available: https://avs.scitation.org/doi/10.1116/1.4758782

[70] S. Logothetidis, I. Alexandrou, and A. Papadopoulos, “In situ spectroscopic ellipsometry to monitor the process of TiNx thin films deposited by reactive sputtering,” *Journal of Applied Physics*, vol. 77, no. 3, pp. 1043–1047, Feb. 1995. [Online]. Available: https://aip.scitation.org/doi/10.1063/1.358963

[71] J. Musschoot, Q. Xie, D. Deduytsche, S. V. den Berghe, R. V. Meirhaeghe, and C. Detavernier, “Atomic layer deposition of titanium nitride from tdmat precursor,” *Microelectronic Engineering*, vol. 86, no. 1, pp. 72 – 77, 2009. [Online]. Available: http://www.sciencedirect.com/science/article/pii/S0167931708004292

[72] J.-D. Kwon and J.-S. Park, “Investigating the TiN Film Quality and Growth Behavior for Plasma-enhanced Atomic Layer Deposition Using TiCl4 and N2/H2/Ar Radicals,” *Journal of the Korean Physical Society*, vol. 57, no. 4, pp. 806–806, 2010. [Online]. Available: http://www.kps.or.kr/jkps/abstract_view.asp?articleuid=DC06AED8-7384-47FC-B549-CABB674CEBC8

[73] S. B. S. Heil, E. Langereis, F. Roozeboom, M. C. M. v. d. Sanden, and W. M. M. Kessels, “Low-Temperature Deposition of TiN by Plasma-Assisted Atomic Layer Deposition,” *Journal of The Electrochemical Society*, vol. 153, no. 11, pp. G956–G965, Nov. 2006. [Online]. Available: http://jes.ecsdl.org/content/153/11/G956

[74] Y. J. Mei, T. C. Chang, J. C. Hu, L. J. Chen, Y. L. Yang, F. M. Pan, W. F. Wu, A. Ting, and C. Y. Chang, “Characterisation of tin film growth by low pressure chemical vapor deposition,” *Thin Solid Films*, p. 5, 1997.

[75] G. V. Naik, J. L. Schroeder, X. Ni, A. V. Kildishev, T. D. Sands, and A. Boltasseva, “Titanium nitride as a plasmonic material for visible and near-infrared wavelengths,” *Optical Materials Express*, vol. 2, no. 4, pp. 478–489, Apr. 2012. [Online]. Available: https://www.osapublishing.org/ome/abstract.cfm?uri=ome-2-4-478

[76] J. Humlicek, A. Nebojsa, J. Hora, M. Stráský, J. Spousta, and T. Šikola, “Ellipsometry and transport studies of thin-film metal nitrides,” *Thin Solid Films*, vol. 332, no. 1, pp. 25–29, Nov. 1998. [Online]. Available: http://www.sciencedirect.com/science/article/pii/S0040609098010141

[77] Z. Michalcik, M. Horakova, P. Spatenka, S. Klementova, M. Zlamal, and N. Martin, "Photocatalytic Activity of Nanostructured Titanium Dioxide Thin Films," *International Journal of Photoenergy*, 2012.

[78] W. Trottier-Lapointe, O. Zabeida, T. Schmitt, and L. Martinu, "Ultralow refractive index optical films with enhanced mechanical performance obtained by hybrid glancing angle deposition," *Applied Optics*, vol. 55, no. 31, pp. 8796–8805, Nov. 2016. [Online]. Available: https://www.osapublishing.org/ao/abstract.cfm?uri=ao-55-31-8796

[79] C. M. Zhou and D. Gall, "Development of two-level porosity during glancing angle deposition," *Journal of Applied Physics*, vol. 103, no. 1, p. 014307, Jan. 2008. [Online]. Available: https://aip.scitation.org/doi/10.1063/1.2828174

[80] K. Robbie and M. J. Brett, "Sculptured thin films and glancing angle deposition: Growth mechanics and applications," *Journal of Vacuum Science & Technology A*, vol. 15, no. 3, pp. 1460–1465, May 1997. [Online]. Available: https://avs.scitation.org/doi/abs/10.1116/1.580562

[81] M. T. Taschuk, K. D. Harris, D. P. Smetaniuk, and M. J. Brett, "Decoupling sensor morphology and material: Atomic layer deposition onto nanocolumn scaffolds," *Sensors & Actuators: B. Chemical*, vol. 162, no. 1, pp. 1–6, 2012. [Online]. Available: https//:doi.org/10.1016/j.snb.2011.08.024

[82] A. Haider, H. Cansizoglu, F. Cansizoglu, T. Karabacak, A. K. Okyay, and N. Biyikli, "Enhanced photoresponse of conformal TiO 2 /Ag nanorod array-based Schottky photodiodes fabricated via successive glancing angle and atomic layer deposition," *Journal of Vacuum Science & Technology A*, vol. 33, no. 1, p. 01A110, 2015. [Online]. Available: https://doi.org/10.1116/1.4898203

[83] O. Albrecht, R. Zierold, C. Patzig, J. Bachmann, C. Sturm, B. Rheinländer, M. Grundmann, D. Görlitz, B. Rauschenbach, and K. Nielsch, "Tubular magnetic nanostructures based on glancing angle deposited templates and atomic layer deposition," *physica status solidi (b)*, vol. 247, no. 6, pp. 1365–1371, 2010. [Online]. Available: http://doi.wiley.com/10.1002/pssb.200945560

[84] H. Im, N. C. Lindquist, A. Lesuffleur, and S.-H. Oh, "Atomic Layer Deposition of Dielectric Overlayers for Enhancing the Optical Properties and Chemical Stability of Plasmonic Nanoholes," *ACS Nano*, vol. 4, no. 2, pp. 947–954, Feb. 2010. [Online]. Available: https://doi.org/10.1021/nn901842r

[85] M. Alevli, A. Haider, S. Kizir, S. A. Leghari, and N. Biyikli, "Comparison of trimethylgallium and triethylgallium as "Ga" source materials for the growth of ultrathin GaN films on Si (100) substrates via hollow-cathode plasma-assisted atomic layer deposition," *Journal of Vacuum Science & Technology A*, vol. 34, no. 1, p. 01A137, Dec. 2015. [Online]. Available: https://avs.scitation.org/doi/10.1116/1.4937725

[86] D. Schmidt, E. Schubert, and M. Schubert, "Generalized Ellipsometry Characterization of Sculptured Thin Films Made by Glancing Angle Deposition," in *Ellipsometry at the Nanoscale*. Berlin, Heidelberg: Springer Berlin Heidelberg, 2013, pp. 341–410. [Online]. Available: http://link.springer.com/10.1007/978-3-642-33956-1_10

[87] D. Schmidt, E. Schubert, and M. Schubert, "Optical properties of cobalt slanted columnar thin films passivated by atomic layer deposition," *Applied Physics Letters*, vol. 100, no. 1, p. 011912, 2012.

[88] A. Mock, R. Korlacki, C. Briley, D. Sekora, T. Hofmann, P. Wilson, A. Sinitskii, E. Schubert, and M. Schubert, "Anisotropy, band-to-band transitions, phonon modes, and oxidation properties of cobalt-oxide core-shell slanted columnar thin films," *Applied Physics Letters*, vol. 108, no. 5, pp. 51 905–113 701, 2016. [Online]. Available: https://doi.org/10.1063/1.4941399

[89] S. Yang and Y. Zhang, "Spectroscopic ellipsometry investigations of porous SiO 2 films prepared by glancing angle deposition," *Surface and Interface Analysis*, vol. 45, no. 11-12, pp. 1690–1694, Nov. 2013. [Online]. Available: http://doi.wiley.com/10.1002/sia.5308

[90] J. Potočnik, M. Nenadović, N. Bundaleski, M. Popović, and Z. Rakočević, "Effect of thickness on optical properties of nickel vertical posts deposited by GLAD technique," *Optical Materials*, vol. 62, pp. 146–151, Dec. 2016. [Online]. Available: https://linkinghub.elsevier.com/retrieve/pii/S0925346716305304

[91] J. Woolam Co., "Ellipsometry tutorial," Available at https://www.jawoollam.com/resources/ellipsometry-tutorial (2019/11/17).

[92] J. N. Hilfiker, "5 - In situ spectroscopic ellipsometry (SE) for characterization of thin film growth," in *In Situ Characterization of Thin Film Growth*, ser. Woodhead Publishing Series in Electronic and Optical Materials, G. Koster and G. Rijnders, Eds. Woodhead Publishing, Jan. 2011, pp. 99–151. [Online]. Available: http://www.sciencedirect.com/science/article/pii/B9781845699345500059

[93] J. N. Hilfiker, N. Singh, T. Tiwald, D. Convey, S. M. Smith, J. H. Baker, and H. G. Tompkins, “Survey of methods to characterize thin absorbing films with Spectroscopic Ellipsometry,” *Thin Solid Films*, vol. 516, no. 22, pp. 7979–7989, Sep. 2008. [Online]. Available: http://linkinghub.elsevier.com/retrieve/pii/S0040609008003623

[94] B. Baloukas, “Thin film-based optically variable security devices : From passive to active,” Ph.D. dissertation, École polytechnique de Montréal, 2012.

[95] T. Smith and J. Guild, “The C.I.E. colorimetric standards and their use,” *Transactions of the Optical Society*, vol. 33, no. 3, p. 73, 1931. [Online]. Available: http://stacks.iop.org/1475-4878/33/i=3/a=301

[96] F. M. Smits, “Measurement of sheet resistivities with the four-point probe,” *The Bell System Technical Journal*, vol. 37, no. 3, pp. 711–718, May 1958.

[97] S. A. Speakerman, “Collecting x-ray reflectivity data using the pathfinder detector abridged sop for manually aligning a sample and collecting data using xrd commander,” Available at http://prism.mit.edu/xray (2019/11/17).

[98] M. Björck and G. Andersson, “*GenX*: an extensible X-ray reflectivity refinement program utilizing differential evolution,” *Journal of Applied Crystallography*, vol. 40, no. 6, pp. 1174–1178, Dec 2007. [Online]. Available: https://doi.org/10.1107/S0021889807045086

[99] X. Meng, J. Lee, A. Ravichandran, Y. Byun, J. Lee, A. T. Lucero, S. J. Kim, M. Ha, C. D. Young, and J. Kim, “Robust SiNx/GaN MIS-HEMTs With Crystalline Interfacial Layer Using Hollow Cathode PEALD,” *IEEE Electron Device Letters*, vol. 39, no. 8, pp. 1195–1198, Aug. 2018.

[100] X. Meng, H. S. Kim, A. T. Lucero, S. M. Hwang, J. S. Lee, Y.-C. Byun, J. Kim, B. K. Hwang, X. Zhou, J. Young, and M. Telgenhoff, “Hollow Cathode Plasma-Enhanced Atomic Layer Deposition of Silicon Nitride Using Pentachlorodisilane,” *ACS applied materials & interfaces*, vol. 10, no. 16, pp. 14 116–14 123, Apr. 2018.

[101] C. G. Granqvist, “Applications of Transparent Conductors to Solar Energy and Energy Efficiency,” in *Handbook of Transparent Conductors*, D. S. Ginley, Ed. Boston, MA: Springer US, 2011, pp. 353–423. [Online]. Available: https://doi.org/10.1007/978-1-4419-1638-9_11

[102] G. B. Smith, “Theory of angular selective transmittance in oblique columnar thin films containing metal and voids,” *Applied Optics*, vol. 29, no. 25, pp. 3685–3693,

Sep. 1990. [Online]. Available: https://www.osapublishing.org/ao/abstract.cfm?uri=ao-29-25-3685

[103] R. J. Ditchburn and G. B. Smith, “Useful angular selectivity in oblique columnar aluminum,” *Journal of Applied Physics*, vol. 69, no. 6, pp. 3769–3771, Mar. 1991. [Online]. Available: https://aip.scitation.org/doi/10.1063/1.348474

[104] V. Leontyev, M. Hawkeye, A. Kovalenko, and M. J. Brett, “Omnidirectional reflection from nanocolumnar TiO_2 films,” *Journal of Applied Physics*, vol. 112, no. 8, p. 084317, Oct. 2012. [Online]. Available: http://aip.scitation.org/doi/10.1063/1.4759138

[105] S. Wang, X. Fu, G. Xia, J. Wang, J. Shao, and Z. Fan, “Structure and optical properties of ZnS thin films grown by glancing angle deposition,” *Appl. Surf. Sci.*, vol. 252, no. 24, pp. 8734–8737, Oct. 2006. [Online]. Available: http://www.sciencedirect.com/science/article/pii/S0169433205016983

[106] N. Schönberg, W. G. Overend, A. Munthe-Kaas, and N. A. Sörensen, “An X-Ray Investigation on Ternary Phases in the Ta-Me-N Systems (Me = Ti, Cr, Mn, Fe, Co, Ni).” *Acta Chemica Scandinavica*, vol. 8, pp. 213–220, 1954. [Online]. Available: http://actachemscand.org/doi/10.3891/acta.chem.scand.08-0213

[107] J. E. Sundgren, B. O. Johansson, S. E. Karlsson, and H. T. G. Hentzell, “Mechanisms of reactive sputtering of titanium nitride and titanium carbide II: Morphology and structure,” *Thin Solid Films*, vol. 105, no. 4, pp. 367–384, Jul. 1983. [Online]. Available: http://www.sciencedirect.com/science/article/pii/004060908390319X

[108] C.-C. Jiang, T. Goto, and T. Hirai, “Non-stoichiometry of titanium nitride plates prepared by chemical vapour deposition,” *Journal of Alloys and Compounds*, vol. 190, no. 2, pp. 197–200, Jan. 1993. [Online]. Available: http://www.sciencedirect.com/science/article/pii/0925838893903998

APPENDIX A: HIGH RATE IN-SITU SE DURING PEALD OF TIN

Figure A.1 shows the thickness of a TiN layer measured by interferences enhanced in-situ SE during deposition as a function of different process steps. As noted, thickness can be determined during deposition with very high accuracy. Such measurements can be used directly for analysis of process dynamics and for uptake optimization from a single cycle. However, in this case, the statistical noise was too great for such analysis to be done because the growth rate of TiN if very low. One can however notice adsorption of the chemical precursor and subsequent reduction by plasma.

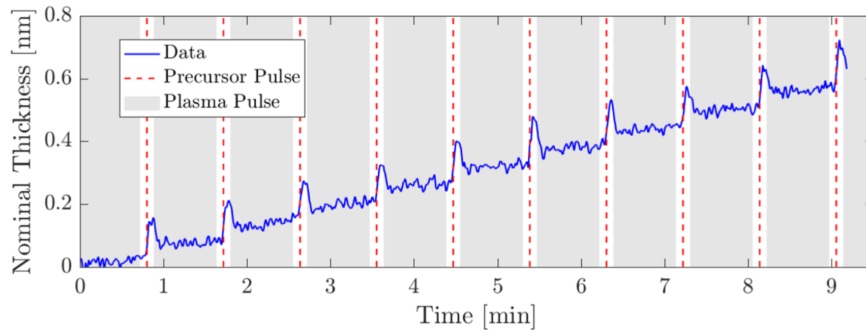

Figure A.1 Thickness of a TiN layer during deposition measured by in-situ SE over a period of 10 cycles. Noise reduction is done by averaging 10 consecutive measurements adjusted to begin at a thickness of 0 nm, hence the nominal thickness. Despite the averaging, data is too noisy to study process cycle dynamics.